1. Report No.	2. Government Accession No.	3. Recipient's Catalog No.
FHWA/TX-07/0-4524-1		

4. Title and Subtitle	5. Report Date
SYSTEM FOR THE EVALUATION OF MOISTURE DAMAGE USING FUNDAMENTAL MATERIAL PROPERTIES	March 2007 Published May 2007
	6. Performing Organization Code

7. Author(s)	8. Performing Organization Report No.
Jonathan Howson, Eyad A. Masad, Amit Bhasin, Veronica Castelo Branco, Edith Arambula, Robert Lytton, and Dallas Little	Report 0-4524-1

9. Performing Organization Name and Address	10. Work Unit No. (TRAIS)
Texas Transportation Institute The Texas A&M University System College Station, Texas 77843-3135	11. Contract or Grant No. Project 0-4524

12. Sponsoring Agency Name and Address	13. Type of Report and Period Covered
Texas Department of Transportation Research and Technology Implementation Office P. O. Box 5080 Austin, Texas 78763-5080	Technical Report: September 2003-August 2006
	14. Sponsoring Agency Code

15. Supplementary Notes

Project performed in cooperation with the Texas Department of Transportation and the Federal Highway Administration.

Project Title: Application of Surface Energy Measurements to Evaluate Moisture Susceptibility of Asphalt and Aggregates

URL: http://tti.tamu.edu/documents/0-4524-1.pdf

16. Abstract

Moisture damage in asphalt mixtures can occur within the mastic (cohesive fracture) or at the aggregate-mastic interface (adhesive fracture or failure). Whether or not a cohesive or adhesive failure occurs depends on the nature of the mastic and the relative thickness of the mastic. This report is part of a project that focused on fundamental understanding of the moisture damage process by carefully considering the micro-mechanisms that influence the adhesive interface between aggregate and asphalt and the cohesive strength and durability of the mastic. The first phase of the project focused on the validation of the surface energy measurements and the dynamic mechanical analysis (DMA) of mastics through the evaluation of the moisture susceptibility of materials with known field performance. The results of the first phase of this project were documented in TxDOT report 0-4524-2. The second phase of the project, which is documented in this report, focused on the evaluation of the surface energy and moisture susceptibility of wide combinations of aggregates and asphalts. The analysis approach of moisture damage that was used for the evaluation of mastics in phase 1 was extended in phase 2 to analyze full asphalt mixtures. Also, the influence of binder modifications made by the manufacturer, aging of the asphalt binder, addition of liquid anti-strip agents to the asphalt binder, and changing of the pH of the water at the asphalt-aggregate interface on surface energy and moisture susceptibility was investigated. The energy ratio *ER* parameter developed under NCHRP 9-37 was used as a screening parameter for evaluating the compatibility of asphalt binders and aggregates in terms of the resistance to moisture damage. The *ER* combines the cohesive and adhesive bond energies into a single term. A comprehensive system was developed for the evaluation of moisture damage. The first step in the system is to examine the compatibility of an asphalt-aggregate combination by evaluating the surface energy components and the *ER*. The second step in the system is to conduct DMA of a mastic specimen made of the asphalt binder and fine aggregate portion of the mix. If the DMA results are favorable, the third step, which is the evaluation of the moisture susceptibility of the full mixture, is conducted in order to examine the suitability of mixture design and volumetrics in resisting moisture damage.

17. Key Words	18. Distribution Statement
Surface Energy, Moisture, Asphalt, Aggregate, Fracture	No restrictions. This document is available to the public through NTIS: National Technical Information Service Springfield, Virginia 22161 http://www.ntis.gov

19. Security Classif. (of this report)	20. Security Classif. (of this page)	21. No. of Pages	22. Price
Unclassified	Unclassified	188	

SYSTEM FOR THE EVALUATION OF MOISTURE DAMAGE USING FUNDAMENTAL MATERIAL PROPERTIES

by

Jonathan Howson
Graduate Assistant Research
Texas Transportation Institute

Eyad A. Masad
Associate Research Engineer
Texas Transportation Institute

Amit Bhasin
Associate Research Engineer
Texas Transportation Institute

Veronica Castelo Branco
Graduate Assistant Research
Texas Transportation Institute

Edith Arambula
Graduate Assistant Research
Texas Transportation Institute

Robert Lytton
Senior Research Fellow
Texas Transportation Institute

Dallas Little
Senior Research Fellow
Texas Transportation Institute

Report 0-4524-1
Project Number 0-4524
Project Title: Application of Surface Energy Measurements to Evaluate Moisture Susceptibility of Asphalt and Aggregates

Performed in cooperation with the
Texas Department of Transportation
and the
Federal Highway Administration

March 2007
Published May 2007

TEXAS TRANSPORTATION INSTITUTE
The Texas A&M University System
College Station, Texas 77843-3135

DISCLAIMER

The contents of this report reflect the views of the authors, who are responsible for the facts and the accuracy of the data presented herein. The contents do not necessarily reflect the official view or policies of the Texas Department of Transportation (TxDOT) and/or the Federal Highway Administration (FHWA). This report does not constitute a standard, specification, or regulation. The engineer in charge of the project was Robert L. Lytton, P.E. (Texas # 27657).

ACKNOWLEDGMENTS

The authors wish to express their appreciation to the Texas Department of Transportation personnel for their support throughout this project, as well as the Federal Highway Administration. We would also like to thank the project directors Darren Hazlett and Jerry Peterson, German Claros and the other members of the project monitoring committee for their valuable technical comments during this project.

TABLE OF CONTENTS

Page

List of Figures x
List of Tables xii
CHAPTER 1. INTRODUCTION 1
Background 1
Surface Free Energy 1
pH of Contact Water 2
Objectives 3
Summary 4
CHAPTER 2. EFFECT OF MODIFICATION PROCESSES ON BOND ENERGY OF ASPHALT BINDERS 7
Introduction 7
Background 9
Surface Free Energy 9
Energy Parameters Related to Performance 10
Materials 13
Results 14
Work of Cohesion 14
Parameter *ER* Related to Moisture Sensitivity 18
Summary 24
CHAPTER 3. ANALYSIS OF THE DATA BASE OF ASPHALT BINDER COHESIVE BOND ENERGY AND BINDER-AGGREGATE ADHESIVE BOND ENERGY 27
Introduction 27
Materials 27
Asphalt Binders 27
Results 30
Surface Energy Components 30
Work of Cohesion 35

TABLE OF CONTENTS (Continued)

Page

Energy Ratio 38
Summary 41
CHAPTER 4. THE EFFECT OF pH VALUE ON THE SURFACE FREE ENERGY COMPONENTS OF WATER 43
Introduction 43
Methodology 44
Materials 49
Results and Discussion 50
Summary 53
CHAPTER 5. IMPROVED METHOD FOR DYNAMIC MECHANICAL ANALYSIS AND SPECIMEN PREPARATION 55
Introduction 55
DMA Specimen Preparation 55
Analyzing of Test Data from DMA Samples 57
Theoretical Background for the Analysis of DMA Data 58
Fracture-Based Analysis Approach for Asphalt Mixtures 65
CHAPTER 6. MOISTURE SUSCEPTIBILITY OF ASPHALT MIXTURES WITH KNOWN FIELD PERFORMANCE USING DYNAMIC ANALYSIS AND A CRACK GROWTH MODEL 71
Introduction 71
Objectives and Tasks 73
Description of Mixtures and Field Performance 74
Fracture Model for Moisture Susceptibility 76
Characterization of Asphalt Mixtures and Model Parameters 77
Viscoelastic Parameters 78
Dissipated Pseudo Strain Energy and Reference Modulus Parameters 79
Tensile Strength Parameter 80
Partial Wet Adhesive Bond Surface Energy Parameter 81

TABLE OF CONTENTS (Continued)

Page

Characterization of Asphalt Mastic Specimens and Model Parameters....84
Results....85
Summary....89
CHAPTER 7. RESEARCH SUMMARY....91
Background....91
Surface Energy of Binders and Aggregates....92
Influence of Modifications Made to Asphalt Binders on its Surface Energy....92
Influence of pH of Water on its Surface Energy....94
Dynamic Mechanical Analysis of Fine Aggregate Matrix....94
Framework to Evaluate Moisture Sensitivity of Asphalt Mixtures....94
REFERENCES....97
APPENDIX A. CURRENT SAND ASPHALT MIXTURE DESIGN METHOD....103
APPENDIX B. IMPROVED DESIGN METHOD FOR SAND ASPHALT MIXTURES....111
APPENDIX C. FRACTURE ANALYSIS AND MOISTURE SUSCEPTIBILITY OF ASPHALT MIXTURES....121
APPENDIX D. PROPOSED TEST METHOD TO USE A WILHELMY PLATE DEVICE TO DETERMINE SURFACE ENERGY COMPONENTS OF ASPHALT BINDERS....145
APPENDIX E. PROPOSED TEST METHOD TO USE A SORPTION DEVICE TO DETERMINE SURFACE ENERGY COMPONENTS OF AGGREGATES....157
APPENDIX F. DESCRIPTION OF TEST EQUIPMENT....169

LIST OF FIGURES

Figure **Page**

2.1 Effect of Manufacturer Modifiers and Additives on Cohesive Bond Strength of Asphalt Binder from Source A 16

2.2 Effect of Manufacturer Modifiers and Aging on Cohesive Bond Strength of Asphalt Binder from Source B 17

2.3 Effect of Manufacturer Modifiers and Aging on Cohesive Bond Strength of Asphalt Binder from Source C....17

2.4 Effect of Manufacturer Modifiers and Additives on *ER* of Asphalt Binder from Source A with Sandstone Aggregate 20

2.5 Effect of Manufacturer Modifiers and Additives on *ER* of Asphalt Binder from Source A with Granite Aggregate....20

2.6 Effect of Manufacturer Modifiers and Aging on *ER* of Asphalt Binder from Source B with Sandstone Aggregate 21

2.7 Effect of Manufacturer Modifiers and Aging on *ER* of Asphalt Binder from Source B with Granite Aggregate 22

2.8 Effect of Manufacturer Modifiers and Aging on *ER* of Asphalt Binder from Source C with Sandstone Aggregate....22

2.9 Effect of Manufacturer Modifiers and Aging on *ER* of Asphalt Binder from Source C with Granite Aggregate 23

3.1 Quartiles of the Lifshitz-van der Waals Component of all Unaged Binders....31

3.2 Quartiles of the Acid Component of all Unaged Binders 31

3.3 Quartiles of the Base Component of all Unaged Binders 32

3.4 Quartiles of Cohesive Bond Energy of all Unaged Binders 35

3.5 Quartiles of the Energy Ratio of all Unaged Binders 38

4.1 Influence of Aggregate Type on pH of the Contacting Water (after Yoon and Tarrer 1989)....44

4.2 Surface Tension versus Pendant Volume (Sessile Drop) 46

LIST OF FIGURES (Continued)

Figure **Page**

4.3 Graph of Surface Free Energy Components of Water Modified with Different Aggregates 52
5.1 DMA Sample Fabrication Methodologies 57
5.2 Illustrations of the Different Possible Responses of Stress-Pseudo Strain Relationships 61
5.3 Illustration of the Idealized Hysteresis Loop and Actual Hysteresis Loop 64
6.1 Aggregate Gradations 75
6.2 Failed Specimens after Tensile Strength Test (a) Wet Specimens Showing Stripping and (b) Dry Specimens Showing Well-Coated Aggregates 81
6.3 Normalized Crack Growth Parameter for Each Mixture Type (a) Mixture A, (b) Mixture B, and (c) Mixture C 87
6.4 Normalized Crack Growth Parameter for the Asphalt Mastic Fraction of Each Mixture Type (a) Mixture A, (b) Mixture B, and (c) Mixture C 88
6.5 Adhesive Bond Energy Ratio versus the Asphalt Mixture Crack Growth Index Ratio 89
7.1 Framework to Select Mixtures Resistant to Moisture Damage 96

LIST OF TABLES

Table		Page
2.1	Matrix of Asphalt Binders Tested for Surface Free Energies	13
3.1	Typical Magnitudes of Surface Free Energy Components (after Little and Bhasin 2006)	28
3.2	A List of Asphalt Binders Used in this Project	29
3.3	Aggregate Surface Free Energy Components (ergs/cm^2)	30
3.4	Surface Free Energy Components due to Addition of Anti-Strip Agents	32
3.5	Surface Free Energy Components of Asphalt Binders before and after Aging	34
3.6	Percent Change in Cohesive Bond Energy due to Addition of Anti-Strip Agents	36
3.7	Percent Change in Cohesive Bond Energy due to Aging of the Asphalt Binder	37
3.8	Percent Change in the Energy Ratio due to Addition of Anti-Strip Agents	39
3.9	Percent Change in the Energy Ratio due to Aging of the Asphalt Binder	40
4.1	Asphalt Surface Free Energy Components	49
4.2	Aggregate Label and Type	50
4.3	Surface Tensions of Water with Different Aggregates Measured Using Sessile Drop Method	50
4.4	Surface Free Energy Components of Water Modified with Different Aggregates in ergs/cm^2	52
6.1	Mixture Descriptions (Lytton et al. [2005]	74
6.2	Adhesive Bond Energy under Dry and Wet Conditions	82
6.3	Weighted Average for the Adhesive Bond Energy under Dry and Wet Conditions	83

LIST OF TABLES (Continued)

Table **Page**

6.4 Average Surface Energy and Mechanical Tests Parameter Results 85
6.5 Average Crack Growth Parameters and Coefficients of Variation.....86
7.1 Preliminary Recommendation of Values to be Used with Decision Tree Shown in Figure 7.1.....95

CHAPTER 1
INTRODUCTION

BACKGROUND

Surface Free Energy

Moisture damage in asphalt mixtures has been a major problem for state and federal highway agencies for many years as is evidenced by the increasing budget needs for maintenance and rehabilitation. In order to reduce these needs, it is necessary to understand the mechanisms causing moisture damage and, consequently, to know how to select materials in an asphalt mixture with good resistance to moisture damage.

Taylor and Khosla (1983), Kiggundu and Roberts (1988), and Terrel and Al-Swalilmi (1994) refer to at least five different mechanisms which contribute to moisture damage in asphalt pavements: detachment, displacement, hydraulic scour, pore pressure, and spontaneous emulsification. Kiggundu and Roberts (1988) suggest that pH instability and the effects of the environment or climate on asphalt-aggregate matrices are additional mechanisms that can contribute to moisture damage.

Schapery (1984) proposed a basic viscoelastic fracture theory, which was derived from first principles of materials science and based on an energy balance. This theory states that the load-induced energy that causes fracture damage is balanced by the energy stored on newly formed crack faces. The energy imparted to the system can be quantified as a product of two properties of the materials in question: tensile creep compliance over the time of loading and the dissipated pseudo-strain energy per unit of crack area produced from one tensile load to the next. The energy stored on fracture faces can be quantified by surface free energy measurements of the material.

A logical extension can be made from understanding adhesive fracture based on surface free energy to understanding the debonding process between asphalt binder and aggregates in the presence of moisture. Cheng et al. (2002) presented a detailed methodology to measure the surface free energy components of asphalt using the Wilhelmy Plate method and the surface free energy components of aggregates using the Universal Sorption Device. They then show how to compute the adhesive bond strength between the

asphalt binder and the aggregate both dry and in the presence of water (third medium). Cheng et al. (2002) further point out that the affinity of the aggregates for water is far greater than it is for the asphalt binder. This means if the water has access to the aggregate surface, it is likely to replace (strip) the asphalt binder with the rate of replacement being a function of the aggregate-asphalt bond strength in the presence of water.

pH of Contact Water

Hughes et al. (1960) and Scott (1982) reported that adhesion between asphalt cement and aggregate in the presence of water became weakened when the pH of the buffer solution was increased from 7.0 to 9.0. Later, Yoon and Tarrer (1989) showed that if different aggregate powders (chert gravel, quartz sand, quartz gravel, granite, limestone, and dolomite) were added to water, the pH of the water would increase. After about 30 minutes, the pH of the water-aggregate blend reached a steady asymptotic value.

Yoon and Tarrer (1989) performed boiling stripping tests to assess the sensitivity of stripping to changes in the pH of water in contact with the aggregate surface. The pH of the water was modified by using a solution of HCl or NaOH. The stripping became more severe as the pH was increased. Yoon and Tarrer (1989) explain that when an aggregate is being coated with asphalt, the aggregate selectively adsorbs some components of the asphalt. The type and quantities of the adsorbed components affect the degree of adhesion. The asphalt-aggregate bond is affected by aggregate mineralogy, adsorbed cations on the aggregate surface, and the surface texture and porosity of the aggregate. Favorable chemical bonding between asphalt and aggregate alone will not optimize the adhesive bond and minimize moisture damage. The bond is partly physical, and therefore, the asphalt must be able to wet and permeate the aggregate surface. This process is dependent on the asphalt rheology at mixing temperature and nature of the aggregate surface, pore size, pore shape, as well as aggregate mineralogy. Furthermore, the ability to bond asphalt to aggregate is dynamic and changes with time. Much of this effect is caused by a shift in pH at the aggregate-water interface that can be triggered by dissociation of the aggregate minerals near the surface and/or by the nature of the pore water.

OBJECTIVES

The main objective of this project is to understand the moisture damage process by carefully considering the micro-mechanisms that influence the adhesive interface between aggregate and asphalt and the cohesive strength and durability of the mastic. This objective is achieved by dividing this project into two main phases. The first phase of the project focused on the validation of the surface free energy measurements and the dynamic mechanical analysis (DMA) of the fine portion of the mix through the evaluation of the moisture susceptibility of materials with known field performance. TxDOT Report 0-4524-2 documented the results of the first phase of this project. The second phase of the project, which is documented in this report, focused on the evaluation of the surface free energy and moisture susceptibility of a wide range of combinations of aggregates and asphalts. The objective of the second phase was achieved by conducting the following tasks:

- Examine the influence of liquid anti-strip agents on the surface free energy of asphalt binders, the cohesive bond energy within the asphalt binder, and the adhesive bond energy of asphalt-aggregate combinations.
- Study the effect of binder aging and modification of the binder by the supplier on surface free energy.
- Catalog surface free energy properties of commonly used aggregates in Texas.
- Catalog surface free energy of commonly used asphalt binders in Texas
- Develop testing protocols for the evaluation of surface free energy of binders and aggregates.
- Develop testing protocols for the evaluation of asphalt mixture resistance to moisture damage.
- Provide specifications for the equipment that can be used for measuring the surface free energy of asphalt binder and aggregates.

SUMMARY

This report includes six chapters and six appendices. Chapter 1 of the report includes a short background of the theory and techniques used, the main objectives of the report and how they were accomplished, and a brief summary of the report chapters.

Chapter 2 of the report discusses the effect of modification processes on bond energy of asphalt binders. This chapter explains how the cohesive bond energy and energy ratio of different asphalt binders and asphalt-aggregate combinations, respectively, change due to the addition of anti-strip agents, manufacturer modifications, and aging of the asphalt binder.

Chapter 3 includes the surface free energy properties of 16 binders from different sources and 11 aggregates used in the state of Texas. A statistical analysis was conducted to determine the influence of various modifications: addition of polymer, addition of liquid anti-strip agents, and aging on the surface free energy components of the asphalt binders.

Chapter 4 of this report documents how the surface free energy of water is affected by changes in its pH. In this project the pH of four water samples were altered by submerging a given amount of aggregate in each respective water sample. After the water-aggregate sample reached a pH equilibrium, the total surface tension and surface free energy components of the water were measured. The total surface tension and surface free energy components of the reference distilled water at a neutral pH were also measured.

Chapter 5 discusses the two current methods used for preparing DMA specimens and proposes a new method for the design of DMA specimens. Also included in this chapter is the procedure and equations used to analyze the data collected from testing a DMA specimen.

Chapter 6 is an evaluation of the moisture susceptibility of asphalt mixtures with known field performance using dynamic analysis and a crack growth model to characterize both the asphalt mixtures and corresponding fine portion of the asphalt mix. The model parameters used in the project were obtained from surface free energy measurements, uniaxial dynamic testing of the asphalt mixtures, and dynamic shear testing for the asphalt mastics. The results showed good differentiation between the moisture conditioned (wet) and unconditioned (dry) specimen behavior and provided a good correlation with the reported field performance of the asphalt mixtures.

There are six appendices contained in this report. Appendix A contains the design procedure used in this project for the preparation of DMA specimens, while Appendix B describes a new mix design procedure for the preparation of DMA specimens where the volume of asphalt used is based on the surface area of the aggregates. An example of the design procedure is included in each of the appendices. Appendix C contains an overview of the method for the evaluation of the moisture susceptibility of asphalt mixtures. The method includes description of the theory, test apparatus, and data analysis. Appendix D contains the proposed test method for using the Wilhelmy Plate device to determine the surface free energy components of asphalt binders. Appendix E contains the proposed test method to use a sorption device to determine the surface free energy components of aggregates. Appendix F contains the specifications for the equipment purchased or used during this project. This includes specifications for the DMA machine, universal sorption device (USD), and the Wilhelmy Plate device.

CHAPTER 2
EFFECT OF MODIFICATION PROCESSES ON BOND ENERGY OF ASPHALT BINDERS

INTRODUCTION

Fatigue cracking and moisture induced damage are major forms of distresses in asphalt pavements. An important material property that influences fatigue cracking and moisture sensitivity of asphalt mixes is the surface free energy of the asphalt binder and the aggregate. Surface free energy of asphalt binders and aggregates is used to compute various energy parameters such as the cohesive bond energy of the asphalt binder, the adhesive bond energy between the asphalt binder and the aggregate in dry condition, and the energy potential for water to displace the asphalt binder from the surface of the aggregate. A combination of one or more of these energy parameters is related to the resistance of the asphalt mix to fatigue cracking and moisture induced damage.

Griffith (1921) demonstrated that the minimum amount of work required for a crack to propagate in an elastic material is a function of its surface free energy (numerically equal to the surface tension). Schapery (1984) used a similar energy balance approach to extend the fundamental principles of crack growth to viscoelastic materials. An important material property to determine the work required for a crack to propagate within a material using the energy balance approach is the cohesive bond energy of that specific material. Cohesive bond energy of a material is defined as the amount of work required to fracture the material to create two new surfaces of unit area each. Numerically, this amount is equal to twice the total surface free energy of the material. Masad et al. (2006) and Little and Bhasin (2006) demonstrated the use of cohesive bond energy of asphalt binders to predict the fatigue cracking characteristics for asphalt mastics and mixes.

Loss of durability of an asphalt mixture due to the action of water depends on the adhesive bond strength between the asphalt binder and the aggregate in dry condition and the magnitude of reduction in free energy when asphalt binder debonds from the aggregate surface in the presence of water. These two properties can be quantified using the surface free energy of these materials. Cheng (2002) correlated the magnitude of reduction in free

energy during debonding in the presence of water to the moisture sensitivity of asphalt mixtures. Several other studies also demonstrated a good correlation between parameters determined using the surface free energy components of asphalt binders and aggregates to the moisture sensitivity of asphalt mixtures (Little and Bhasin [2006] and Bhasin and Masad [2006]). These correlations were made based on the performance of asphalt mixtures in the field and in the laboratory.

Most of the previous work related to the application of surface free energy to predict performance of asphalt mixtures is based on neat asphalt binders. A pertinent question that has arisen from these studies regards the effect of modifications to the asphalt binder on its surface free energy and, consequently, on the predicted performance. The term *modification* is used to imply the different natural and/or engineering processes that asphalt binders are subjected to during production and in service. The modifications that were addressed in this project are:

- Made by the manufacturer to achieve a certain performance grade (PG) in accordance with the Superpave specifications. The original PG grade asphalt binder is referred to as the base asphalt.
- Made by materials and/or design engineers to improve the performance of the asphalt mixture. A typical example of this is the addition of liquid anti-strip agents to improve moisture resistance of the asphalt mixture. These modifications can be made to either a base asphalt binder or an asphalt binder that is already modified by the manufacturer.
- Caused by environmental effects. An example of this modification is oxidative aging, which significantly alters the chemistry of the binder and, consequently, its mechanical properties.

The objective of this project was to evaluate the effect of the aforementioned three types of modification on the surface free energy of asphalt binders. Comparison of differences in the surface free energies of the asphalt binders due to modification is of little value by itself. It is more important to investigate the differences in the

performance-related energy parameters due to the modifications made to the asphalt binders. This chapter includes three sections:

- background and description of the energy parameters related to the performance of the asphalt mixes,
- brief description of the test method and materials used in this project, and
- comparison of the changes in the energy parameters due to modifications made to the asphalt binders and its implication on the performance of asphalt mixtures.

BACKGROUND

The overall performance of an asphalt mixture depends on the combined positive or negative impact of several different material properties such as bond energy within the mixture, viscoelasticity of the asphalt binder, and internal structure distribution. A continuum mechanics-based, comprehensive materials characterization model can determine the interactive effects of these properties on the performance of the mixture (Little and Bhasin [2006] and Masad et al. [2006]). Previous research studies have shown that bond energy is an important material property that is an integral part of these models and has significant impact on performance (Little and Bhasin [2006] and Masad et al. [2006]). Consequently, the focus of this project will be on using parameters formulated based on bond energy to estimate the positive or negative impact of different types of modifications to the asphalt binder. For brevity, the term *energy parameters* will be used in this chapter to describe the parameters that are computed using the surface free energy components of materials. These parameters have been shown to have a very good correlation with the performance of asphalt mixtures (Little and Bhasin [2006] and Masad et al. [2006]).

Surface Free Energy

Surface free energy of a material is defined as the amount of work required to create a unit area of a new surface of that specific material in a vacuum. The Good-van Oss-Chaudhury theory (van Oss [1994]), also referred to as the acid-base theory, provides a popular and well-accepted explanation of the source and classification of surface free

energy of materials. According to this theory, the surface free energy of a material is divided into three separate components based on the source of the intermolecular forces. These components are the:

- monopolar acidic, γ^+;
- monopolar basic, γ^-; and
- apolar, or Lifshitz-van der Waals (LW), γ^{LW} component. The total surface free energy of a material, γ^{Total}, is obtained from the three components as shown in Equation 2.1.

$$\gamma^{Total} = \gamma^{LW} + 2\sqrt{\gamma^+\gamma^-} \tag{2.1}$$

This theory was used as the basis for all underlying computations to determine the surface free energy of the asphalt binders and energy parameters that are related to the performance of the asphalt mixtures.

Energy Parameters Related to Performance

Schapery's theory of damage in viscoelastic materials was used to develop equations that model the growth of fatigue cracks in asphalt mastics using fundamental properties of its constituent materials (Masad et al. [2006], and Masad et al. [2006]). One of these material properties is the fracture energy, ΔG_f. A very simple definition of fracture energy is the amount of work that must be supplied to a material for a crack to propagate and create two new surfaces of unit area each.

Theoretically, the fracture energy derives from surface free energy of the material and is related to fracture toughness or strain energy release rate calculated from mechanical tests on specimens. However, in addition to surface energy, the mechanical measurement of fracture introduces factors such as heat dissipation, acoustic emissions, and plastic deformation. There is also a difference in the scale at which energy is calculated from mechanical tests versus fracture energy calculated from surface energy measurements. A nominal surface area at the macro scale is typically used in the mechanical tests, while the true crack area of propagating micro cracks can be several times higher.

A higher magnitude of cohesive bond energy implies that more energy is required for the crack to propagate due to fracture. The cohesive bond energy of asphalt binders is computed using its surface free energy components and is shown in Equation 2.2:

$$\Delta G_{coh} = 2\gamma^{Total} = 2\left(\gamma^{LW} + 2\sqrt{\gamma^{+}\gamma^{-}}\right) \quad (2.2)$$

The effect of various modifications on cohesive bond energy of selected asphalt binders and the implications of this effect are discussed later in this report.

Little and Bhasin (2006) reported four different energy parameters that were correlated to the moisture sensitivity of asphalt mixtures. These parameters were computed using the surface free energy components of materials used in the asphalt mixtures. All four parameters were developed using similar hypotheses and demonstrated similar trends with the moisture sensitivity of asphalt mixtures. One of these four parameters was used in this project to assess the change in moisture sensitivity of asphalt mixtures due to the modifications made to the asphalt binders. This parameter is a function of the surface free energy components of water, the asphalt binder and the aggregate and is expressed as:

$$ER = \left| \frac{W_{AS} - W_{AA}}{W_{ASW}} \right| \quad (2.3)$$

In Equation 2.3, the terms W_{AS}, W_{AA}, and W_{ASW} represent the work of adhesion between the asphalt binder and the aggregate, work of cohesion of the asphalt binder, and work of debonding when water displaces asphalt binder from its interface with the aggregate. A higher value of W_{AS} indicates that more work is required to break the adhesive bond between the asphalt binder and the aggregate and, hence, implies better resistance to moisture damage. A lower magnitude of W_{ASW} indicates a lower energy potential for water to displace asphalt binder from its interface with the aggregate and, hence, a higher resistance to moisture damage. The use of $W_{AS} - W_{AA}$ in Equation 2.3 provided a more reliable index of successful performance. The parameter, Energy Ratio (ER), is easily computed for any combination of asphalt binder and

aggregate if their respective surface free energy components are known from Equations 2.4-2.6.

$$W_{AS} = 2\sqrt{\gamma_A^{LW}\gamma_S^{LW}} + 2\sqrt{\gamma_A^{+}\gamma_S^{-}} + 2\sqrt{\gamma_A^{-}\gamma_S^{+}} \quad (2.4)$$

$$W_{AA} = 2\left(\gamma_A^{LW} + 2\sqrt{\gamma_A^{+}\gamma_A^{-}}\right) \quad (2.5)$$

$$W_{ASW}^{wet} = \gamma_{AW} + \gamma_{SW} - \gamma_{AS} \quad (2.6)$$

In Equations 2.4 – 2.6, the subscripts A, S, and W represent the asphalt binder, aggregate (stone), and water, respectively. On the right-hand side of Equation 2.7, γ_{ij} represents the energy of the interface between any two materials "i" and "j" and are computed from their surface free energy components as follows:

$$\gamma_{ij} = \gamma_i + \gamma_j - 2\sqrt{\gamma_i^{LW}\gamma_j^{LW}} - 2\sqrt{\gamma_i^{+}\gamma_j^{-}} - 2\sqrt{\gamma_i^{-}\gamma_j^{+}} \quad (2.7)$$

Note that the parameter ER is a function of the surface free energy components of both the asphalt binder and the aggregate. In this project, only the effect of modifications on the surface free energy of asphalt binders was investigated. Therefore, in order to demonstrate the effect of these modifications on the parameter ER, two aggregates—sandstone and granite—were carefully selected to represent a range of different surface energy components typically encountered with aggregates.

In summary, the work of cohesion and the parameter ER were identified as two energy parameters that are related to the performance of asphalt mixtures based on previous research that establishes the correlations between these parameters and mixture performance. These parameters can be computed using the surface free energy components of the asphalt binder and aggregate. The effect of various types of modifications made to the asphalt binders on these two parameters and, consequently, on the performance of asphalt mixtures are presented in the following sections of this report.

MATERIALS

Table 2.1 displays the matrix of base asphalt binders and their modified forms. This project included three base asphalt binders from three different sources, labeled as A, B, and C. Each manufacturer modified its respective base asphalt binder to produce a total of seven modified asphalt binders. These modifications were achieved by using additives to the base asphalt binder. The additives included materials such as styrene-butadiene-styrene (SBS) and tire rubber (TRS). The exact nature, amount, and process of modification varied from one manufacturer to another; the details of which were not known to the authors.

The base and manufacturer-modified asphalt binders from sources B and C were used to evaluate the effect of aging on their surface free energy and concomitant energy parameters. Two aging methods were used in this project. The first type was the stirred air-flow test (SAFT), and the second type was the pressurized aging vessel (PAV). According to the literature, SAFT is a suitable simulation of short-term aging, especially for polymer modified asphalt binders (Vassiliev et al. 2001). PAV simulates long-term aging, representing about 5 to 10 years of aging in asphalt pavements.

Table 2.1. Matrix of Asphalt Binders Tested for Surface Free Energies.

Source	**Asphalt A**			**Asphalt B**				**Asphalt C**		
PG Grade and Modifier	**64-22 B**	**70-22 S**	**76-22 S**	**64-22 B**	**70-22 S**	**76-22 TRS**	**76-22 S**	**64-22 B**	**70-22 S**	**76-22 TRS**
Unaged Binder	■	■	■	■	■	■	■	■	■	■
SAFT Aging				■	■	■	■	■	■	■
PAV Aging				■	■	■	■	■	■	■
Anti-strip agent 1	■	■	■							
Anti-strip agent 2	■	■	■							

Note: Descriptions provided by binder suppliers: B = Base asphalt binder; S = SBS modifier; TRS = Tire rubber & SBS modifiers.

■ Indicates surface energy measurements were made on that specific binder.

The base and manufacturer-modified asphalt binders from source A were used to evaluate the effect of liquid anti-strip agents on their surface free energy components. Two different types of liquid anti-strip agents, commonly used by the TxDOT in various field mixtures, were included in this project. The manufacturer's recommended amount of anti-strip agent was added to the asphalt binder.

The asphalt binders are labeled by the source followed by the PG grade followed by the type of modifier. For example, binder A 64-22 B indicates source A, PG 64-22 binder, and a base (B) or unmodified binder. A binder with the label A 70-22 S indicates source A, grade PG 70-22, and modified using SBS. As discussed earlier, the binder surface energy was used to calculate the work of cohesion using Equation 2.2; however, the *ER* in Equation 2.3 requires the use of surface free energy components of both the asphalt binder and the aggregate. For this purpose, two carefully selected aggregates with known surface energies, sandstone $\left(\gamma^{LW} = 63, \gamma^{+} = 2, \gamma^{-} = 223 \text{ ergs/cm}^2\right)$ and granite $\left(\gamma^{LW} = 56, \gamma^{+} = 43, \gamma^{-} = 783 \text{ ergs/cm}^2\right)$ were used (Masad et al. [2006]).

The Wilhelmy Plate device was used in this project to measure contact angles of the asphalt binder with five probe liquids (water, glycerol, ethylene glycol, formamide, and diiodomethane). The contact angles were then used to compute the three surface free energy components of the asphalt binder. Details of the test method and the analysis technique that were used are documented in the appendices to this report. The surface energy components of various asphalt binders obtained from these measurements were in the same range as those reported in other independent studies (Little and Bhasin [2006], and Wasiuddin et al. [2006]).

RESULTS

Work of Cohesion

Effect of Modifications Made by Manufacturer

The first bar from each stack within each figure (Figures 2.1–2.3) is compared to evaluate the effect of modifications made by the manufacturer on the work of cohesion of unaged binders without additives. In all cases, the work of cohesion increased for the modified asphalt binders when compared to their respective base or unmodified asphalt binder. The only exception to this was asphalt binder A 70-22 S from source A. For this

particular asphalt binder, the work of cohesion dropped slightly as compared to the unmodified asphalt binder. Furthermore, the magnitude of change in the work of cohesion, although not very significant in most cases, depended on the type of modification to the base or unmodified asphalt binder. An increase in the work of cohesion indicates that more work is required for a crack to propagate within the asphalt binder. Modifications to the unmodified asphalt binder also resulted in an increase of the PG grade. Increase in the PG grade together with an increase in the work of cohesion for the modified binders indicates an overall improvement in the fracture resistance due to the modification of the base asphalt binder.

Effect of Additives

Figure 2.1 illustrates the effect of liquid anti-strip agents on the work of cohesion of the binders. For the unmodified asphalt binder, the work of cohesion did not change significantly due to the addition of liquid anti-strip agents. For the two manufacturer modified asphalt binders (A 70-22 S and A 76-22 S), the work of cohesion dropped by varying amounts upon the addition of the liquid anti-strip agent as compared to the respective binders without the additive. A reduction in the work of cohesion implies that less external work is required for a crack to propagate. However, it also implies a reduction in the surface free energy of the asphalt binder, which enables better coating of the aggregate surface by the binder and improved overall interfacial adhesion. Therefore, a reduction in the work of cohesion due to the addition of liquid anti-strip agents can be indirectly related to improved overall fracture resistance of the asphalt binder aggregate matrix. Furthermore, according to the literature, better adhesion between a polymer phase (such as the asphalt binder) and filler particles (such as aggregate fines) improves the fracture resistance of the matrix (Lucic et al., 1998). Better adhesion also improves moisture resistance of the mixture which will be discussed in a later section using the parameter *ER*.

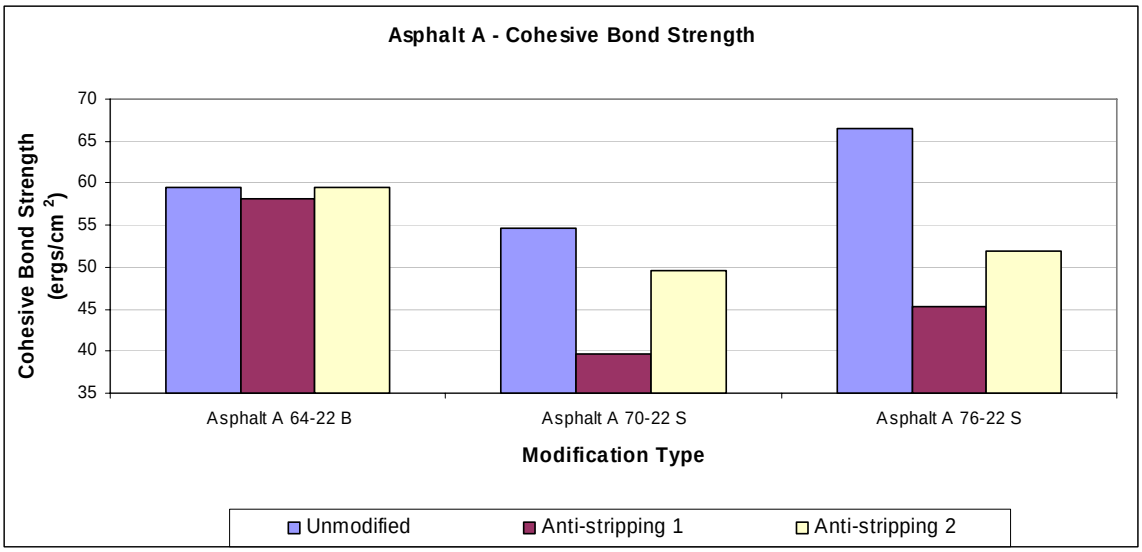

Figure 2.1. Effect of Manufacturer Modifiers and Additives on Cohesive Bond Strength of Asphalt Binder from Source A.

Effect of Aging

Figures 2.2 and 2.3 illustrate the effect of aging on the work of cohesion of unmodified and manufacturer modified asphalt binders. For the unmodified asphalt binder from source B (Figure 2.2), short-term aging using SAFT caused the work of cohesion to decrease by a small magnitude compared to the unaged unmodified binder. Manufacturer modified asphalt binders from this source showed very little variation in the work of cohesion due to short-term aging. However, upon long-term aging, the work of cohesion increased for the unmodified and B 76-22 S modified asphalt binders and decreased for the B 70-22 S and B 76-22 TRS modified binders. For the asphalt binders from source C (Figure 2.3), both the short-term and long-term aging caused the work of cohesion to decrease consistently for all the binders.

A decrease in the work of cohesion implies that less work is required for a crack to propagate and cause fracture. According to the literature, long-term aging of asphalt binders typically leads to the deterioration of its fracture properties (Walubita et al. [2005]). Therefore, a reduction in work of cohesion due to long-term aging, as observed for five of the eight asphalt binders, corroborates well with this experience. The two anomalies to this were the unmodified and modified asphalt binders (B 76-22 S) from source B (Figure 2.2).

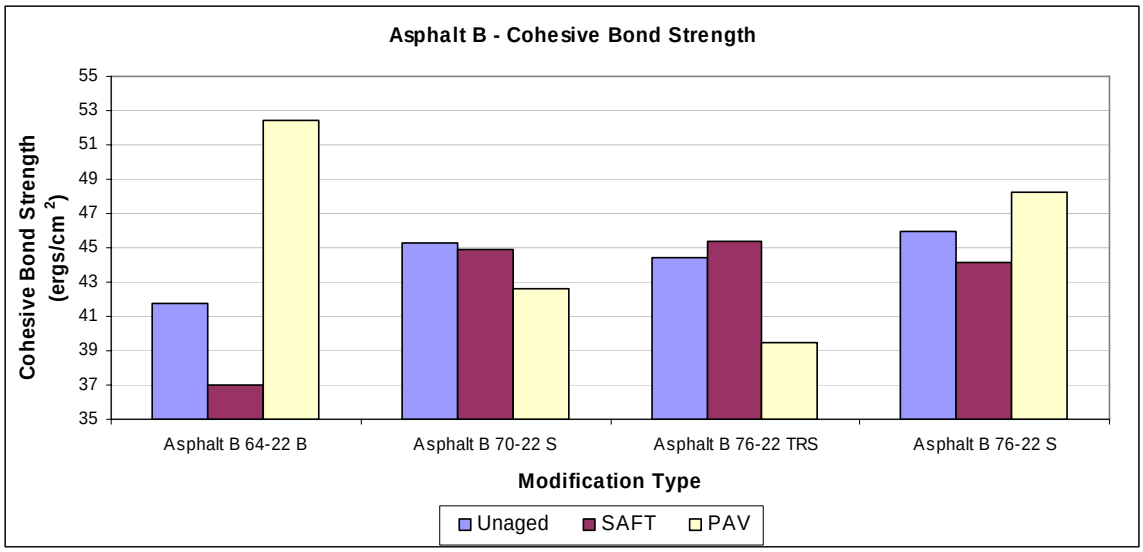

Figure 2.2. Effect of Manufacturer Modifiers and Aging on Cohesive Bond Strength of Asphalt Binder from Source B.

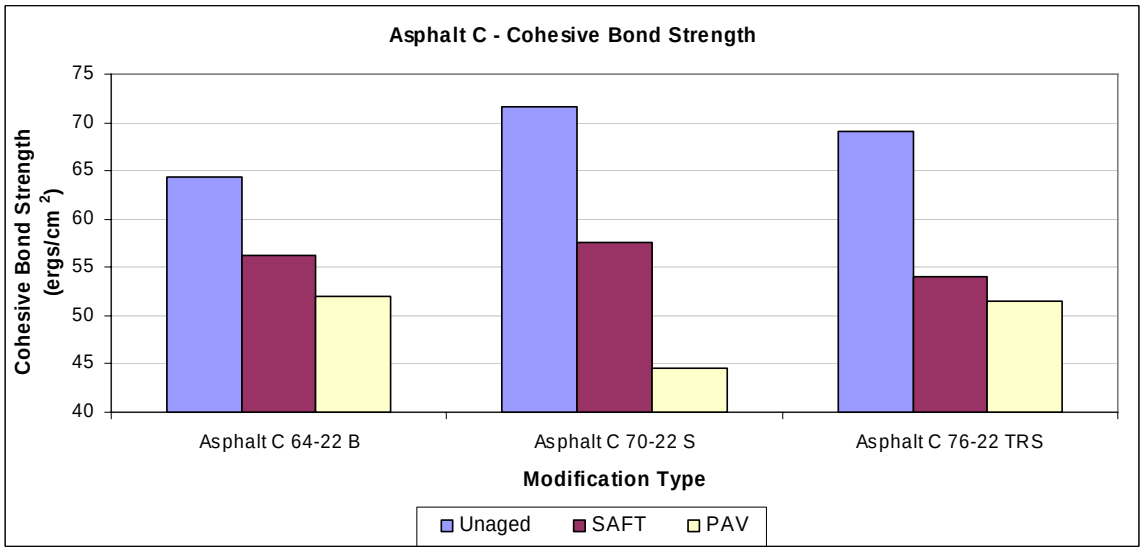

Figure 2.3. Effect of Manufacturer Modifiers and Aging on Cohesive Bond Strength of Asphalt Binder from Source C.

In both cases, the improvement in the work of cohesion was due to the increase in the LW component of surface free energy. Furthermore, according to the literature, the effect of aging on the chemistry and rheology of modified binders depends on the nature of the base bitumen and characteristics of the polymers (Lu and Isacsson [2000]).

An important distinction must be made between the reduction in work of cohesion due to addition of additives such as the liquid anti-strip agents and the reduction in work of cohesion due to aging. The former modification occurs during the mixing and compaction process and can improve properties of the asphalt binder and aggregate fines matrix due to better coating. Whereas, the latter modification occurs in situ after the asphalt mixture is put in place and, therefore, cannot provide the same benefit of better coating as in the previous case.

Parameter *ER* Related to Moisture Sensitivity

Effect of Modifications Made by Manufacturer

Comparison of the first bar from each stack within each figure (Figures 2.4–2.9) provides information about the change in *ER* due to modifications made to the base asphalt binder by the manufacturer. A higher value of *ER* is desirable for better resistance to moisture damage. From these results, it appears that the addition of SBS to the base asphalt binder (producing asphalt binders with suffix S) typically caused little change in the magnitude of *ER* for binder (Figures 2.6 and 2.7). The influence of SBS on binder C was very small for the unaged binder; however, the benefit of the SBS modification in binder C is very clear for the aged binders (Figures 2.8 and 2.9). Addition of TRS, as in the case of asphalt binder from source B, resulted in a significant percentage increase in the *ER* with both aggregates indicating an improvement in the moisture resistance. Further examination of the surface free energy components of the binders revealed that addition of TRS increased the acid component of surface free energy compared to the base asphalt binder. Since most aggregates have a very high base component of surface free energy, it is easy to see from Equation 2.4 that an increase in the acid component of the asphalt binder will cause the adhesive bond strength with the aggregates to increase and improve the resistance to moisture damage.

As discussed earlier, the energy ratio is only a performance indicator and not a comprehensive performance prediction model. Researchers base the latter on analytical modeling of performance using various material and mixture properties such as viscoelasticity of the binder and surface free energy. The addition of polymers to asphalt binders can significantly alter its viscoelastic properties, and therefore, a more detailed analysis is required to evaluate the effect of these modifications on the moisture resistance of the mixture.

Effect of Additives

Liquid anti-strip agents are frequently added to asphalt mixtures to improve their resistance to moisture damage. Figures 2.4 and 2.5 illustrate the change in the magnitude of *ER* and, consequently, the moisture sensitivity of the asphalt mixtures due to addition of liquid anti-strip agents from two different sources. Addition of liquid anti-strip agents to the asphalt binder either decreased or did not significantly change the moisture sensitivity of the mixture. The effect of the anti-strip agent depended on the source of this material and the type of asphalt binder. For example, use of anti-strip agent 1 with the asphalt binder A 70-22 S resulted in an improvement in the moisture resistance with granite aggregate (Figure 2.5), whereas the use of anti-strip agent 2 with the same asphalt binder and aggregate resulted in a small decrease in the moisture resistance. Differences in the efficiency of the liquid anti-strip agents when used with different asphalt binders and aggregates are well-documented in the literature (Western Research Institute [2006]).

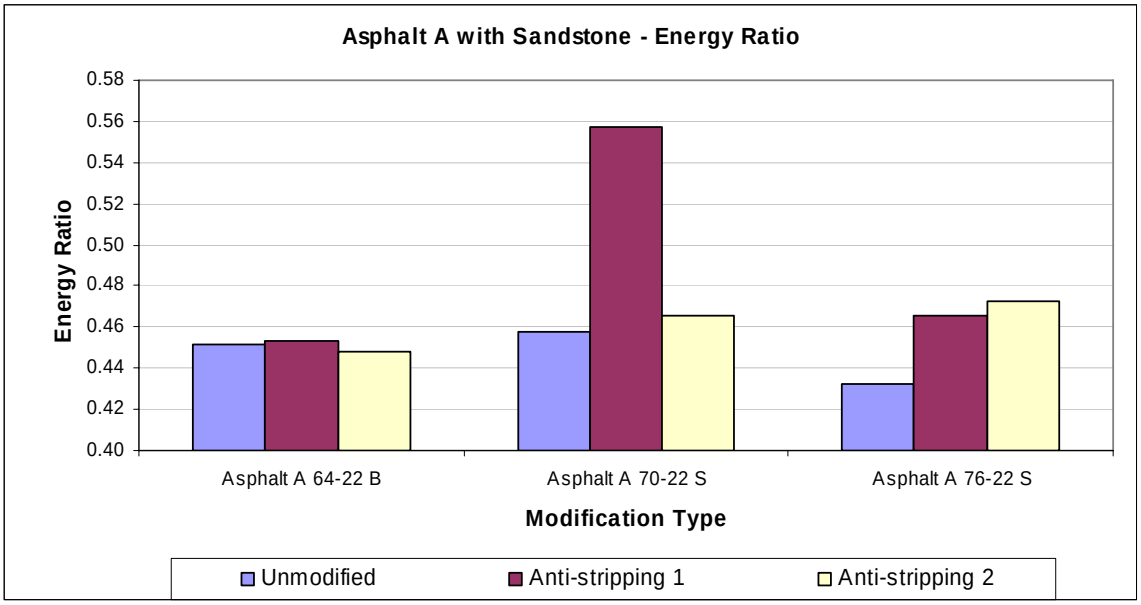

Figure 2.4. Effect of Manufacturer Modifiers and Additives on *ER* of Asphalt Binder from Source A with Sandstone Aggregate.

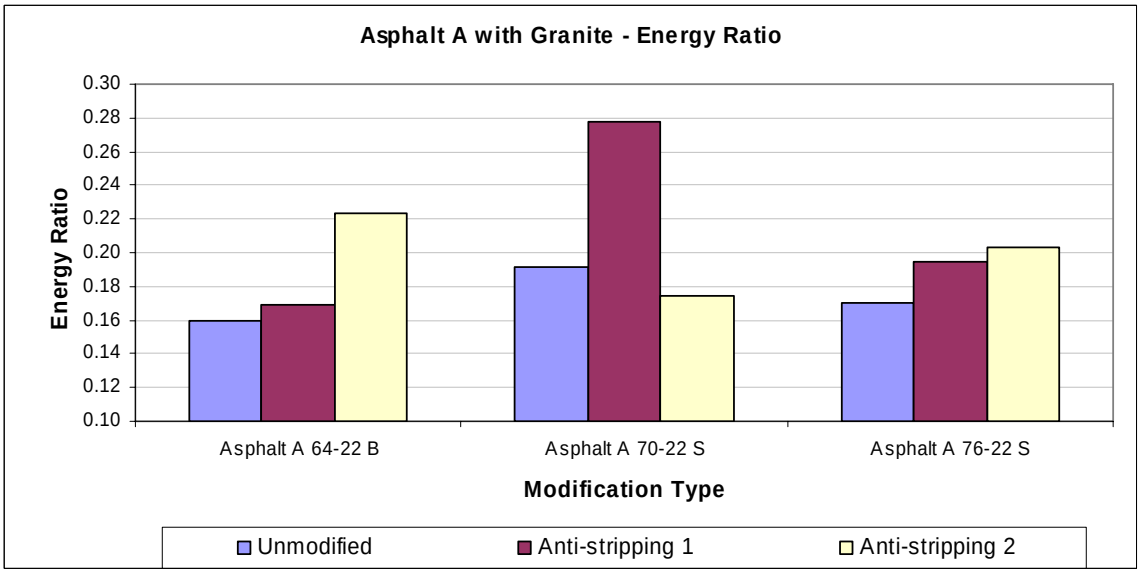

Figure 2.5. Effect of Manufacturer Modifiers and Additives on *ER* of Asphalt Binder from Source A with Granite Aggregate.

Effect of Aging

Figures 2.6 through 2.9 demonstrate the effect of short-term and long-term aging on the moisture resistance of the asphalt binder when combined with the sandstone and granite aggregates based on the magnitude of *ER*. Both an increase and a decrease in the magnitude of *ER*, and hence, moisture sensitivity of the mixture was observed due to short-term aging of asphalt binders from source B. The effect of short-term aging on binder from this source depended on the manufacturer-based modification as well as the type of aggregate used. For example, short-term aging of the asphalt binder B 70-22 S resulted in a small increase in the value of *ER* when combined with the sandstone aggregate (Figure 2.6). However, no change in this value was observed when the aged binder was combined with the granite aggregate (Figure 2.7). Short-term aging of the asphalt binders from source C demonstrated a consistent increase in the magnitude of *ER* (Figures 2.8 and 2.9).

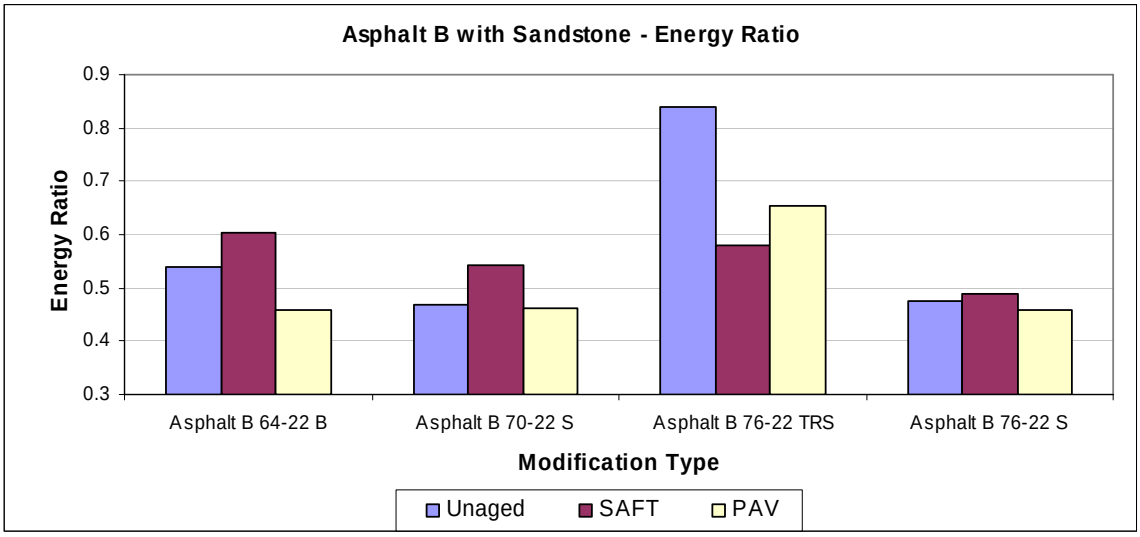

Figure 2.6. Effect of Manufacturer Modifiers and Aging on *ER* of Asphalt Binder from Source B with Sandstone Aggregate.

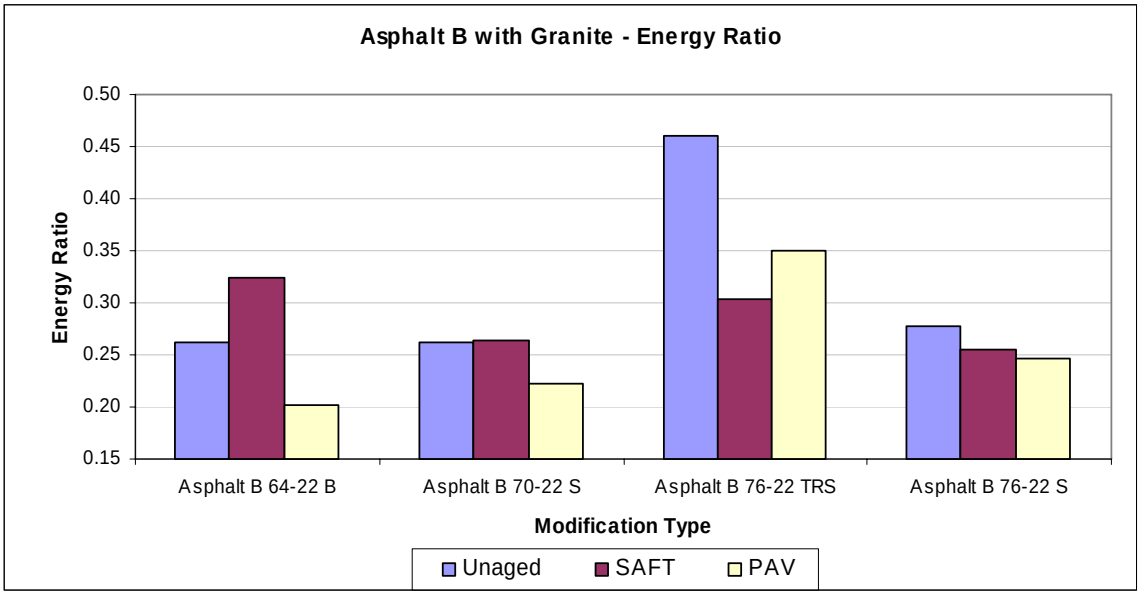

Figure 2.7. Effect of Manufacturer Modifiers and Aging on *ER* of Asphalt Binder from Source B with Granite Aggregate.

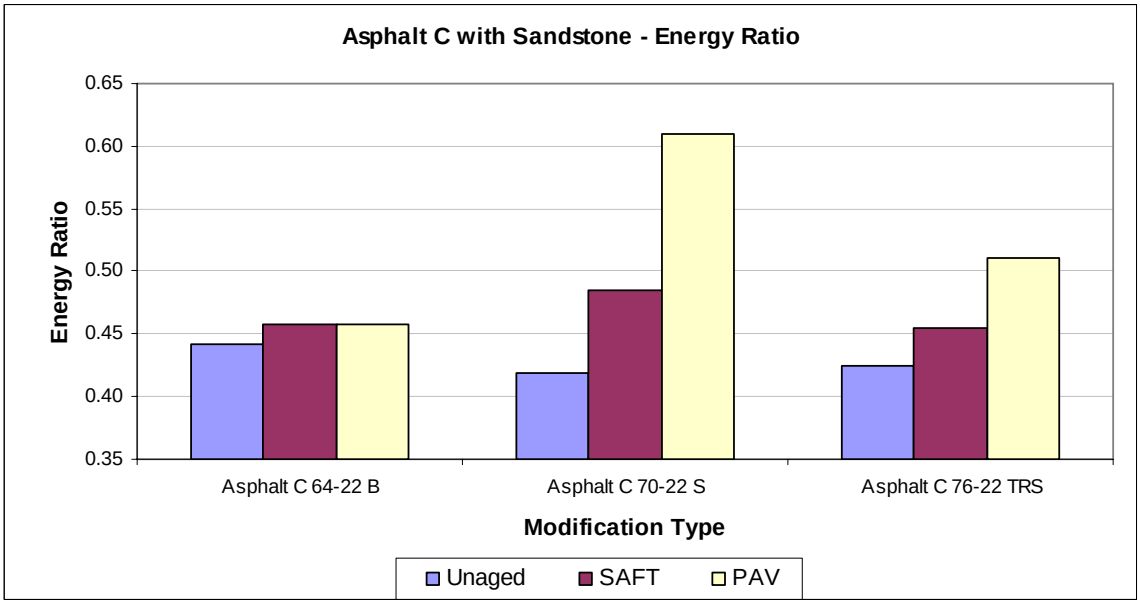

Figure 2.8. Effect of Manufacturer Modifiers and Aging on *ER* of Asphalt Binder from Source C with Sandstone Aggregate.

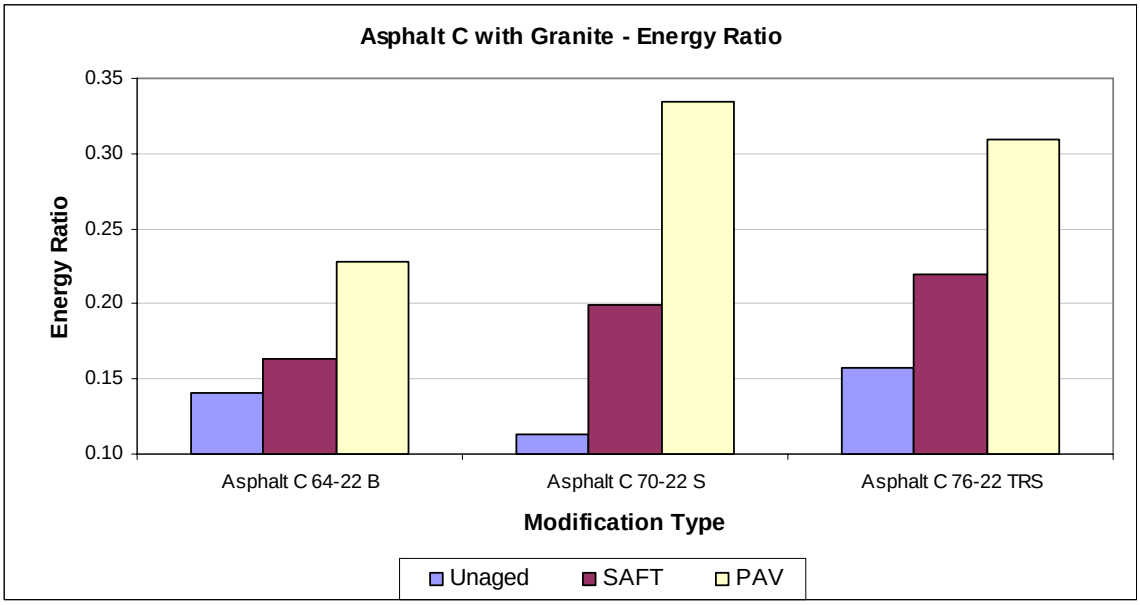

Figure 2.9. Effect of Manufacturer Modifiers and Aging on *ER* of Asphalt Binder from Source C with Granite Aggregate.

Long-term aging and its effect on the moisture resistance of asphalt mixes while the pavement is in service is relatively more important than short-term aging. All asphalt binders from source B demonstrated a decrease in the magnitude of *ER* due to long-term aging indicating a reduction in the moisture resistance when combined with either one of the aggregates (Figures 2.6 and 2.7). On the contrary, all asphalt binders from source C demonstrated an increase in the magnitude of *ER* due to long-term aging (Figures 2.8 and 2.9). This was due to the fact that long-term aging typically increased the polar components of surface free energy of the asphalt binders from source C. The increase in polar components of the asphalt binder due to aging is well-corroborated by existing literature (Lu and Isacsson [2000]). This effect was opposite in the case of asphalt binders from source B. Although small in magnitude, polar components of the asphalt binder contribute significantly to their adhesive bond strength with the aggregates. The authors speculate that the initial differences in polar functional groups of the unaged asphalt binders could have led to the differences in the surface properties of the binder after aging.

SUMMARY

Three types of modifications were investigated in this project. These included: modifications made to the binder by the manufacturer, modification due to addition of liquid anti-strip agents, and modification due to in service oxidative aging of the binder. Important conclusions related to the effect of each type of modification on the fracture properties and moisture sensitivity of asphalt mixtures based on the changes observed in the energy parameters are as follows:

- Modifications made to a base asphalt binder by the manufacturer to produce a higher PG grade typically increased the work of cohesion indicating better fracture resistance of the modified binders. These modifications did not change the moisture sensitivity of the asphalt binder-aggregate combinations significantly except when TRS was used as a modifier. In this case, the acid component of the asphalt binder increased providing a potential improvement in the adhesive bond strength with most types of aggregates. For one of the asphalt binders, addition of SBS also showed improved in the moisture resistance after aging.
- Addition of liquid anti-strip agents typically reduced the surface free energy and, consequently, the work of cohesion of the asphalt binders. This can indirectly improve the fracture resistance by promoting better adhesion between the fines and the binder during the mixing and compaction process. Use of liquid anti-strip agents either improved or did not significantly change the moisture resistance of the asphalt binder with the selected aggregates (gauged using the parameter *ER*). The liquid anti-strip agents from the two different sources demonstrated different levels of changes in the moisture resistance when used with the same combination of asphalt binder and aggregate. It appears that the effect of the liquid anti-strip agent on the ER is specific to both the binder and aggregate.
- In most cases, long-term aging reduced the work of cohesion indicating lower fracture resistance of the aged binder. In the case of one unmodified binder and one modified binder, the work of cohesion increased after long-term aging. After long-term aging, asphalt binders from one source demonstrated a decrease in the moisture sensitivity, while asphalt binders from the other source demonstrated an

increase or no change with the moisture sensitivity with the two aggregates used in this project. The difference in the behavior of the two asphalt binders is attributed to the influence of aging on the magnitudes of the polar functional groups.

CHAPTER 3
ANALYSIS OF THE DATABASE OF ASPHALT BINDER COHESIVE BOND ENERGY AND BINDER-AGGREGATE ADHESIVE BOND ENERGY

INTRODUCTION

The previous chapter provides the basic principles of surface energy of binders and aggregates. This chapter uses these principles to conduct statistical analysis of the cohesive and adhesive bond energy for the materials tested in this project. The objective of this analysis is to provide a range of cohesive bond energy for binders with different PG grades and modified using different processes, and adhesive bond energy for these binders when used with aggregates from different sources. Recent documentation of a range of surface free energy values is given by Little and Bhasin (2006), who presented the information in Table 3.1 based on testing of 21 unmodified and modified binders from different sources in the United States. Bhasin et al. (2006) compared energy parameters of asphalt-aggregate combinations (determined using their respective surface energy components) to moisture damage of mixtures that included these combinations. As a result, they recommended the use of a bond energy ratio and threshold values for this ratio in order to identify asphalt-aggregate combinations that are susceptible to moisture damage.

MATERIALS

Asphalt Binders

Table 3.2 includes a list of asphalt binders tested during this project. The asphalt binders were obtained from 16 different sources and labeled as A, B, C, etc. Base asphalt binders from sources A through J were modified by their respective manufacturer to produce a total of 21 modified asphalt binders. These modifications were achieved by introducing additives to the base asphalt binder. The additives included materials such as SBS, SBR, and tire rubber. The exact nature, amount, and process of modification varied from one manufacturer to another; the details of which were not disclosed to the authors. The asphalt binders are labeled by the source followed by the PG grade followed by the

type of modifier. For example, binder A 64-22 B indicates source A, PG 64-22 binder, and a base (B) or unmodified binder. A binder with the label A 70-22 S indicates source A, grade PG 70-22, and modified using SBS. A shaded cell in Table 3.2 indicates that surface energy was measured for this binder at the listed condition.

Table 3.1. Typical Magnitudes of Surface Free Energy Components (after Little and Bhasin 2006).

Parameter	Asphalt Binders
Total Surface Free Energy	The total surface free energy is typically in the range of 15 to 45 ergs/cm^2.
Lifshitz-van der Waals component	This component is the most significant contributor to the total surface free energy. Based on results from the Wilhelmy Plate and sessile drop tests, this component varies significantly depending on the type of binder.
Acid-Base component	Most asphalt binders have very small magnitudes of the acid or base component, typically of the order of 0 to 3 ergs/cm^2. This is consistent with the fact that most asphalt binders are weak acids or bases. These small magnitudes can be scaled when multiplied with larger magnitudes of the acid-base components of the aggregate while computing the work of adhesion.

The base and manufacturer-modified asphalt binders from sources B, C, and D were used to evaluate the effect of aging on their surface free energy components and concomitant energy parameters. Chapter 2 gives the description of these aging methods. The base and manufacturer-modified asphalt binders from source A were used to evaluate the effect of liquid anti-strip agents on their surface free energy components. Two different types of liquid anti-strip agents, commonly used by TxDOT in various field mixtures, were included in this project. The manufacturer's recommended amount of anti-strip agent was added to the asphalt binder.

Table 3.2. A List of Asphalt Binders Used in this Project.

Source	PG Grade and Modifier	Unaged	SAFT Aged	PAV Aged	Anti-Strip Agent 1	Anti-Strip Agent 2
Asphalt A	64-22 B	■			■	■
	70-22 S	■			■	■
	76-22 S	■			■	■
Asphalt B	64-22 B	■	■	■		
	70-22 S	■	■	■		
	76-22 TRS	■	■	■		
	76-22 S	■	■	■		
Asphalt C	64-22 B	■	■	■		
	70-22 S	■	■	■		
	76-22 TRS	■	■	■		
Asphalt D	58-22 B	■	■	■		
	70-28 S	■	■	■		
Asphalt E	64-22 B	■				
	70-22 S	■				
	76-22 S	■				
	70-28 S	■				
	76-28 S	■				
Asphalt F	58-28 B	■				
	58-34 S	■				
	58-40 S	■				
Asphalt G	64-22 B	■				
	70-22 S	■				
	76-22 S	■				
Asphalt H	64-22 B	■				
	70-22 S	■				
	76-22 S	■				
Asphalt I	64-22 B	■				
	70-22 S	■				
	76-22 S	■				
Asphalt J	64-22 B	■				
	76-22 SR	■				
Asphalt K	76-22 S	■				
Asphalt L	76-22 S	■				
Asphalt M	76-22 S	■				
Asphalt N	76-22 S	■				
Asphalt O	76-22 S	■				
Asphalt P	76-22 S	■				

B = Base asphalt binder; S = SBS modifier; SR = SBR modifier;
TRS = Tire rubber & SBS modifiers.
Shaded cells indicate the type of binder that was tested.

The surface free energy components of 11 different aggregates were measured in this project. Table 3.3 includes a list these aggregates and their corresponding surface free energy components. Similar aggregates with different suffix (e.g., Limestone-1, Limestone-2, Limestone-3) indicate that the generic aggregate type was obtained from different sources with a unique suffix assigned to each source.

Table 3.3. Aggregate Surface Free Energy Components (ergs/cm^2).

Aggregate	Γ^{LW}	Γ^{+}	Γ^{-}
Quartizite	60.86	8.89	544.98
Light Sandstone	62.46	2.03	222.61
Granite	56.35	43.45	782.70
Gravel - 1	59.49	1.20	285.98
Dark Sandstone	63.97	8.51	316.90
Limestone - 1	59.89	18.82	561.11
Limestone - 2	58.01	1.76	401.07
Gravel - 2	63.48	7.70	546.26
Gravel - 3	81.34	1.10	426.85
Limestone - 3	57.70	5.50	340.40
Gravel - 4	57.50	23.00	973.00

RESULTS

Surface Energy Components

The surface free energy components of all binders were determined using the Wilhelmy Plate method. The values of the surface free energy components were then arranged in an ascending order, and the quartiles of the distribution were determined. The first, second (median), and third quartiles refer to the values at which 25 percent, 50 percent and 75 percent of the measurements are less, respectively. Figures 3.1 - 3.3 display these quartiles for the LW, acid, and base components of the surface free energy of unaged binders, respectively. The LW, component is the largest among the three components, usually followed by the basic component, with the acidic component is the smallest. It is important to have as high an acidic component as possible since the acidic component of the asphalt bonds with the basic component of the aggregate, as seen in Equation 2.4.

Aggregates have much larger values of surface free energy compared to asphalt and have very large basic components, as shown in Table 3.3.

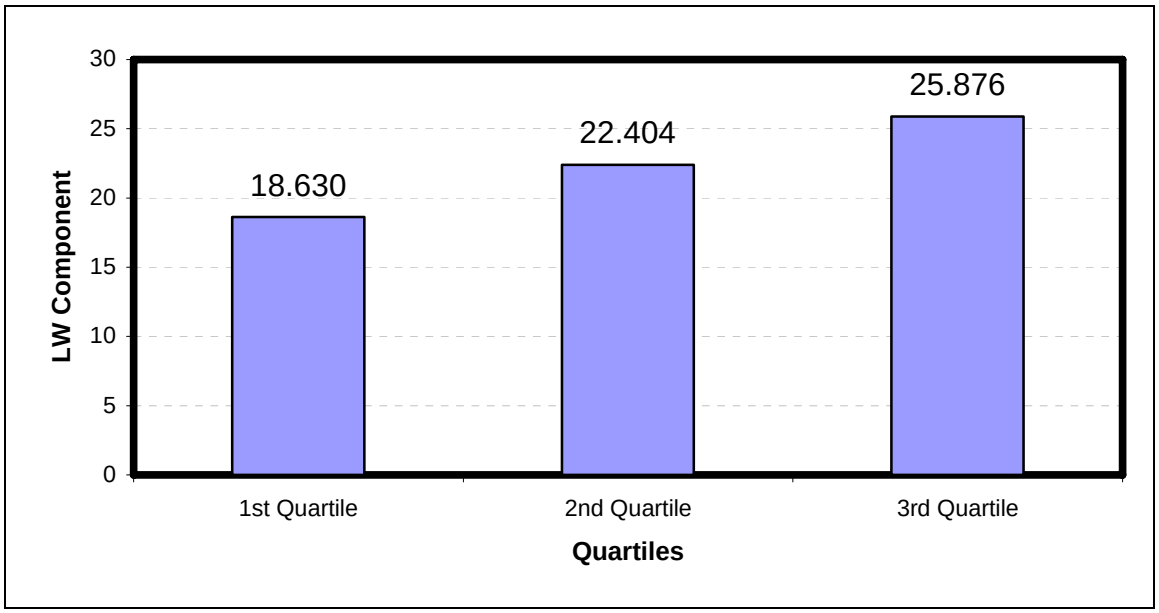

Figure 3.1. Quartiles of the Lifshitz-van der Waals Component of all Unaged Binders.

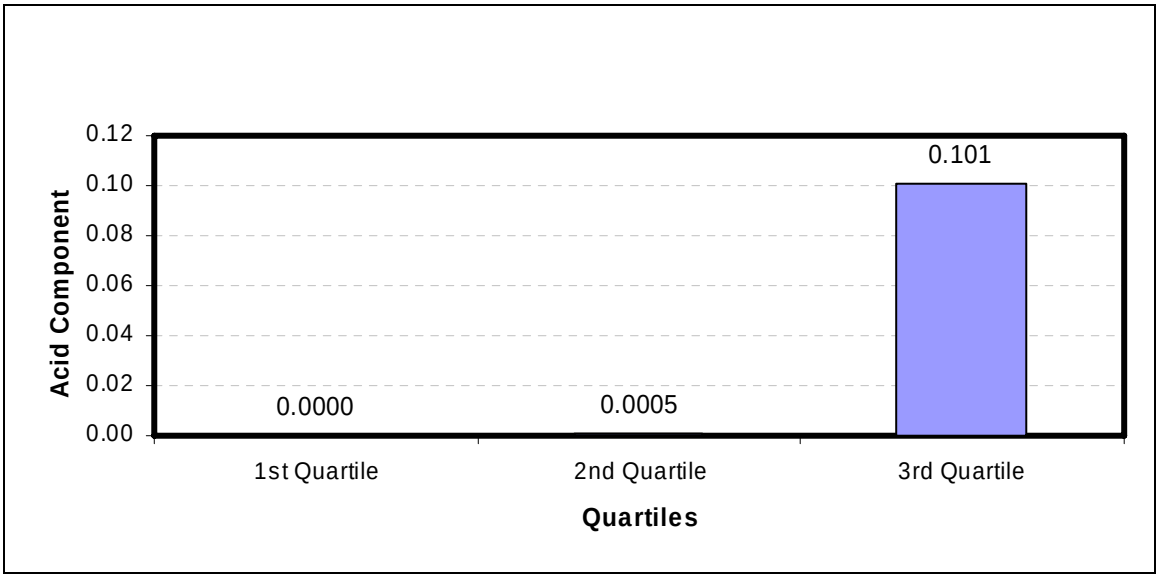

Figure 3.2. Quartiles of the Acid Component of all Unaged Binders.

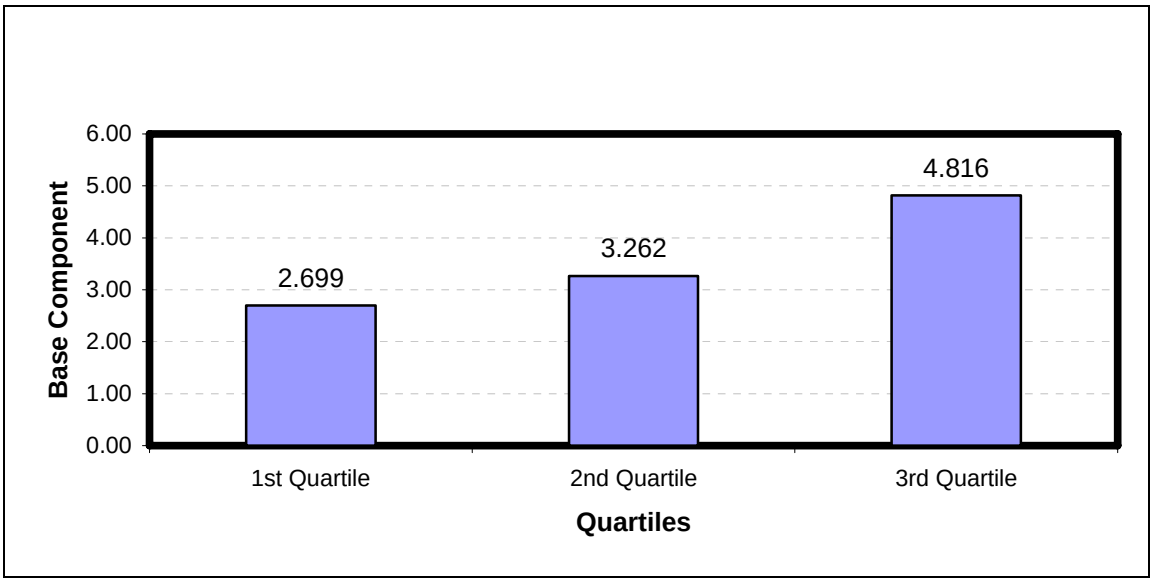

Figure 3.3. Quartiles of the Base Component of all Unaged Binders.

Table 3.4 shows the change in the surface free energy components caused by the addition of anti-strip agents. It can be seen that all asphalt binders except one had an increase in either the acid or base component of surface free energy, and some had increases in both, due to the addition of liquid anti-strip agents. As shown later, the asphalt binder that did not have an increase, Asphalt A 70-22 S with Anti-strip 2, is also the asphalt binder that showed the greatest decrease in *ER*. This indicates that the acid and base components of an asphalt binder are very important to moisture resistance. The non-polar component of surface free energy, γ^{LW}, decreased for all binders when liquid anti-strip agent was added.

Table 3.4. Surface Free Energy Components due to Addition of Anti-Strip Agents.

Asphalt	Anti-Strip	Γ^{LW}	Γ^{+}	Γ^{-}	Γ^{Total}
Asphalt A 64-22 B	None	29.79	0.000	1.42	29.80
	1	29.10	0.000	1.78	29.11
	2	29.72	0.000	5.12	29.75
Asphalt A 70-22 S	None	27.34	0.000	2.77	27.34
	1	18.89	0.055	3.81	19.80
	2	24.79	0.000	1.67	24.80
Asphalt A 76-22 S	None	33.22	0.000	2.30	33.22
	1	22.66	0.000	2.49	22.66
	2	25.91	0.001	2.91	26.00

Table 3.5 displays the change in the surface free energy components caused by aging of the asphalt binders. The results are much more varied than those from the anti-strip study. Asphalt binders from source B showed mixed results after being SAFT aged. Three of the four asphalt binders from source B exhibited a decrease in the γ^{LW} component of surface free energy, one of the four asphalts showed a decrease in the γ^{+} component of surface free energy, and two of them showed a decrease in the γ^{-} component of surface free energy. After PAV aging, two of the asphalts from source B showed a decrease in the γ^{LW} component of surface free energy, and all asphalt binders from source B showed a decrease in the polar components of surface free energy. Asphalt binders from source C all showed a decrease in the γ^{LW} component of surface free energy and an increase in either the γ^{+} or γ^{-} component of surface free energy or both. Asphalt D 58-28 B showed an increase in the γ^{LW} component of surface free energy after being short- and long-term aged, but Asphalt D 70-28 S showed a decrease in the γ^{LW} component of surface free energy after being short- and long-term aged. The only change to the γ^{+} component occurred after long-term aging of Asphalt D 70-28 S. The basic component of Asphalt D decreased in all cases except 58-28 B after PAV aging.

The lack of trend in the surface energy components of short- and long-term aged asphalt binders can be explained on the basis of asphalt chemistry. Researchers at the Western Research Institute (WRI) have extensively investigated the aging phenomenon in asphalt binders and determined that the properties of short- and long-term aged asphalt binders depend on the chemistry of the unaged binder (Western Research Institute 2006). Two important compounds that are formed during the oxidative aging of asphalt binders are sulfoxides and ketones. An asphalt binder with low sulfur is unlikely to produce a high concentration of sulfoxides after short term aging. Therefore, depending on the initial chemistry, each unaged asphalt binder reacts differently to aging. Since the physio-chemical surface properties of the asphalt binder are dictated by its chemistry, it is reasonable to expect that different asphalt binders exhibit different trends due to aging.

Table 3.5. Surface Free Energy Components of Asphalt Binders before and after Aging.

Asphalt	Aging	γ^{LW}	γ^{+}	γ^{-}	γ^{Total}
Asphalt B 64-22 B	Unaged	20.16	0.033	3.75	20.87
	SAFT	16.91	0.137	4.51	18.48
	PAV	26.2	0.000	3.2	26.23
Asphalt B 70-22 S	Unaged	22.50	0.001	6.79	22.66
	SAFT	21.72	0.036	3.74	22.45
	PAV	21.3	0.000	4.1	21.29
Asphalt B 76-22 TRS	Unaged	18.75	0.663	4.57	22.23
	SAFT	21.4	0.083	4.8	22.67
	PAV	17.8	0.219	4.4	19.73
Asphalt B 76-22 S	Unaged	22.67	0.003	7.86	22.96
	SAFT	21.72	0.006	5.35	22.06
	PAV	24.1	0.000	6.4	24.10
Asphalt C 64-22 B	Unaged	32.17	0.000	0.92	32.17
	SAFT	28.1	0.000	1.4	28.12
	PAV	26.0	0.000	5.1	25.97
Asphalt C 70-22 S	Unaged	35.78	0.000	0.44	35.78
	SAFT	28.6	0.004	2.5	28.80
	PAV	20.5	0.137	5.4	22.25
Asphalt C 76-22 TRS	Unaged	34.55	0.000	1.85	34.55
	SAFT	27.0	0.000	4.6	26.99
	PAV	24.8	0.027	8.5	25.78
Asphalt D 58-28 B	Unaged	18.96	0.000	3.26	18.96
	SAFT	21.3	0.000	2.9	21.28
	PAV	24.6	0.000	3.3	24.63
Asphalt D 70-28 S	Unaged	23.01	0.000	5.44	23.01
	SAFT	20.3	0.000	2.9	20.26
	PAV	17.7	0.441	4.7	20.57

For any given asphalt binder, the difference in trends between short-term and long-term aging are explained on the basis of kinetics of the oxidation reaction. For example, sulfoxides (weak bases) form at a much faster rate compared to ketones (weak acids). As a result, it is not possible to extrapolate the effect of short-term oxidation on surface energy to predict surface energy components that may be formed after long-term aging. The net impact of aging on the chemical and physio-chemical properties of asphalt binders can be different depending on the duration of aging.

The different trends in surface energy components exhibited by the asphalt binders due to short-and long-term aging ultimately translate into different values of the energy ratio and, hence, different expected trends in moisture resistance of the asphalt binders due

to aging. Researchers at WRI have conducted freeze thaw tests on asphalt mixtures using several different aged and unaged asphalt binders (Western Research Institute 2006). They have demonstrated that the moisture resistance of asphalt mixtures either decreased or increased after oxidative aging of the binder, depending on the type of binder.

Work of Cohesion

Figure 3.4 displays the quartiles for the cohesive bond energy for all the unaged binders tested in this project. The cohesive bond energy values range from 26 ergs/cm^2 to 71.5 ergs/cm^2. These values can determine the relative ranking of a binder with respect to a comprehensive list of binders such as those used in this project.

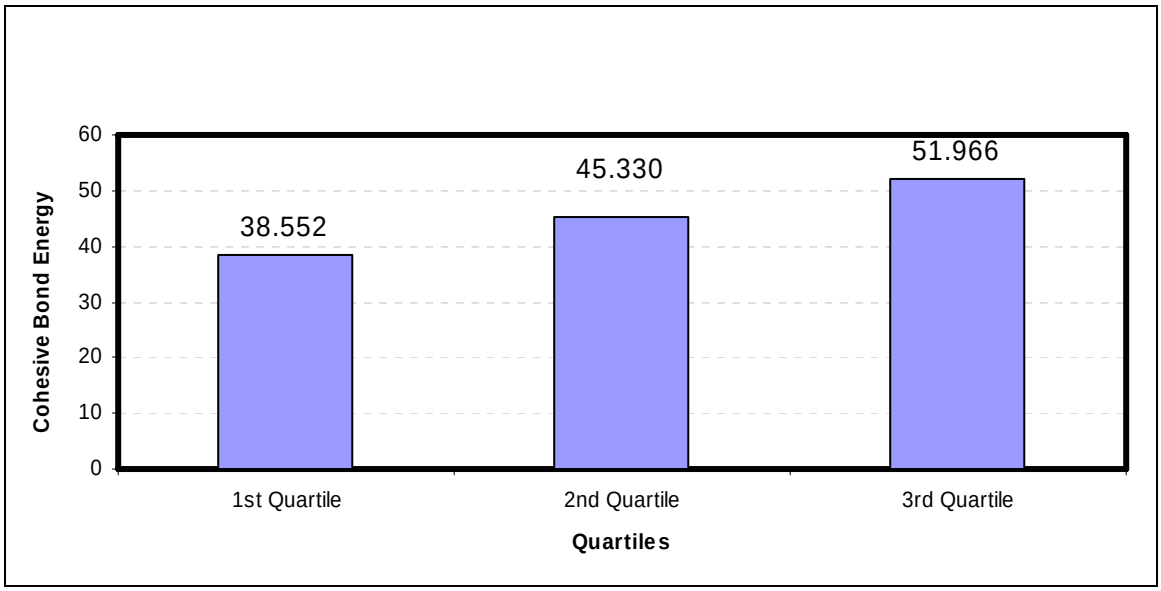

Figure 3.4. Quartiles of Cohesive Bond Energy of all Unaged Binders.

Table 3.6 shows the percent change in cohesive bond energy caused by the addition of anti-strip agents. It can be seen that the addition of anti-strip agents to the asphalt binder caused an overall decrease in the cohesive bond energy. There are two main implications from a decrease in the cohesive bond energy of an asphalt binder. The first is a reduction in the amount of work needed for a crack to propagate through the asphalt binder. The second is a reduction in the surface free energy or surface tension of the asphalt binder, which enables better coating of the aggregate by the asphalt binder and, thus, improves adhesion

between the two. The reduction in the amount of work needed for a crack to propagate through a mix will reduce the fracture resistance of the mix; however, this is offset by the reduction in the non-polar component of surface free energy of the asphalt binder, which is explained as follows. The reduction in the surface free energy of the asphalt binder enables better coating of the aggregate surface by the asphalt binder and, thus, improves the adhesion between the two. Since the anti-strip agent is added before mixing occurs, the asphalt-aggregate matrix will benefit from the reduction in surface free energy. This is supported by Lucic et al. (1998) who found that the fracture resistance of a matrix increases due to improved adhesion between a polymer phase (asphalt binder) and filler particles (aggregate fines). Therefore, a reduction in the cohesive bond energy due to the addition of liquid anti-strip agents can be indirectly correlated to improved fracture resistance of the asphalt-aggregate matrix.

Table 3.6. Percent Change in Cohesive Bond Energy due to Addition of Anti-Strip Agents.

Asphalt	Anti-Strip	Γ Cohesive	% Change in Cohesive Bond Energy (Increase Positive)
Asphalt A 64-22 B	None	59.59	
	1	58.21	-2.32
	2	59.50	-0.15
Asphalt A 70-22 S	None	54.67	
	1	39.60	-27.56
	2	49.59	-9.30
Asphalt A 76-22 S	None	66.44	
	1	45.31	-31.80
	2	52.00	-21.74

B = Base asphalt binder; S = SBS modifier

From Table 3.7, it can be seen that the percent change in the cohesive bond energy due to aging of the asphalt binder is more variable; however, the overall trend is a decrease in cohesive bond energy due to aging. Seven of the nine asphalt binders that were short-term aged showed a decrease in their cohesive bond energy, and six of the nine asphalt binders that were long-term aged showed a decrease in their cohesive energy. Of the five asphalt binders that showed an increase in the cohesive bond energy after aging, three were from base binders. By evaluating the surface free energy components of the

asphalt binders, it can be seen that the increase or decrease of the cohesive bond energy is due mainly to an increase or decrease in the γ^{LW} component of surface free energy, respectively.

As stated earlier, a decrease in the cohesive bond energy of an asphalt binder implies that less work is needed for a crack to propagate through an asphalt binder. In the case of the anti-strip agents, which were added prior to mixing, this was counteracted by the increase in the coating of the asphalt binder to the aggregate. However, with aging, the reduction in the cohesive bond energy occurs after mixing has occurred, and there is no benefit of better coating due to reduction of cohesive bond energy.

Table 3.7. Percent Change in Cohesive Bond Energy due to Aging of the Asphalt Binder.

Asphalt	Aging	Γ Cohesive	% Change in Cohesive Bond Energy (Increase Positive)
Asphalt B 64-22 B	Unaged	41.73	
	SAFT	36.96	-11.45
	PAV	52.46	25.70
Asphalt B 70-22 S	Unaged	45.33	
	SAFT	44.90	-0.95
	PAV	42.57	-6.08
Asphalt B 76-22 TRS	Unaged	44.46	
	SAFT	45.34	1.97
	PAV	39.45	-11.26
Asphalt B 76-22 S	Unaged	45.92	
	SAFT	44.12	-3.92
	PAV	48.19	4.95
Asphalt C 64-22 B	Unaged	64.34	
	SAFT	56.24	-12.58
	PAV	51.93	-19.28
Asphalt C 70-22 S	Unaged	71.56	
	SAFT	57.59	-19.52
	PAV	44.50	-37.81
Asphalt C 76-22 TRS	Unaged	69.09	
	SAFT	53.97	-21.89
	PAV	51.56	-25.37
Asphalt D 58-28 B	Unaged	37.92	
	SAFT	42.56	12.23
	PAV	49.25	29.88
Asphalt D 70-28 S	Unaged	46.02	
	SAFT	40.52	-11.94
	PAV	41.14	-10.60

B = Base asphalt binder; S = SBS modifier; TRS = Tire rubber.

Energy Ratio

Figure 3.5 displays quartiles for the *ER* of all the unaged asphalt binders in combination with the aggregates listed in Table 3.3. From the previous chapters, researchers know that a higher value of *ER* is desirable for better resistance to moisture damage. Therefore, it is important to determine the ranking of an asphalt binder-aggregate combination with respect to other choices in order to determine the compatibility of the asphalt binder and aggregates based on its resistance to moisture damage.

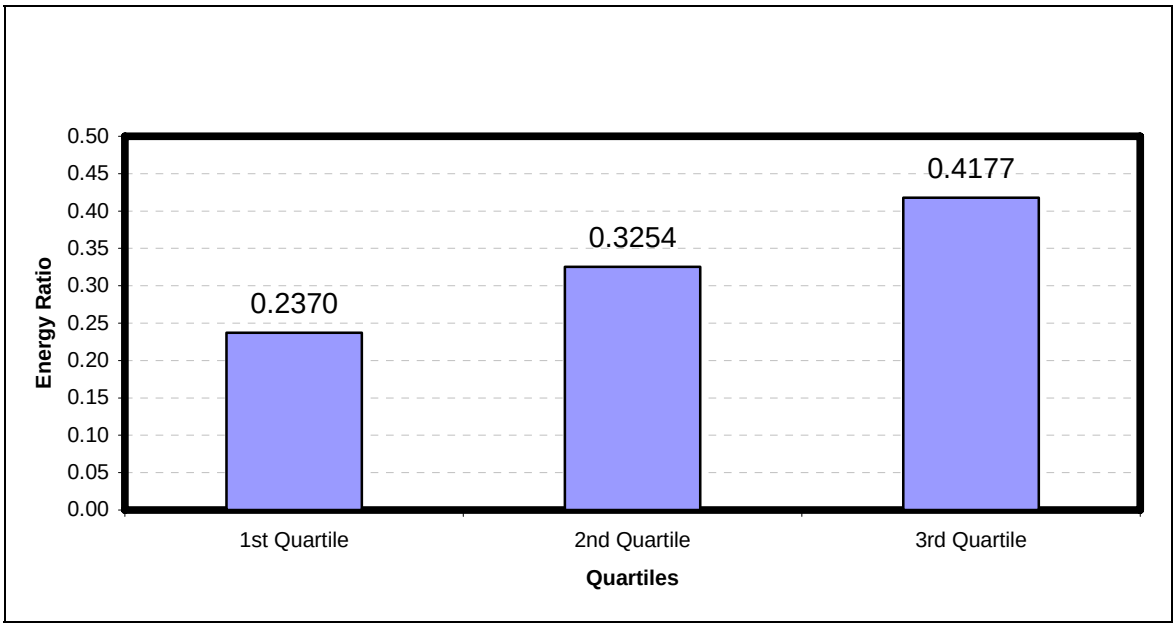

Figure 3.5. Quartiles of the Energy Ratio of all Unaged Binders.

Table 3.8 shows the percent change in the *ER* caused by the addition of anti-strip agents. The energy ratio is a function of the surface free energy of both the asphalt binder and the aggregate as explained in Chapter 2. For this reason, an asphalt binder might show an improvement in *ER* with one aggregate, but a decrease in *ER* with another aggregate. From Table 3.8, it can be observed that the addition of anti-strip agents increased the *ER* in the majority of the cases. Only 11 out of the 66 cases showed a decrease in the *ER*, and only three had a decrease greater than 5 percent. This implies that the addition of anti-strip agents, in the majority of cases, will increase an asphalt mixture's resistance to moisture-induced damage.

There are three factors that determine the effectiveness of the anti-strip agents—the source of anti-strip agent, the type and mineralogy of the aggregate, and the chemical composition of the asphalt binder. Looking at Asphalt A 70-22 S in Table 3.8, Anti-strip 1 increased *ER* by at least 20 percent in every case, whereas Anti-strip 2 decreased *ER* in seven of the 11 cases. The effect of aggregate mineralogy can best be seen by looking at the case of Asphalt A 64-22 B with Anti-strip 2 in Table 3.8. Gravel 1 and Gravel 3 decrease *ER*; however, Gravel 2 and Gravel 4 increase *ER*. This effect can be seen in several other cases and shows that aggregate mineralogy plays a large role in resisting moisture-related damage in asphalt concrete. This also implies that not all limestone, river gravel, or granite aggregates can be treated as the same; there are differences in the mineralogical makeup that will manifest themselves as differences in the moisture resistance of the mixture. The effect of the chemical composition of the asphalt binder used can be seen by looking at Asphalt A 64-22 B with Anti-strip 1 and Asphalt A 70-22 S with Anti-strip 1 in Table 3.8. The unmodified base asphalt binder shows little or no improvement in *ER* when coupled with Anti-strip 1; however, when Anti-strip 1 is used with the modified asphalt binder, 70-22 S, a much larger improvement in *ER* is observed.

Table 3.8. Percent Change in the Energy Ratio due to Addition of Anti-Strip Agents.

Percent Difference in ER - Addition of Anti-Strip Agents												
Asphalt	Anti-Strip	Q	LS	Granite	G1	DS	L1	L2	G2	G3	L3	G4
Asphalt A 64-22 B	1	3	0	6	1	2	4	2	3	0	3	5
	2	17	-1	40	-1	14	26	5	15	-1	12	31
Asphalt A 70-22 S	1	39	22	45	31	27	39	40	37	19	35	51
	2	-3	2	-9	3	-3	-5	2	-2	0	-1	-6
Asphalt A 76-22 S	1	13	8	14	14	9	13	17	11	0	15	16
	2	16	9	20	14	12	17	18	15	4	17	20

Q = Quartzite; LS = Light Sandstone; DS = Dark Sandstone; G1 – G4 = Gravel 1 – Gravel 4; L1 – L3 = Limestone 1 – Limestone 3

From Table 3.9, it can be seen that the percent change in the *ER* due to aging varies among the different binder-aggregate combinations. Upon closer inspection, it can be seen that the changes can be correlated with modifications made by the manufacturer. Asphalts B 64-22 B and 70-22 S both show increases in *ER* after SAFT aging; however, Asphalts B 76-22 TRS and 76-22 S both show decreases in *ER* after SAFT aging. Asphalt D 58-28

B showed a decrease in *ER* after PAV aging, but Asphalt D 70-28 S showed an increase in *ER* after PAV aging. This shows that modifications made by the manufacturer can have an effect, positive or negative, on the moisture susceptibility of an asphalt pavement once the asphalt binder has been aged.

Asphalt C from Table 3.9 showed an increase in *ER* for all PG grades, aggregates, and aging except for one case, Asphalt C 64-22 B with aggregate Gravel 3 after being PAV aged. Upon inspection of the surface free energy components of the aged binders, researchers noted that the increase or decrease of the polar components of surface free energy, γ^+ and γ^-, was directly proportional to the increase or decrease of an asphalt mix's moisture resistance, respectively. The acidic and/or basic components of surface free energy increased for both types of aging for Asphalt C. Looking at another asphalt binder, Asphalt B 64-22 B from Table 3.9, it can be seen that an increase in *ER* occurs after SAFT aging, and a decrease in *ER* occurs after PAV aging. After inspection of surface free energy components, it is noted that SAFT aging increases in the polar components and PAV aging decreases the polar components; see Table 3.5.

Table 3.9. Percent Change in the Energy Ratio due to Aging of the Asphalt Binder.

Percent Difference in ER - SAFT and PAV Aging												
Asphalt	Aging	Q	LS	Granite	G1	DS	L1	L2	G2	G3	L3	G4
Asphalt B	SAFT	21	12	23	16	15	21	20	20	13	18	26
64-22 B	PAV	-22	-15	-23	-19	-16	-21	-23	-21	-13	-20	-26
Asphalt B	SAFT	11	16	1	19	8	5	19	11	17	11	8
70-22 S	PAV	-9	-2	-15	-2	-7	-12	-4	-8	-3	-7	-13
Asphalt B	SAFT	-36	-31	-34	-35	-30	-34	-37	-35	-32	-34	-38
76-22 TRS	PAV	-25	-22	-24	-24	-22	-24	-25	-25	-24	-23	-26
Asphalt B	SAFT	-8	-10	-2	-12	-6	-5	-12	-8	-11	-8	-7
76-22 S	PAV	-14	-13	-9	-16	-10	-11	-18	-13	-12	-13	-14
Asphalt C	SAFT	10	4	17	6	8	13	9	9	0	10	15
64-22 B	PAV	30	4	63	7	23	42	16	26	-1	25	50
Asphalt C	SAFT	44	16	76	23	32	54	33	38	8	40	66
70-22 S	PAV	120	46	195	66	82	140	96	106	35	103	184
Asphalt C	SAFT	24	7	40	12	18	30	18	21	1	22	35
76-22 TRS	PAV	61	20	97	30	44	72	46	54	14	52	90
Asphalt D	SAFT	-2	1	-4	0	-1	-3	-1	-1	2	-2	-3
58-28 B	PAV	-2	0	-2	-2	0	-2	-3	-1	3	-3	-3
Asphalt D	SAFT	-6	1	-14	2	-6	-10	0	-6	-1	-4	-11
70-28 S	PAV	83	62	74	79	60	73	92	81	68	74	96

Q = Quartzite; LS = Light Sandstone; DS = Dark Sandstone; G1 – G4 = Gravel 1 – Gravel 4; L1 – L3 = Limestone 1 – Limestone 3

SUMMARY

This project looked at the distribution of cohesive and adhesive bond energy parameter, *ER*, and the individual surface free energy components and how these changed due to the addition of anti-strip agents and aging of the asphalt binder. The main conclusions from the results discussed in this chapter are:

- Asphalt binders can be ranked based on their cohesive bond energy or any of its surface free energy components. This ranking can be used to compare binders against each other and determine the ones that have the best resistance to fracture and moisture damage when used with aggregates.
- The addition of anti-strip agents to Asphalt A resulted in a decrease of the cohesive bond energy of each PG grade of asphalt. Upon further examination, it was found that the decrease in the cohesive bond energy of the asphalt binder resulted from a decrease in the non-polar γ^{LW} component of the surface free energy; see Table 3.6. A reduction in the γ^{LW} component of the surface free energy allow better coating of the aggregate by the asphalt, improving interfacial adhesion and, thus, improving the fracture resistance of the matrix (Lucic et al. [1998]).
- Aging can have different impacts on different asphalt binders depending on the initial chemistry of the asphalt binder. Furthermore, differences in kinetics of different compounds formed during oxidative aging also influence the chemistry and, consequently, the surface free energy components and performance of different asphalt binders after short- and long-term aging.
- In all but one case, the addition of liquid anti-strip agents to an asphalt binder increased *ER* and, thus, the moisture resistance of the mixture. In the case that did not improve, Asphalt A 70-22 S Anti-strip 2, the addition of the liquid anti-strip agent decreased the polar components of surface free energy.

CHAPTER 4
THE EFFECT OF pH VALUE ON THE SURFACE FREE ENERGY COMPONENTS OF WATER

INTRODUCTION

Stripping of asphalt binder from aggregates is caused by an adhesive failure at the interface of the two materials in the presence of water. From a thermodynamic standpoint, the increase in stripping is due to the fact that water has a higher affinity to aggregate than asphalt does. For this reason, water will always strip asphalt binder from the surface of aggregates. However, the thermodynamic energy potential that drives the stripping phenomenon depends on the surface properties of both the asphalt binder and the aggregate. During the stripping process, water diffuses through the thin layer of asphalt binder or mastic and collects on the surface of the aggregate. When this occurs, the pH of the contact water will typically increase (become more basic) due to the adsorption of hydrogen ions from the water and onto the surface of the aggregate. The change in pH of water affects its surface energy components. The change in surface energy components of water can consequently aggravate or retard the stripping process. Therefore, it is important to assess and quantify the impact of change in surface energy components of water due to the change in its pH after coming into contact with aggregate surfaces.

Higher basic character of aggregate surface and larger specific surface areas will typically result in greater adsorption of hydrogen ions. Figure 4.1 below is from Yoon and Tarrer (1989) and shows how the pH of water increases when different aggregate fines are added to it. The limestone aggregate most likely had the lowest acidic and highest basic surface free energy components and/or relatively higher specific surface area. The chert, however, had the highest acidic and lowest basic surface free energy components and/or relatively lower specific surface area.

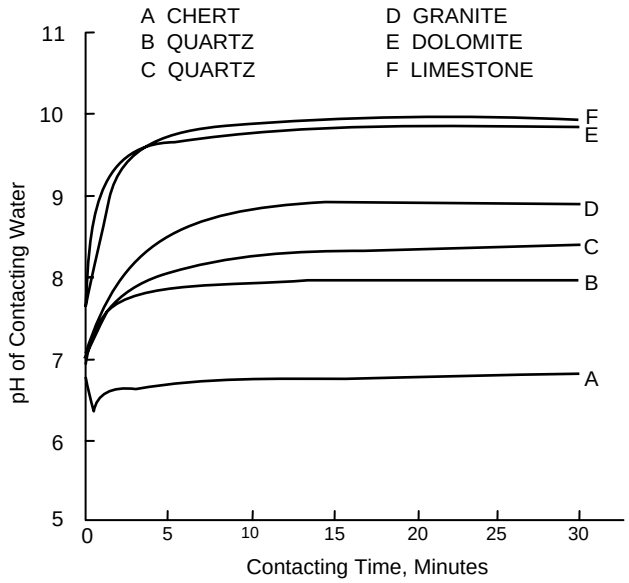

Figure 4.1. Influence of Aggregate Type on pH of the Contacting Water (after Yoon and Tarrer 1989).

METHODOLOGY

The methodology used for this testing begins by using the Wilhelmy Plate to measure the surface free energy of at least three asphalt binders. Twenty thin glass slides per asphalt sample are cleaned, dried, and then coated with a thin film of asphalt binder. These slides are then suspended from a balance and immersed into a probe liquid. Five replicate slides are used for each probe liquid, and the contact angle is measured for each slide. The contact angle can be calculated using Equation 4.1 as follows:

$$\cos\theta = \left(\Delta F + V_{im}\left(\rho_L - \rho_{air}\right)g\right)/\left(P_t\gamma_L\right) \tag{4.1}$$

where θ is the contact angle, ΔF is the change in force measured by the balance, V_{im} is the volume of the immersed plate, ρ_L is the density of the probe liquid, ρ_{air} is the density of the air, g is the local acceleration of gravity, P_t is the perimeter of the asphalt coated plate, and γ_L is the total surface free energy of the probe liquid. By using Equation 4.1 and the

Young-Dupre equation, with the assumption that equilibrium film pressure is neglected for asphalt, Equation 4.2 can be obtained as follows:

$$\gamma_L(1+\cos\theta_i) = 2\sqrt{\gamma_S^{LW}\gamma_L^{LW}} + 2\sqrt{\gamma_S^-\gamma_L^+} + 2\sqrt{\gamma_S^+\gamma_L^-} \quad (4.2)$$

where γ_L^{LW}, γ_L^-, and γ_L^+ are the three surface free energy components of the liquid and γ_S^{LW}, γ_S^-, and γ_S^+ are the three surface free energy components of the solid being tested. θ_i is the contact angle between probe liquid and the solid being tested and can be measured using the Wilhelmy Plate method.

Since there are three components of surface free energy that will be measured for each asphalt binder, there needs to be at least three probe liquids used. The probe liquids used in this project were distilled water, glycerol, ethylene glycol, formamide, and diiodomethane (methylene iodide). The use of five probe liquids adds some redundancy into the results and allows better confirmation that no interactions occurred between the asphalt and probe liquid using the Newman criteria (Hefer et al. 2006).

Once the surface free energy of the asphalt binder is known, the surface free energy of the different pH water can be measured. By using a similar process to that which Yoon and Tarrer (1989) used, the pH of different waters was altered. Various crushed aggregates passing sieve #16 (1.18 mm) retained on sieve #30 (0.6 mm) were placed in separate glass beakers, and the pH was allowed to come to equilibrium. Distilled water is placed in another beaker, and its pH was also measured. The distilled water was used to serve as a reference to evaluate the pH altered water.

Two properties were measured after the pH of the different water with aggregate immersed in them reached equilibrium. The first property is the total surface tension of the water using the sessile drop method (which is equivalent to the total surface free energy), and the second is the surface free energy components of the water using the Wilhelmy Plate method.

The total surface tension, or surface free energy, of the water using the sessile drop method was determined using an image analysis software accompanying the sessile drop device based on the pendant drop volume method (Adamson and Gast 1997). The

following test procedure was followed to accomplish this. A reusable glass syringe with a threaded and labeled volume adjustment cap for very accurate volume changes attached to a stainless steel needle was used in this test. The drop of the water to be tested was suspended from the syringe needle. The syringe needle was held vertically downward, and the volume of the drop was increased steadily. A high resolution digital camera was used to take pictures of the suspended drop of water every 3 seconds in order to calculate the corresponding surface tension in real time as the volume of the drop increases. As seen in Figure 4.2, the volume of the drop was increased until the equilibrium surface tension was achieved. The volume of the drop was then increased and decreased several times to ensure the equilibrium surface tension was, in fact, reached. Once a stable surface tension value was achieved, a best fit line was drawn through the points, and the average surface tension value was recorded.

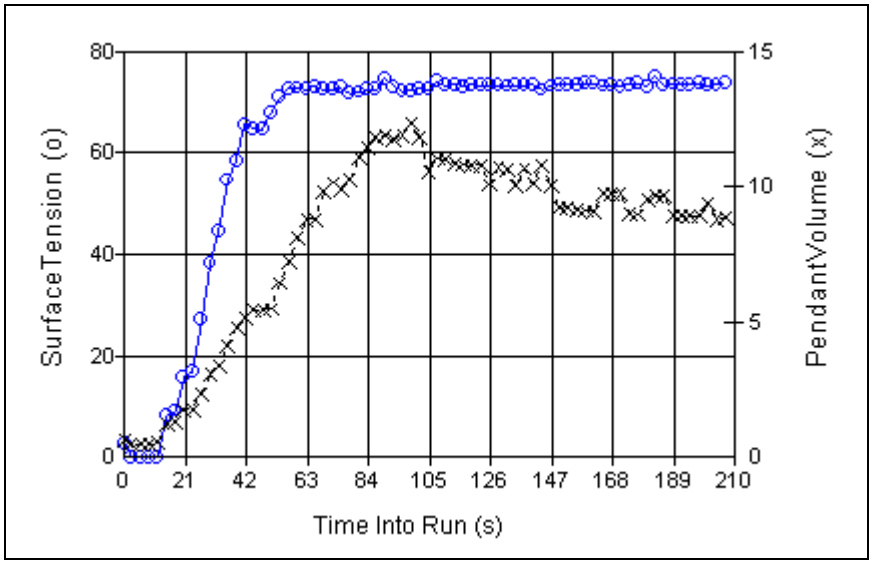

Figure 4.2. Surface Tension versus Pendant Volume (Sessile Drop).
O – Surface Tension; X – Pendant Volume

The surface free energy components of the pH altered and reference distilled water were determined using the Wilhelmy Plate method in a new fashion. As discussed earlier, the typical procedure to determine the surface free energy components of an asphalt binder is to measure its contact angle with at least three different probe liquids with known surface free energy components and then backcalculate the surface free energy components of the

binder. In this case, it is of interest to determine the surface free energy components of the liquid (pH altered and reference distilled water). Therefore, contact angles of at least three asphalt binders with known surface free energy components were measured with the liquid, and the unknown surface energy components of the liquid were backcalculated. In this project four asphalt binders were used to introduce redundancy and improve the robustness of the backcalculated values. The four asphalt binders, for which the surface energy components were measured previously, were dipped into each pH altered water and reference distilled water, and the contact angle was recorded. The surface tension used by the Wilhelmy Plate device as an input to compute the contact angle from the test is the theoretical surface tension for distilled water, not water with an altered pH. To correct for this, Equation 4.1 was employed. ΔF , V_{im}, ρ_L, ρ_{air}, g, and P_t are all constants and do not change with a change in pH, assuming that the change in density of water due to change in pH is negligible. However, θ and γ_L do change and, therefore, need to be corrected in order for the contact angle between the asphalt and the water with an altered pH to be accurate. Equation 4.3 will be used subsequently to correct the contact angle for the difference in surface tension:

$$\gamma_{LpH}^{Total} \cos\theta_i^{pH} = \gamma_L^{Total} \cos\theta_i \tag{4.3}$$

where θ_i is the apparent contact angle determined by the Wilhelmy Plate device, θ_i^{pH} is the corrected contact angle due to a change in the pH of the water , γ_L^{Total} is the theoretical total surface tension of water (=72.8 ergs/cm^2), and γ_{LpH}^{Total} is the surface tension of the water with an altered pH, which was determined using the sessile drop device.

Once the corrected contact angle was determined, Equation 4.4, which is a different form of Equation 4.3, was used to determine the three surface free energy components of the pH altered water and the reference distilled water:

$$\gamma_{LpH}^{Total}\left(1+\cos\theta_i^{pH}\right) = 2\sqrt{\gamma_i^{LW}\gamma_{LpH}^{LW}} + 2\sqrt{\gamma_i^{-}\gamma_{LpH}^{+}} + 2\sqrt{\gamma_i^{+}\gamma_{LpH}^{-}} \tag{4.4}$$

where γ_{LpH}^{Total} is the surface tension of the water with a pH altered or reference distilled water determined using the sessile drop device, θ_i^{pH} is the corrected contact angle determined from the Wilhelmy Plate device using i^{th} binder, subscript i denotes the i^{th} binder, subscript *LpH* denotes the pH altered water or reference distilled water as the case may be, and superscripts Total, LW, +, and – denote the total, Lifshitz-van der Waals, acid, and base components, respectively. Equation 4.4 can be rewritten using Equation 4.3 in terms of the apparent contact angle measured using the Wilhelmy Plate device as follows:

$$\gamma_{LpH}^{Total} + \gamma_L^{Total}\cos\theta_i = 2\sqrt{\gamma_i^{LW}\gamma_{LpH}^{LW}} + 2\sqrt{\gamma_i^-\gamma_{LpH}^+} + 2\sqrt{\gamma_i^+\gamma_{LpH}^-}$$

or

$$\gamma_{LpH}^{LW} + 2\sqrt{\gamma_{LpH}^+\gamma_{LpH}^-} + 72.8(\cos\theta_i) = 2\sqrt{\gamma_i^{LW}\gamma_{LpH}^{LW}} + 2\sqrt{\gamma_i^-\gamma_{LpH}^+} + 2\sqrt{\gamma_i^+\gamma_{LpH}^-} \quad (4.5)$$

From Equation 4.5, it is evident that the three surface free energy components of the water are unknowns, and therefore, contact angles with at least three different asphalt binders are required to backcalculate the surface energy components. As mentioned earlier, in order to improve the robustness of the results, redundancy was introduced in Equation 4.4 by using four asphalt binders with known surface energy components with each pH altered water.

The following procedure was used to compute the three surface free energy components for each pH altered water or reference distilled water. Initial values for three surface free energy components of the pH altered water or reference distilled water were assumed from the theoretical values of distilled water. The sum of square of error (SSE) for the four asphalt binders was determined using Equation 4.6 as follows:

$$SSE = \sum_{i=1}^{4}\left(\gamma_{LpH}^{LW} + 2\sqrt{\gamma_{LpH}^+\gamma_{LpH}^-} + 72.8\cos\theta_i - 2\sqrt{\gamma_i^{LW}\gamma_{LpH}^{LW}} - 2\sqrt{\gamma_i^-\gamma_{LpH}^+} - 2\sqrt{\gamma_i^+\gamma_{LpH}^-}\right)^2 \quad (4.6)$$

Microsoft Excel© Solver was used to minimize the SSE by changing the Lifshitz-van der Waals, acid, and base components of the surface free energy of the pH altered water or reference distilled water using an iterative procedure. Since Equation 4.6 is nonlinear, the

possibility of multiple false solutions exists. In order to minimize this error, the nonpolar, or γ^{LW}, component of surface free energy was fixed at its theoretical value of 21.8 ergs/cm^2 in this project because a change in pH is caused by an increase or decrease in the positively or negatively charged ions in a solution, and therefore, theoretically, should not affect the γ^{LW} component of surface free energy. Once this is completed, the acid and base components of surface free energy of the different pH modified waters can be calculated.

MATERIALS

There were four asphalts and four aggregates used in this project. Since the asphalt binders were also used in the previous chapter, the same labeling system was followed. All asphalt binders were PG 76-22 S with no aging and no anti-strip agents added. These asphalt binders were chosen for their variable surface free energy components, measured using the Wilhelmy Plate method, shown in Table 4.1. Asphalt O had a very high acid component, Asphalt K and P had a higher basic component, and Asphalt L was almost totally non-polar.

Table 4.1. Asphalt Surface Free Energy Components.

Asphalt	γ^{LW}	γ^{+}	γ^{-}	γ^{TOTAL}
K	22.68	0.00	0.88	22.77
L	19.24	0.00	0.07	19.24
O	10.24	1.50	1.27	13.00
P	17.20	0.19	1.18	18.14

The four aggregates used in this project were granite, sandstone, granite-sandstone mix, and river gravel. Table 4.2 displays the labeling scheme used for the aggregates. Aggregate W is a granite with low concentration of quartz, a high concentration of albite and anorthite, and appears to be quartz monzodiorite. Aggregate C is a quartz rich sandstone. Aggregate M is a mixture of granite and sandstone, and aggregate R is a river gravel. A detailed mineralogical composition of these aggregates was not available to the authors at the time of this project.

Table 4.2. Aggregate Label and Type.

Aggregate	Mineralogy
W	Granite
C	Sandstone
M	Granite-Sandstone Mix
R	River Gravel

RESULTS AND DISCUSSION

The total surface tensions of the pH altered water were measured using the sessile drop method. Table 4.3 below displays the results of the tests. Researchers acquired these results using the same procedure listed in the methodology and the same technique shown in Figure 4.2. The total surface tension of the five measured liquids does not change significantly, as is clearly shown in Table 4.3. The highest percent change between the total surface tension of the theoretical water and one of the measured waters occurred in water modified with aggregate W. This percent change was only 0.824 percent (or 0.6 ergs/cm^2) and is not large enough to warrant a change in the surface free energy. If distilled water is used as a basis, then the maximum percent change occurs with water modified with aggregate C. This percent change was less than 1 percent (or 0.7 ergs/cm^2). The differences in the total surface tension of the various waters are not great enough to warrant concluding that there is any change in the total surface tension of the waters due to a change in the pH.

Table 4.3. Surface Tensions of Water with Different Aggregates Measured Using Sessile Drop Method.

Water with Aggregate	Total Surface Tension
Theoretical	72.80
W	73.4
C	72.3
M	72.9
R	73
Distilled Water	73

While the total surface tension or surface free energy of the pH altered water did not change significantly, the Wilhelmy Plate device was used to assess if there are any differences in the surface energy components of the pH altered water. Table 4.4 displays the surface free energy components and total surface free energy of the water with the different aggregates submerged in it. Figure 4.3 displays the same information, except it is in a graphical form. These values were calculated from the contact angles measured using the Wilhelmy Plate method as described in the previous section.

The total surface free energy of the pH altered water was not significantly different from the reference distilled water as determined using the Wilhelmy Plate device (Table 4.4). This conclusion is consistent with the conclusion made based on measurements using the sessile drop device. However, there is a bias between the results obtained for the total surface energy using the Wilhelmy Plate device versus the sessile drop method. This bias was attributed to two factors. Firstly, there is a systematic error in the Wilhelmy Plate balance calibration that was corrected subsequent to the completion of the tests. Secondly, there is an inherent systematic error involved in this methodology because theory and lab measurements are used twice consecutively to arrive at the final values. Intrinsic theoretical and measurement errors are propagated when the surface free energy components of the four asphalt binders were determined using measurements with four probe liquids. These errors are further propagated when the four asphalt binders were used to calculate the surface free energy components of the pH altered water. The apparently lower acid component compared to the base component is also an artifact of these error propagations. Not withstanding these limitations in the backcalculation approach, a comparison between the respective surface energy components for the pH altered water and reference distilled water can still be made.

With respect to the reference distilled water, the total surface tension or surface free energy of the pH altered waters varied from -1.03 to 0 ergs/cm^2 with no specific trend with respect to the pH value. Similarly, the variation in acid and base components with reference to the distilled water was -0.50 to +1.07 and -2.42 to +0.92 ergs/cm^2, respectively. In general, the variations in the surface energy components were small compared to the reference values and showed no specific trend with respect to the pH of the water.

Table 4.4. Surface Free Energy Components of Water Modified with Different Aggregates in ergs/cm^2.

Water with Aggregate	pH	Acid Component (Δ with respect to distilled water)	Base Component (Δ with respect to distilled water)	Total (Δ with respect to distilled water)
Distilled Water	7.27	16.77 (+0.00)	30.64 (+0.00)	67.14 (+0.00)
Aggregate C	8.13	17.57 (+0.80)	28.54 (-2.10)	66.59 (-0.55)
Aggregate R	8.24	17.11 (+0.34)	28.68 (-1.96)	66.11 (-1.03)
Aggregate M	8.28	16.27 (-0.50)	31.56 (+0.92)	67.12 (-0.02)
Aggregate W	8.42	17.84 (+1.07)	28.22 (-2.42)	66.68 (-0.46)

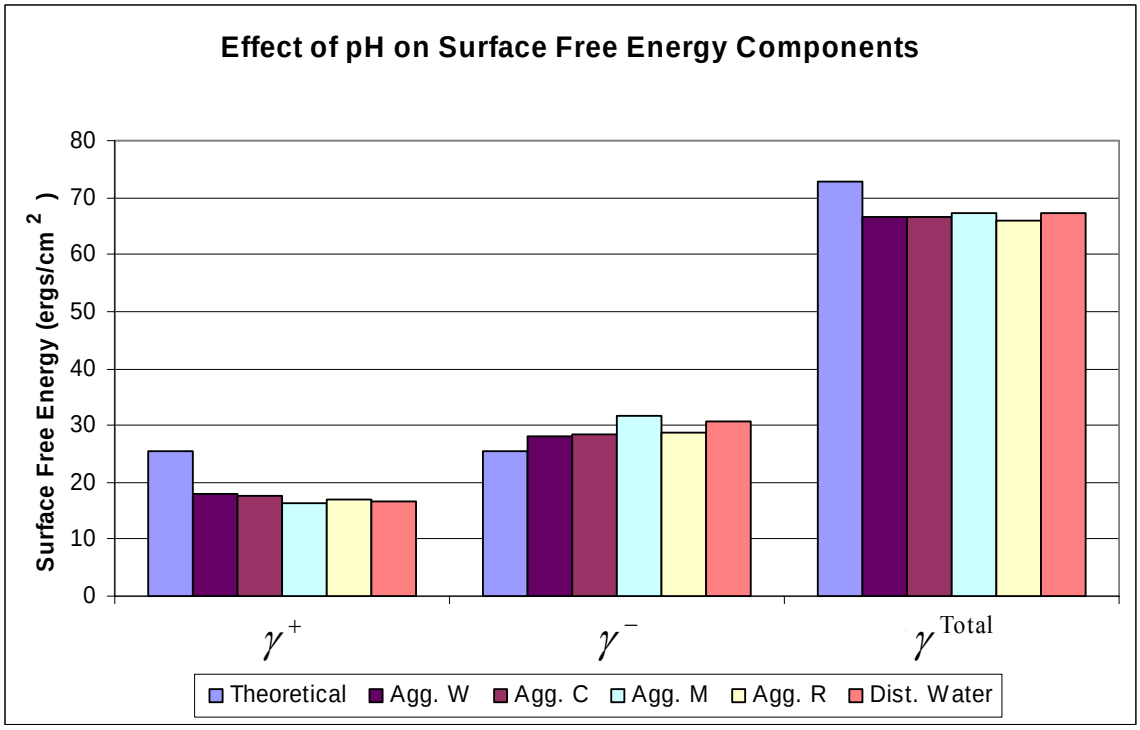

Figure 4.3. Graph of Surface Free Energy Components of Water Modified with Different Aggregates.

SUMMARY

No significant changes in the total surface free energy or the acid and base components of surface free energy were observed with respect to the reference distilled water. Within the range of pH that was achieved by exposing distilled water to aggregates in this project, there is no significant correlation between the change in surface free energy components and the pH of the water.

CHAPTER 5
IMPROVED METHOD FOR DYNAMIC MECHANICAL ANALYSIS AND SPECIMEN PREPARATION

INTRODUCTION

In the first phase of this project, the researchers evaluated the moisture susceptibility of asphalt mixtures by testing mixtures of asphalt and fine aggregates using the DMA method. TxDOT Report 0-4524-2 documented the results of the DMA experiments and results. In the second phase of the project, the researchers refined the methods for the preparation of the DMA specimens and the data analysis. The new analysis method can be used for DMA testing under both controlled stress and controlled strain loading. This chapter provides a description of these refined methods. Appendix A includes description of the method that was used in phase 1 for the preparation of DMA specimens. Appendix B includes a description of the refined method in which the asphalt binder in the DMA specimen is calculated based on the asphalt content in the full mixture.
The proportions of the fine aggregate used to fabricate the DMA specimen were scaled to represent the gradation of the full mixture (Masad et al., 2006)

DMA SPECIMEN PREPARATION

Two methods documented in the current literature to prepare DMA specimens were proposed and used by Kim and Little (2003) and Lytton et al. (2005). The first method, by Kim and Little, focused on testing mastic (filler and binder). In this method, the filler volume to asphalt binder volume proportion is fixed at 10 percent. The mastic is mixed with Ottawa sand such that the mastic weight divided by the weight of Ottawa sand is 8 percent. The total weight of mixture is 15 g. After it is cooled, 11.5 g of the mixture is reheated and placed in a special mold fabricated for this purpose and compacted using static pressure. The mixture is allowed to cool in the mold for 30 minutes, after which specimens are extracted. A DMA specimen is, 50 mm in height, 12 mm in diameter, and has a typical air void content around 17 percent. Figure 5.1(a) shows the mold used by Kim and Little to compact DMA specimens (Kim and Little, 2003).

The second method, proposed by Lytton et al. (2005), was developed to test sand asphalt mixtures in which the fine aggregate from the actual mixture, rather than Ottawa sand, is used to prepare DMA specimens. The proportions of the fine aggregate used to fabricate the DMA specimen were scaled to represent the gradation of the full mixture. However, the filler volume to asphalt binder volume and the filler weight to the fine aggregate weight were kept similar to the method by Kim and Little (2003). The total weight of mixture is 15 g. In this method, the asphalt mastic is mixed with the fine aggregates using a mechanical mixer, rather than by hand. The mixture is then short-term aged for 2 hours at mixing temperature and 1 hour at compaction temperature. The Superpave gyratory compactor (SGC) is used in this method to compact the mixture and prepare gyratory specimens of 152 mm in diameter and 85 mm in height. The target air void is 11 percent. SGC specimens are then cored from top to bottom to obtain DMA specimens (50 mm in height and 12 mm in diameter). Approximately 32 DMA samples are extracted from an SGC specimen. Figure 5.1(b) shows a gyratory specimen after coring DMA specimens. The proportions of the fine aggregate used to construct the DMA specimen were based on their subsequent proportions in the full mix. These proportions are determined using simple volumetric analysis as shown in Appendix A. Prior to test execution, all specimens were glued to sample holders at the top and bottom using Devcon 5, which requires at least 30 minutes to stiffen. It is important to fill the holder completely with the glue to avoid cracks in the top of the sample. One shortcoming Zollinger noted was the use of exactly the same binder content regardless of aggregate shape characteristics (Zollinger, 2005).

In the second phase of the project, the researchers refined the method used in phase 1 such that the asphalt binder in DMA specimens is calculated based on the asphalt binder in the full asphalt mixtures. Appendix B summarizes this refined method.

(a) Sample compaction mold (1st method)

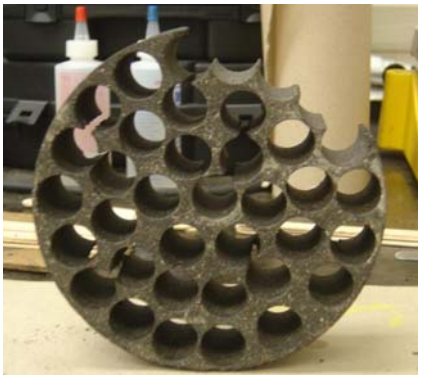

(b) SGC sample after DMA sample extraction (2nd method)

Figure 5.1. DMA Sample Fabrication Methodologies.

ANALYSIS OF TEST DATA FROM DMA SAMPLES

The frequency sweep mode is used for both the controlled-strain and controlled-stress tests. This specific mode applies a fixed frequency (in this case 10 Hz) with a fixed value of either shear stress or shear strain. During the tests, the DMA sample is subjected to sinusoidal torsional loading. All tests are conducted at 25ºC. Both the controlled-strain and controlled-stress tests are performed in two different stages: (1) using low strain or stress amplitude to obtain material properties in the linear viscoelastic range, and (2) using high strain or stress amplitude to induce fatigue damage. The stresses used in the low-amplitude testing are selected to correspond to a strain of 0.0065 percent. The stresses used in the high-amplitude loading in controlled-stress testing correspond to the stresses measured at 50 percent of the fatigue life in the controlled-strain tests. Data are collected every five cycles with 128 points being recorded per cycle. Relaxation tests are also performed to determine relaxation moduli as a function of time; see Equation 5.1.

$$E(t) = \frac{\sigma(t)}{\varepsilon_o} = E_\infty + E_1 t^{-m} \tag{5.1}$$

Theoretical Background for the Analysis of DMA Data

The stress-pseudo strain relationship within the framework of continuum damage mechanics has been used for the characterization of damage in asphalt mixtures. The underlying concept in this approach is based on separating the energy that is dissipated by causing damage from the viscoelastic energy. Two tests are needed to develop the stress-pseudo strain relationship. The first test was conducted at small stress or strain values and is used to determine the linear viscoelastic properties. Next, a fatigue test was conducted at higher stress or strain values in order to induce damage and characterize the asphalt mixture's fatigue resistance. In principle, it is possible to induce damage by conducting long term fatigue loading at the same stress or strain values that are used to determine the linear viscoelastic properties. However, this approach is time-consuming, and it might even prohibit characterization of fatigue damage if the applied stress or strain magnitudes are within the endurance limit of the asphalt mixture.

Under sinusoidal stress loading, the stress and strain functions for an undamaged viscoelastic material are described using Equations 5.2 and 5.3, respectively.

$$\sigma = \sigma_0 \sin(wt) \tag{5.2}$$

$$\varepsilon = \varepsilon_{0VE} \sin(wt - \delta_{VE}) \tag{5.3}$$

where σ_0 and ε_{0VE} are the stress and strain amplitudes, respectively; w is the angular frequency; t is the time; and δ_{VE} is the viscoelastic phase angle between the stress and strain responses. The subscript VE refers to viscoelastic properties that the material would attain if it did not exhibit damage at the stress and strain levels used in the fatigue test. As will be discussed later, subscript VE can refer to either linear or nonlinear viscoelastic response and properties. The 0 subscript refers to the amplitude of the strain sinusoidal function.

The pseudo energy can be calculated using a pseudo stress-strain relationship or using a stress–pseudo strain relationship. The latter relationship is formulated here in order to allow direct comparison between the results from the controlled-stress and

controlled-strain tests. Under controlled-strain fatigue loading, the applied strain and the stress response will have the forms listed in Equations 5.4 and 5.5, respectively.

$$\sigma = \sigma_{0NF} \sin(wt + \delta_{NF}) \tag{5.4}$$

$$\varepsilon = \varepsilon_{0F} \sin(wt) \tag{5.5}$$

where the F subscript indicates that the labeled quantities (stress, strain, and material properties) are associated with the fatigue test. The N subscript indicates that the parameter changes as a function of the number of loading cycles. The pseudo strain is given by Equation 5.6:

$$\varepsilon^R = \frac{E^*_{VE}\varepsilon_{0F} \sin(wt + \delta_{VE})}{E_R} \tag{5.6}$$

where E_R is the reference modulus, and its selection is discussed later. Basically, the pseudo strain is the viscoelastic stress response of the material divided by E_R. This is based on the assumption that the material is not damaged under the applied strain function shown in Equation 5.4.

Under controlled-stress fatigue loading, the applied stress and the strain response will have the forms presented in Equations 5.7 and 5.8, respectively.

$$\sigma = \sigma_{0F} \sin(wt) \tag{5.7}$$

$$\varepsilon = \varepsilon_{0NF} \sin(wt - \delta_{NF}) \tag{5.8}$$

If the material is undamaged and subjected to the strain function in Equation 5.8, then the corresponding undamaged stress for this strain is shown in Equation 5.9.

$$\sigma = E_{VE}^{*}\varepsilon_{0NF}\sin(wt - \delta_{NF} + \delta_{VE}) \tag{5.9}$$

The pseudo strain under stress-controlled loading is the function in Equation 5.9 divided by the reference modulus:

$$\varepsilon^{R} = \frac{E_{VE}^{*}\varepsilon_{0NF}\sin(wt - \delta_{NF} + \delta_{VE})}{E_{R}} \tag{5.10}$$

The various stress-pseudo strain behaviors are illustrated in Figure 5.2 for different material conditions (linear viscoelastic, nonlinear viscoelastic, and damage). Consider the case where the linear viscoelastic condition is taken as the undamaged reference state (the linear viscoelastic properties are used in the pseudo strain functions in Equations 5.6 and 5.10), and the fatigue test starts with a stress level within the linear viscoelastic range. In this case, $\delta_{NF} = \delta_{VE}$ and the stress-pseudo strain response will be represented by the line "A" because Equations 5.7 and 5.10 are in phase. If the applied stress increases but remains within the linear viscoelastic range, then the stress-pseudo strain relationship will be represented by the line labeled "B" in Figure 5.2. However, an increase in stress can cause one of the following responses:

- damage of the linear viscoelastic material,
- nonlinear viscoelastic response of the intact (undamaged) material, and
- combined nonlinear viscoelastic response of the intact material and damage.

Damage is identified by a decrease in the modulus and an increase in the phase angle. The values of these properties, as well as the area of the hysteresis loop continue to change as loading cycles are applied. This case is represented by curve "C," which becomes curve "D" as fatigue loading and damage proceed.

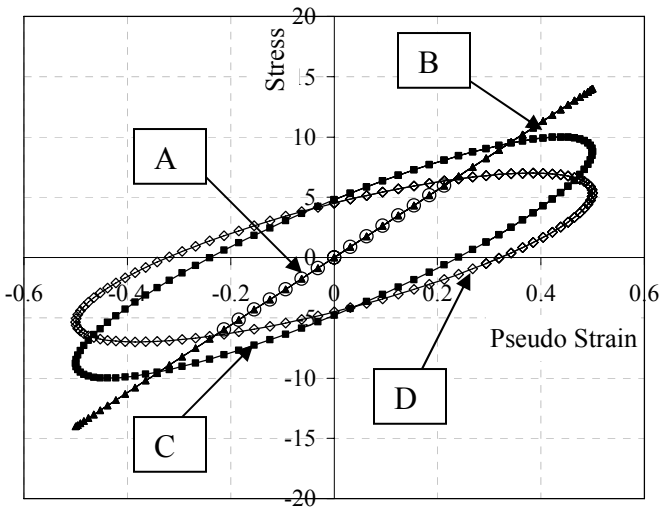

Figure 5.2. Illustrations of the Different Possible Responses of Stress-Pseudo Strain Relationships.

A decrease in the modulus and an increase in the phase angle relative to the linear viscoelastic properties also occur due to the nonlinear behavior of the intact material. However, as pointed out by Si et al. (Si et al., 2002), the nonlinear viscoelastic properties (phase angle and modulus) and the nonlinear hysteresis loop remain unchanged as further loading is applied. This behavior is represented in Figure 5.2 by the curve labeled "C" that does not shift to position "D" with further loading as long as damage is not initiated.

It is also possible that the response combines both nonlinear viscoelastic behavior and damage. The energy consumed by the nonlinear viscoelastic behavior can be separated from damage by properly selecting stress and strain magnitudes used in the fatigue test. These magnitudes can be selected such that no damage is observed (no change in the stress-pseudo strain relation) for a number of load cycles. Following this, loading can proceed in order to determine the energy associated with damage. Once the nonlinear viscoelastic properties are determined, they can be used as $\left|E^*_{VE}\right|$ and δ_{VE} in Equations 5.6 and 5.10 in order to calculate the pseudo strain that accounts for the undamaged nonlinear state at the high stresses and strains used in the fatigue test. In this case, Curve "C" in Figure 5.2 will become a line indicating that there is no damage at this state of stress.

Fatigue damage in Hot Mix Asphalt (HMA) is manifested as an increase in the apparent phase angle and a decrease in the pseudo stiffness. The term "apparent" is used here to indicate that this phase angle is not the same as the phase angle associated with viscoelastic deformation as it accounts for the effect of damage. In controlled-strain loading, the decrease in stiffness is associated with a decrease in the applied stress and a decrease in the area of the hysteresis loop, while the increase in the apparent phase angle causes an increase in the hysteresis loop. As such, the two manifestations of damage (increase in phase angle and decrease in stiffness) have opposing effects on the hysteresis loop area but with the net results being a decrease in the area. In controlled-stress loading, changes in both the apparent phase angle and stiffness cause an increase in the hysteresis loop area. Hence, the effect of damage on the hysteresis loop area depends on the mode of loading, and consequently, the loop areas calculated from the two modes of loading are not comparable.

A new approach is proposed here by which to calculate the dissipated energy. This approach divides the dissipated pseudo strain energy (DPSE) into three components. The first component accounts for damage that causes an increase in the apparent phase angle and an increase in the hysteresis loop area with respect to a reference modulus that represents the intact undamaged material. For controlled-strain loading, the hysteresis loop in the stress-pseudo strain domain can be represented by the following equation:

$$DPSE = \pi\sigma_{0NF}\varepsilon_0^R \sin(\delta_{NF} - \delta_{VE}) \tag{5.11}$$

The above equation can also be written as follows:

$$DPSE = \pi\sigma_{0NF}\frac{\sigma_{0VE}}{E_R}\sin(\delta_{NF} - \delta_{VE}) = \pi\sigma_{0NF}\frac{E_{VE}^*\varepsilon_{0F}}{E_R}\sin(\delta_{NF} - \delta_{VE}) \tag{5.12}$$

The reference modulus E_R can be selected to be equal to the undamaged modulus E^*_{VE}. This selection has the advantage of making the amplitude of the pseudo strain equal to the amplitude of the actual strain. The DPSE becomes equal to:

$$DPSE = \pi\sigma_{0NF}\varepsilon_{0F}\sin(\delta_{NF} - \delta_{VE}) = \pi E^*_{NF}\varepsilon^2_{0F}\sin(\delta_{NF} - \delta_{VE}) \tag{5.13}$$

As discussed earlier, as the level of material damage increases, the modulus E^*_{NF} decreases while the apparent phase angle δ_{NF} increases, and the net result is a decrease in the DPSE. The effect of these two factors can be separated by dividing the DPSE by the ratio of the damage stiffness to the undamaged stiffness $\left(\frac{E^*_{NF}}{E^*_{VE}}\right)$ as follows:

$$W_{R1} = \pi E^*_{VE}\varepsilon^2_{0F}\sin(\delta_{NF} - \delta_{VE}) \tag{5.14}$$

The above expression gives the dissipated energy due to an increase in the apparent phase angle at a given reference undamaged modulus. It can also be viewed as the change in the viscoelastic energy $E^*_{VE}\varepsilon^2_{0F}$ due to damage that is quantified by the change in the phase angle from δ_{VE} to δ_{NF}.

The second component of the dissipated energy is due to permanent deformation caused by the loading and unloading within each cycle. The hysteresis loop area divided by $\frac{E^*_{NF}}{E^*_{VE}}$ is always larger than the area calculated using Equation (5.14). The difference between the actual hysteresis loop and the idealized loop, shown in Figure 5.3, is attributed to permanent deformation in the mixture and is denoted as W_{R2}. During the first quarter of a loading cycle, damage is induced due to the increase in stress magnitude. Upon unloading in the second quarter of the cycle, some permanent strain remains in the specimen, which is manifested by a variable apparent phase angle within the cycle.

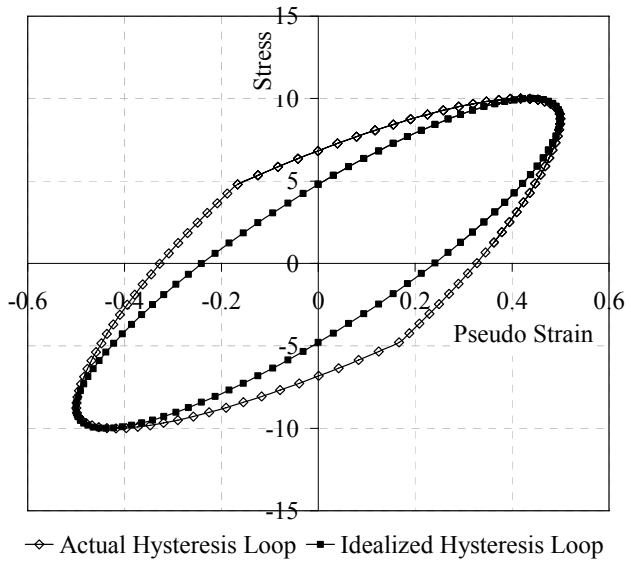

Figure 5.3. Illustration of the Idealized Hysteresis Loop and Actual Hysteresis Loop.

The third component of the dissipated energy, W_{R3}, is associated with the difference between the pseudo stiffness of the undamaged material and the pseudo stiffness after damage. The dissipated energy associated with the reduction in the pseudo stiffness is calculated as follows:

$$W_{R3} = \frac{1}{2}\varepsilon_{0F}^{R}\left(\sigma_{0VE} - \sigma_{0NF}\right) = \frac{1}{2}\frac{\sigma_{0VE}}{E_R}\left(\sigma_{0VE} - \sigma_{0N}\right) \tag{5.15}$$

and for $E_R = E_{VE}^{*}$, W_{R3} becomes:

$$W_{R3} = \frac{1}{2}\frac{E_{VE}^{*}\varepsilon_{OF}}{E_{VE}^{*}}\left(E_{VE}^{*}\varepsilon_{OF} - E_{NF}^{*}\varepsilon_{OF}\right) = \frac{1}{2}\varepsilon_{OF}^{2}\left(E_{VE}^{*} - E_{NF}^{*}\right) \tag{5.16}$$

The same analysis presented above can be applied in the controlled-stress case, and the DPSE can be written as in Equation 5.17:

$$DPSE = \pi\sigma_{0F}\varepsilon_{0NF}\sin(\delta_{NF} - \delta_{VE}) = \pi\frac{\sigma_{0F}^{2}}{E_{NF}^{*}}\sin(\delta_{N} - \delta_{VE}) \tag{5.17}$$

The above equation is multiplied by $\left(\frac{E^*_{NF}}{E^*_{VE}}\right)$ in order to calculate the dissipated energy in the hysteresis loop at the reference undamaged pseudo stiffness. The expression for W_{R1} becomes:

$$W_{R1} = \pi \frac{\sigma^2_{OF}}{E^*_{VE}} sin\left(\delta_{NF} - \delta_{VE}\right) \tag{5.18}$$

The above expression has the same significance as in controlled-strain loading as it represents the effect of damage, which changes the phase angle from δ_{VE} to δ_{NF} on the viscoelastic energy $\frac{\sigma^2_{0F}}{E^*_{VE}}$. The expression for W_{R3} is:

$$W_{R3} = \frac{1}{2}\sigma_{0F}(\varepsilon^R_{0NF} - \varepsilon^R_{0VE}) = \frac{1}{2}\sigma_{0F}\left(\frac{E^*_{VE}\sigma_0}{E^*_{NF}E_R} - \frac{E^*_{VE}\sigma_0}{E^*_{VE}E_R}\right) \tag{5.19}$$

and for $E_R = E^*_{VE}$, W_{R3} becomes:

$$W_{R3} = \frac{1}{2}\sigma^2_{0F}\left(\frac{1}{E^*_{NF}} - \frac{1}{E^*_{VE}}\right) \tag{5.20}$$

Fracture-Based Analysis Approach for Asphalt Mixtures

The crack growth potential was used to evaluate the moisture susceptibility of the asphalt mix specimens. The equation to estimate the crack growth was derived from Paris' law, which can be expressed in terms of the J-integral as follows (Lytton et al. 1993):

$$\frac{dr}{dN} = A\left(J_R\right)^n \tag{5.21}$$

where r is the average crack radius, N is the number of load cycles, A and n are material constants, and J_R is the J-integral, which can be expressed as the change in pseudo strain energy per unit volume of the intact material with respect to the change in crack surface area (*c.s.a*) as follows:

$$J_R = \frac{\partial W_R}{\partial (c.s.a.)} = \frac{\frac{\partial W_R}{\partial N}}{\frac{\partial (c.s.a)}{\partial N}} \tag{5.22}$$

Researchers assumed that *c.s.a.* has a value of $2\pi r^2$. Based on the experimental results, it was found that a linear relationship exists between the normalized pseudo strain energy and the natural logarithm of the load cycles, $W_R = a + b \ln(N)$. Therefore, $b = \partial WR / \partial \ln(N)$ and the expression for the J-integral become:

$$J_R = \frac{\frac{\partial W_R}{\partial \ln N}\frac{d \ln N}{dN}}{4\pi r \frac{dr}{dN}} = \frac{b}{4\pi r N \frac{dr}{dN}} \tag{5.23}$$

$$J_R = \frac{b}{4\pi r N \frac{dr}{dN}} \tag{5.24}$$

The value of the constant A has been expressed by Lytton et al. (1993) as:

$$A = k\left(\frac{E_R}{E_1 \Delta G_f - E_1 E_\infty E_R J_R}\right)^n \left(\frac{1}{\sigma_t^{\,2} I_1}\right)^n \int_0^{\Delta t} (w(t))^n \, dt \tag{5.25}$$

where k is a material constant, E_1 is the initial relaxation modulus, ΔG_f is the partial wet adhesive bond surface energy between the asphalt binder and the aggregate, E_∞ is the final value of the relaxation modulus after a long elapsed time, E_R is the reference modulus, σ_t is the tensile strength of the material, I_1 is a parameter that describes the shape of the

stress-strain curve, and *w(t)* is a function that describes the shape of the applied load with respect to time.

The material constant *k* is different for each material but varies only slightly between various materials. For simplicity, *k* is assumed to have a value of 1. In the type of tests conducted in this project the term with E_∞ is much smaller than $E_1\Delta G_f$. Therefore, the denominator of the first bracket is reduced to $E_1\Delta G_f$. The shapes of the stress-strain curves are similar for the mixtures used in this project, and thus, the parameter I_1 can be assumed to be the same and equal to 1 for all mixes. In addition, since an identical sinusoidal loading shape is applied to all specimens, the value of $\int_0^{\Delta t} (w(t))^n \, dt$ is equal for all specimens. These considerations reduce the expression for *A* to:

$$A = k\left(\frac{E_R}{E_1 \Delta G_f \sigma_t^{\,2}}\right)^n \tag{5.26}$$

Substituting the terms of *A* and J_R back in the Paris' law equation gives:

$$\frac{dr}{dN} = k\left(\frac{E_R}{E_1 \Delta G_f \sigma_t^{\,2}}\right)^n \left(\frac{b}{4\pi r N \frac{dr}{dN}}\right)^n \tag{5.27}$$

The above equation can be rearranged to give the following expression:

$$\left(\frac{dr}{dN}\right)^{1+n} r^n = k\left(\frac{E_R}{E_1 \Delta G_f \sigma_t^{\,2}}\right)^n \left(\frac{b}{4\pi N}\right)^n \tag{5.28}$$

$$(dr)^{1+n} r^n = k\left(\frac{E_R}{E_1 \Delta G_f \sigma_t^{\,2}}\right)^n \left(\frac{b}{4\pi}\right)^n \left(\frac{dN^{1+n}}{N^n}\right) \tag{5.29}$$

Integrating both sides gives the following:

$$\int_{r_0}^{r} r^{\frac{n}{1+n}} dr = k^{\frac{1}{1+n}} \left(\frac{E_R}{E_1 \Delta G_f \sigma_t^{\,2}} \right)^{\frac{n}{1+n}} \int_1^N \left(\frac{b}{4\pi} \right)^{\frac{n}{1+n}} \left(\frac{dN}{N^{\frac{n}{1+n}}} \right) \tag{5.30}$$

$$\frac{(r)^{\frac{2n+1}{1+n}} - (r_o)^{\frac{2n+1}{1+n}}}{\left(\frac{2n+1}{1+n} \right)} = k^{\frac{1}{1+n}} \left(\frac{E_R}{E_1 \Delta G_f \sigma_t^{\,2}} \right)^{\frac{n}{1+n}} \left(\frac{b}{4\pi} \right)^{\frac{n}{1+n}} (1+n) \left(N^{\frac{1}{1+n}} - 1^{\frac{1}{1+n}} \right) \tag{5.31}$$

The equation to estimate the crack growth in the asphalt mix specimens can be expressed as:

$$r = \left[r_o^{\frac{2n+1}{1+n}} + (2n+1) \left(\frac{bE_R}{4\pi E_1 \Delta G_f \sigma_t^{\,2}} \right)^{\frac{n}{1+n}} \left(N^{\frac{1}{1+n}} - 1^{\frac{1}{1+n}} \right) \right]^{\frac{1+n}{2n+1}} \tag{5.32}$$

The r_o corresponds to the initial damage in the mix. Since all specimens were prepared using the same method, the analysis was conducted by assuming r_o to be the same for the mixtures, and consequently, r_o was dropped from Equation (5.14). The crack growth index used in this project is shown in Equation 5.33:

$$r = \left[(2n+1) \left(\frac{bE_R}{4\pi E_1 \Delta G_f \sigma_t^{\,2}} \right)^{\frac{n}{1+n}} \left(N^{\frac{1}{1+n}} - 1^{\frac{1}{1+n}} \right) \right]^{\frac{1+n}{2n+1}} \tag{5.33}$$

The viscoelastic properties of the intact material ahead of the crack affect the rate of crack propagation. Schapery (1981) derived the relationship between the exponent *n* in Equation 5.21 and *m,* which is the exponent of time in the power law equation of the relaxation modulus. He found that if the surface energy of the material and the fracture

process zone with length α ahead of the crack are constants, then $n = 1/m$. If the tensile strength of the material and surface energy are constants during fracture, then $n = 1 + 1/m$. The third case is when the crack opening displacement at the left end of the failure zone and α are constants. In this case, $n = 1/(m \times (1+N))$. N is the nonlinearity exponent for the continuum in the neighborhood of the crack tip.

CHAPTER 6
MOISTURE SUSCEPTIBILITY OF ASPHALT MIXTURES WITH KNOWN FIELD PERFORMANCE USING DYNAMIC ANALYSIS AND A CRACK GROWTH MODEL

INTRODUCTION

Moisture damage in asphalt mixtures refers to the loss in strength and durability due to the presence of water. The level and extent of moisture damage, also called moisture susceptibility, depends on environmental, construction, and pavement design factors; internal structure distribution; and the quality and type of materials used in the asphalt mixture.

This project evaluates the moisture susceptibility of asphalt mixtures with known field performance using dynamic analysis and a crack growth model to characterize both the asphalt mixtures and corresponding asphalt mastics. The model parameters were obtained from surface energy measurements, uniaxial dynamic testing for the asphalt mixtures, and dynamic shear testing for the asphalt mastics. The results showed good differentiation between the moisture conditioned (wet) and unconditioned (dry) specimen behavior and provided a good correlation with the reported field performance of the asphalt mixtures.

Many of the principal distresses that affect asphalt pavements relate to a phenomenon called moisture damage, a term that refers to the detrimental effects of water. The level and extent of the damage relates to the environmental conditions, the quality of the construction techniques, the adequacy of the pavement structure and mixture design, the type of aggregate and asphalt binder used in the asphalt mixture, and the internal structure distribution in the asphalt mixture. Although not necessarily initiated by the presence of water, most distresses increase their extent and severity due to the presence of water and moisture and cause a loss of bond between the aggregate and the asphalt binder (Miller and Bellinger [2003]).

Two of the principal mechanisms that induce moisture damage in the asphalt mixture are advective flow and water diffusion (Kringos and Scarpas [2005]). Advective

flow occurs when water causes desorption of the outer layers of the asphalt mastic ultimately breaking the bond between the asphalt mastic and the aggregate. Diffusion, on the other hand, occurs when water coming from an underground source or moisture from the environment permeates through the asphalt mastic, diminishing its cohesive bond strength. When the asphalt mastic coating the aggregate is completely displaced by water, a distress called stripping becomes visible in the asphalt mixture. The chemical composition of the aggregate and its affinity to the asphalt binder influence the severity of stripping (Emery and Seddik [1997]). In addition, the aggregate surface characteristics such as roughness and texture also play an important role in the occurrence of stripping, with smooth and rounded aggregates exhibiting greater stripping potential (McGennis et al. [1984]).

In the past, researchers focused on evaluating moisture damage by performing laboratory tests on asphalt mixtures, which indirectly measured damage either qualitatively or quantitatively. In the 1920s, the first tests to evaluate moisture damage were the static immersion test and the boiling test (Solaimanian [2003]). Both tests, applied to loose asphalt mixtures, were based on a visual inspection of the specimens after moisture conditioning to determine the degree of damage. Consequently, the evaluation of damage in these qualitative tests was subjective. During the 1940s and 1950s, quantitative test methods performed on compacted asphalt mixtures, including the immersion compression test, were introduced. In those tests, the ratio of results on unconditioned (dry) and moisture conditioned (wet) specimens was used to determine moisture susceptibility (Solaimanian [2003]). During the 1960s and 1970s, greater understanding of moisture damage mechanisms resulted in the development of different test protocols, including the modified Lottman test. This procedure is still widely used and required by the state-of-the-practice Superpave system, (The Asphalt Institute [1995]). An indirect tensile test and a ratio of wet to dry strength greater than or equal to 0.8 is required for an adequate performance. In the 1980s and 1990s, new test procedures were developed including the Environmental Conditioning System and the Hamburg wheel tracking device (Solaimanian [2003]).

The reduction of strength in the asphalt mixture after moisture conditioning is related to the air void content and structure. Based on this observation, researchers

classified asphalt mixtures as impermeable, pessimum voids (7 to 13 percent air voids), and free drainage (Terrel and Al-Swailmi [1994]). The pessimum voids range, where maximum moisture damage occurred, was further explored by analyzing asphalt mixtures with different gradations but the same air void content. The average void diameter was determined using X-ray computed tomography (CT) and correlated with parameters such as the energy ratio and the number of cycles to failure (Masad et al. [2006]) and Birgisson et al. [2003]). The observed shape of the correlation curves was the same as the one obtained by Terrel and Al-Swailmi (1994), indicating that a pessimum size concept also exists and a specific range of air void sizes maximizes moisture damage.

A crack growth model was recently developed to evaluate the performance and moisture sensitivity of asphalt mixtures and asphalt mastics, which includes several mechanical and surface energy properties. This model gave promising results in distinguishing wet and dry behavior and the effect of air void distribution (Lytton et al. [2005] and Arambula et al. [In press]).

OBJECTIVES AND TASKS

The primary objective of this project was to examine the validity and applicability of the crack growth model in predicting the moisture susceptibility of asphalt mixtures with known field performance. This objective was achieved by:

- dynamic testing of asphalt mixtures,
- analysis to determine the crack growth model parameters,
- surface energy measurements of the aggregates and asphalt binders,
- dynamic testing and analysis for asphalt mastics, and
- comparison of the analysis results with field performance.

Subsequent sections describe the methodology and results of this project. The first section describes the characteristics of the selected asphalt mixtures and asphalt mastics. The next section includes a brief description of the crack growth model with details provided elsewhere (Arambula et al. [In press]). Then, a description of the materials' characterization and the mechanical and surface energy tests performed to obtain the inputs

for the model is provided. The following section includes the results, and a summary section completes the chapter.

DESCRIPTION OF MIXTURES AND FIELD PERFORMANCE

A description of the mixtures selected for this project in terms of their type, location, aggregate and asphalt binder type, and reported field performance is presented in Table 6.1. Figure 6.1 presents the aggregate gradations. The in-place air voids required for dense-graded mixtures in Texas is from 5 to 9 percent, and in Ohio, the requirement is approximately 4 to 8 percent Texas Department of Transportation [2004] and Ohio Department of Transportation [2005].

Table 6.1. Mixture Descriptions (Lytton et al. [2005]).

Mixture	Highway	Mixture Type	Location	Field Moisture Performance	Aggregate Type	Binder Grade
A	Texas IH 20	Superpave	Atlanta, TX	Good	River Gravel	PG 76-22
B	Ohio SR 511	Type 1	Ashland County, OH	Fair to Poor	Gravel, Limestone, Reclaimed Asphalt Pavement (RAP)	PG 64-22
C	Ohio SR 226	Type 1 Intermediate	Wayne County, OH	Poor	Gravel, RAP	PG 64-28

Mixture A was used by the TxDOT in Harrison County in the construction of Interstate Highway 20. The mixture design included 67 percent siliceous river gravel, 32 percent limestone screenings, and 1 percent hydrated lime. The asphalt binder content was 5 percent by weight of the mixture. Based on field and laboratory test results, Mixture A exhibited overall good performance and did not exhibit evidence of moisture damage (Lytton et al. [2005]). Mixture A is the same as Mixture 5 in the report by Lytton et al. (2005).

Mixture B was constructed on State Route 511 in Ashland County, Ohio. It included 32 percent limestone, 22 percent gravel, 26 percent natural sand, and 20 percent reclaimed asphalt pavement (RAP). During specimen preparation, the RAP material was proportionally replaced with the other aggregates in the mixture. Therefore, the final mixture proportion included 40 percent limestone, 27.5 percent gravel, and 32.5 percent natural sand. The asphalt binder content was 5.4 percent by weight of the mixture.

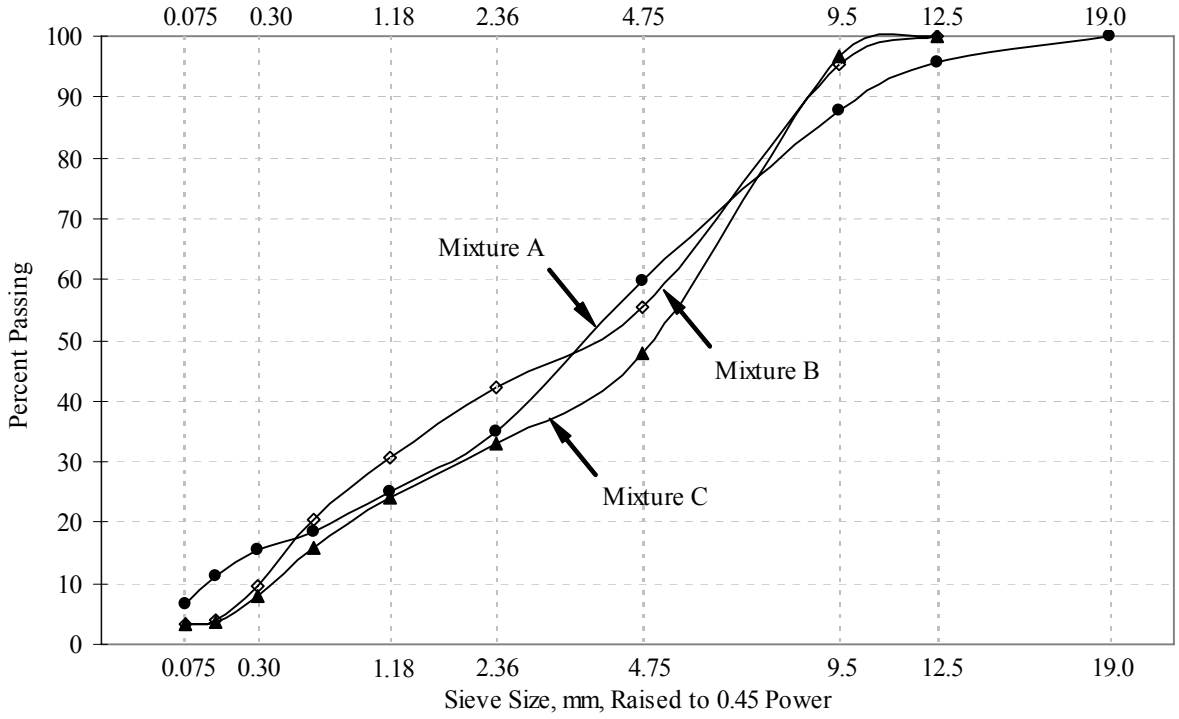

Figure 6.1. Aggregate Gradations.

Mixture C was constructed on State Route 226 in Wayne County, Ohio. It consisted of 52 percent gravel, 14 percent limestone sand, 14 percent natural sand, and 20 percent RAP. Again, the RAP material was replaced for a final mixture proportion of 65 percent gravel, 17.5 percent limestone, and 17.5 percent natural sand. The asphalt binder content was 5 percent by weight of the mixture. Mixtures B and C are the same as Mixtures 7 and 8, respectively, in the report by Lytton et al. (2005).

The Ohio Department of Transportation (ODOT) performed a field evaluation of the pavement sections where mixtures B and C were used. The reported Pavement Condition Rating (PCR) for mixture B dropped from 95 to 89 from 2000 to 2004 and for Mixture C dropped from 97 to 60 from 1998 to 2004. Extensive amounts of cracking and raveling were observed in these pavements, especially in the sections where Mixture C was applied. According to ODOT, the primary cause of the moisture-induced distresses is the type of gravel aggregate used (Lytton et al. [2005]).

FRACTURE MODEL FOR MOISTURE SUSCEPTIBILITY

A fracture model was developed to assess the moisture susceptibility of several asphalt mixtures prepared and characterized in the laboratory (Arambula et al. [2007]). Equation 6.1 is used to estimate the crack growth derives from Paris' law, which describes the average crack growth with respect to the change in pseudo strain energy per unit volume or J-integral:

$$\frac{dr}{dN} = A\left(J_R\right)^n \tag{6.1}$$

where r is the average crack radius in the specimen, n and A are material constants, and J_R is the J-integral, which is the pseudostrain energy release rate per unit crack area expressed as:

$$J_R = \frac{\frac{\partial W_R}{\partial N}}{\frac{\partial (c.s.a)}{\partial N}} \tag{6.2}$$

where W_R is the DPSE per unit volume of the intact material or the volume of the material that is capable of dissipating energy, and $c.s.a$ is the crack surface area. W_R is estimated as the area in the hysteresis loop of the stress-pseudo strain domain divided by the volume of the intact material. Arambula et al. (In press) provide a detailed discussion on the

stress-pseudo strain relationship and its application in characterizing asphalt mixture performance.

As shown in Chapter 5, the equation to estimate the crack growth parameter denoted by r is expressed as (Arambula et al. [2007]):

$$r = \left[(2n+1) \left(\frac{bE_R}{4\pi E_1 \Delta G_f \sigma_t^2} \right)^{\frac{n}{1+n}} \left(N^{\frac{1}{1+n}} - 1^{\frac{1}{1+n}} \right) \right]^{\frac{1+n}{2n+1}} \tag{6.3}$$

where n is a function of the slope of the relaxation curve, b represents the rate of change of the DPSE with respect to load cycles N, E_R is the reference modulus, E_1 is the initial relaxation modulus, ΔG_f is the partial wet adhesive bond surface energy between the asphalt binder and the aggregate, and σ_t is the tensile strength of the material.

As shown subsequently, variability in the crack growth parameter can be reduced by normalizing with respect to tensile strength. Therefore, the normalized crack growth parameter denoted by R is estimated as:

$$R = r\left(\sigma_t^2\right)^{\frac{2n+1}{n}} \tag{6.4}$$

$$R = (2n+1)^{\frac{1+n}{2n+1}} \left(\frac{bE_R}{4\pi E_1 \Delta G_f} \right)^{\frac{n}{2n+1}} \left(N^{\frac{1}{1+n}} - 1^{\frac{1}{1+n}} \right)^{\frac{1+n}{2n+1}} \tag{6.5}$$

CHARACTERIZATION OF ASPHALT MIXTURES AND MODEL PARAMETERS

The crack growth model was used in this study to evaluate the moisture susceptibility of mixtures *A*, *B*, and *C*. Six replicates for each mixture type were prepared and compacted in the laboratory using the Superpave gyratory compactor (SGC). The compacted specimens with a dimension of 150 mm in diameter and 165 mm in height were cored and trimmed to a final size of 100 mm in diameter and 150 mm in height. Three of the six replicates were moisture conditioned following the modified Lottman test procedure that specifies 70 to 80 percent vacuum saturation with water by weight, AASTO (2002). To

satisfy this requirement, Mixture *A* required 25 s of saturation time, while Mixtures *B* and *C* required 900s.

After measuring the degree of saturation, the specimens were kept in water and transported to a water bath at 60°C with water 25 mm above the specimen surface. After 24 hours inside the hot water bath, the specimens were removed and placed in water at room temperature for an additional 2 hours. The specimens were then removed from the water bath at room temperature and left to air dry before testing.

To measure the load-induced displacement, three axial linear variable differential transducer (LVDT) holders 120° from each other were attached to the replicates of each mixture type. The gauge length was 100 mm. To obtain the parameters required to estimate *r*, relaxation, uniaxial dynamic tension and tensile strength tests were performed on the specimens, and surface energy values were obtained to estimate the partial wet adhesive bond energy value. The next section presents details of these procedures.

Viscoelastic Parameters

Relaxation tests at 10ºC, 20ºC, and 30ºC were conducted on the asphalt mixtures. To prevent damage to the specimen, a low-level trapezoidal-shaped tensile strain of 200 microstrain (με) was applied during 60 s. After a rest period of 600 s, a trapezoidal compressive strain of 200 με was also applied for a period of 60 s.

The following power law equation was used to describe the master curve of the relaxation modulus as a function of loading time:

$$E(t) = E_1 t_{red}^{-m} \tag{6.6}$$

where $E(t)$ is the time-dependent relaxation modulus, E_1 is the initial relaxation modulus, t_{red} is the reduced time equal to t/a_T, and m is the modulus relaxation rate. The shift factors, a_T, were obtained using the Arrhenius equation (Medani et al. [2004]):

$$\log a_T = \log(e)\left(\frac{\Delta H}{R}\right)\left(\frac{1}{T} - \frac{1}{T_{ref}}\right) \tag{6.7}$$

where T *is* the test temperature, T_{ref} is the reference temperature, ΔH is the activation energy, and R is the universal gas constant equal to 8.314 J/(mol K). The relaxation moduli at the three different temperatures were shifted to a reference temperature of 30ºC. The values for E_1, m, and ΔH were obtained by minimizing the sum of squared errors between the observed and estimated relaxation moduli.

The relationships between n in Equation 6.1 and m in Equation 6.6 were derived by Schapery (1981) for different scenarios. Further, strain-controlled loading with constant surface energy of the material and length of the fracture process zone ahead of the crack tip was associated with a value of $n = 1/m$ (Lytton et al. [1993]). This relationship was, therefore, adopted in this project.

Dissipated Pseudo Strain Energy and Reference Modulus Parameters

A uniaxial dynamic tension test at 30ºC was used to estimate the DPSE and E_R parameters for the crack growth model. The test consisted of application of a haversine-shaped strain of 350 με for 0.1 s followed by a rest period of 0.9 s. The total number of applied load cycles was 1000. The applied strain level during the uniaxial dynamic tension test was higher than in the relaxation modulus test to induce damage in the specimen, where damage was detected by the change in the stress versus pseudo strain relationship.

The applied stress was calculated as the ratio of the recorded load to the cross-sectional area of the specimen. Then, the viscoelastic stress was computed for each load cycle using Boltzmann superposition (Si [2001]):

$$\sigma_{VE} = \Sigma_{i=1}^{n} E_1 (\tau - t_i)^{-m} \left(\frac{d\varepsilon}{dt} \right)_i dt \qquad (6.8)$$

where E_1 is the initial relaxation modulus, τ is the last value of time in the load cycle, t is the i^{th} value of time in the load cycle, m is the modulus relaxation rate, $\frac{d\varepsilon}{dt}$ is the change in

strain for every i^{th} time increment, dt is the time increment, and n is the number of data points recorded during each load cycle.

The pseudo strain, ε_R, was calculated as the ratio of σ_{ve} and the reference modulus, E_R, which was computed as the ratio of the maximum applied stress recorded during the first load cycle (nonlinear response) to the maximum applied strain of 350 με (Si [2001]). The values of the applied stress were then plotted versus ε_R, forming an oval-shaped loop. The area inside the loop represents the DPSE in each load cycle and was computed using the area by coordinates method (Wolf and Ghilani [2002]). To account for the reduction in the material capable of dissipating energy, the DPSE was normalized by the pseudostiffness ratio:

$$W_R = \frac{DPSE}{\left(\frac{S_i}{S_1}\right)} \tag{6.9}$$

where S_i is the pseudostiffness and is computed for each load cycle as the ratio of the maximum applied stress with respect to ε_R, and S_1 is the pseudostiffness in the first load cycle.

There is a linear relationship between W_R and the logarithm of the number of load cycles, ln(N); the parameter b in Equation 6.5 represents the slope of that relationship. The intercept of the line represents the energy associated with the initial damage and material nonlinearity due to the difference in the strain level used in determining the viscoelastic properties (200 με) and the strain level used in the uniaxial dynamic tension test (350 με).

Tensile Strength Parameter

After the uniaxial dynamic tension test, a tensile strength test at 30ºC and a rate of 0.25 mm/min was conducted on the specimens until failure. As expected, the wet specimens differed from the dry specimens after failure. As shown in Figure 6.2, the wet specimens exhibited stripping or loss of adhesion between the asphalt binder and the aggregate, while the dry specimens had fully coated aggregates throughout the section of the specimen.

(a) **(b)**

Figure 6.2. Failed Specimens after Tensile Strength Test (a) Wet Specimens Showing Stripping and (b) Dry Specimens Showing Well-Coated Aggregates.

Partial Wet Adhesive Bond Surface Energy Parameter

The thermodynamic theory establishes the relationship between the Gibbs free energy, the work of adhesion, and surface energy. The surface energy of a single-phase material is defined as the work required to create a unit area of a new surface, and it is comprised of a polar acid-base component (γ^{AB}) and a non-polar Lifshitz-van der Waals (γ^{LW}) component. When a material cracks, the energy required to create the new two faces is known as the work of adhesion and equals the surface energy of each material (represented by the indices *1* and *2*) minus the interfacial energy lost when the new surfaces are created (represented by the index *12*). The Gibbs free energy or adhesive bond energy (ΔG^a) is equal and opposite in magnitude to the work of adhesion Hefer (2004):

$$\Delta G_{12}^{a} = \gamma_{12} - \gamma_1 - \gamma_2 = \Delta G_{12}^{aLW} + \Delta G_{12}^{aAB} \tag{6.10}$$

where:
$$\Delta G_{12}^{aLW} = -2\sqrt{\gamma_1^{LW}\gamma_2^{LW}} \tag{6.11}$$

$$\Delta G_{12}^{aAB} = -2\left(\sqrt{\gamma_1^{+}\gamma_2^{-}} + \sqrt{\gamma_1^{-}\gamma_2^{+}}\right) \tag{6.12}$$

The polar acid-base component in Equation 6.12 is calculated from its individual acid (positive superscript) and basic (negative superscript) parts. When water (represented by the index *3*) is present at the interface of the system, the expression for ΔG^a becomes:

$$\Delta G_{123}^{a} = \gamma_{12} - \gamma_{13} - \gamma_{23} = \Delta G_{123}^{aLW} + \Delta G_{123}^{aAB} \qquad (6.13)$$

The Wilhelmy Plate (WP) and the USD were used to estimate the values of the surface energy components of the asphalt binder and the aggregates, respectively. In the USD, the spreading pressure of several probe gases onto the surface of the aggregate is used to estimate the surface energy components. In the WP, the contact angle between a thin plastic plate coated with asphalt binder submerged (wetting) and withdrawn (dewetting) from several probe liquids is used to estimate the individual surface energy values of the asphalt binder. Details about these test protocols and calculations can be found elsewhere (Lytton et al. [2005]). The dry and wet ΔG^a results for the different types of aggregates are presented in Table 6.2, which were calculated using the wetting contact angle measured with the WP.

The values presented in Table 6.2 correspond to each individual type of aggregate. Since more than one aggregate type is present in each mixture, to obtain ΔG^a for the mixture, a weighted average based on the corresponding aggregate proportions was utilized (Table 6.3).

Table 6.2. Adhesive Bond Energy under Dry and Wet Conditions.

Mixture	Field Moisture Performance	Aggregate	Adhesive Dry ΔG^a_{12} (ergs/cm^2)	Adhesive Wet ΔG^a_{123} (ergs/cm^2)
A	Good	Gravel	93.36	-75.20
		Limestone	118.87	-151.14
B	Fair to Poor	Limestone	87.49	-115.58
		Gravel	94.56	-160.22
C	Poor	Limestone	81.27	-119.82
		Gravel	90.92	-161.87

Table 6.3. Weighted Average for the Adhesive Bond Energy under Dry and Wet Conditions.

Mix-ture	High-way	Mixture Des-cription	Loc-ation	Reported Per-formance	Agg-regates	Weighted Adhesive Dry ΔG_f^{dry} (ergs/cm^2)	Weighted Adhesive Wet ΔG_f^{wet} (ergs/cm^2)	Ratio $\left\lvert \frac{\Delta G_f^{dry}}{\Delta G_f^{wet}} \right\rvert$
A	Texas IH 20	Superpave	Atlanta, TX	Good	Gravel and TXI Limestone	101.6	-99.7	1.0186
B	Ohio SR 511	TY 1	Ashland County, OH	Fair to Poor	Gravel and Limestone	90.4	-133.8	0.6756
C	Ohio SR 226	TY 1 Inter-mediate	Wayne County, OH	Poor	Gravel and Limestone	88.9	-153.0	0.5811

The ΔG^a values presented in Table 6.3 correspond to a fully dry or a fully wet condition. The dry bond energy, ΔG_f^{dry}, represents the condition where no moisture is present in the asphalt mixture, while the wet bond energy, ΔG_f^{wet}, represents the condition when water fully saturates the aggregate-binder interface. During testing, the material is not completely dry or fully saturated, but a partial wet condition exists at the interface of the aggregate and the asphalt binder (Lytton et al. [2005]) and Kim et al. [2004]). Thus, in Equation 6.5 the adhesive bond surface energy between the asphalt binder and the aggregate, ΔG_f, represents the value in a partial wet condition. The ratio of the partial wet bond energy to the dry one was assumed proportional to the ratio of the normalized pseudostiffness under wet conditions to that under dry conditions as follows:

$$\Delta G_f = \frac{\left(\frac{S_i}{S_1}\right)^{wet}}{\left(\frac{S_i}{S_1}\right)^{dry}} \Delta G_f^{dry} \tag{6.14}$$

CHARACTERIZATION OF ASPHALT MASTIC SPECIMENS AND MODEL PARAMETERS

Cylindrical asphalt mastic specimens made of a mixture of the aggregate portion smaller than 1.18 mm and the asphalt binder were tested using the DMA (Lytton et al. [2005]). The testing of the asphalt mastic was similar to that of the asphalt mixtures, except that the DMA applies dynamic shear while the asphalt mixtures were tested using a uniaxial dynamic tension test. The asphalt mastic of Mixture A consisted of 97 percent limestone screenings and 3 percent hydrated lime; Mixture B consisted of 72 percent natural sand and 28 percent limestone sand; and Mixture C consisted of 50 percent natural sand and 50 percent limestone sand.

The DMA specimens were prepared by mixing the filler and the asphalt binder prior to mixing with the rest of the aggregates using a mechanical mixer (Lytton et al. [2005]). After short-term oven aging for 2 hours at 135 °C, the SGC was used to compact the asphalt mastic specimens to 152 mm in diameter and 85 mm in height. Afterwards, the sides of the specimens were trimmed to a height of 50 mm, and several specimens of 12 mm in diameter were cored. Some of the asphalt mastic specimens were moisture conditioned following a method established by Kim et al. (2004), in which the specimens are placed in distilled water under vacuum for 1 hour. The saturation level of the specimens, measured using Equation 6.15, was 125 percent on average, indicating that water not only permeated into the voids but also diffused into the asphalt binder.

$$\%S = \frac{100 * (W_{SSD} - W_{DRY})}{V_a} \tag{6.15}$$

where W_{SSD} is the saturated surface dry weight of the specimen after vacuum saturation, W_{DRY} is the initial dry specimen weight, and V_a is the volume of air voids in the specimen.

The dry and wet asphalt mastic specimens were then subjected to a sinusoidal shear strain in the DMA in order to evaluate the accumulation of damage. The linear viscoelastic properties of the asphalt mastic specimens were determined by applying a low strain level, and fatigue damage was evaluated by applying a high strain level (Lytton et al. [2005]). The data were used to compute the number of cycles to failure, dynamic modulus, and the

normalized crack growth parameter, R. This data analysis is identical to that applied to the asphalt mixtures and presented previously.

RESULTS

Table 6.4 presents a summary of the average input parameters used in Equations 6.3 and 6.5 to estimate r and R, including the values of E_1, m, n, E_R, a, b, σ_t, and ΔG_f.

Table 6.4. Average Surface Energy and Mechanical Tests Parameter Results.

Mixture	E_1 (MPa)	m	$n = 1/m$	E_R* (MPa)	a (J/m^3)	b	σ_t (kPa)	ΔG_f** (J/m^2)
A dry	1728.2	0.1231	8.24	2132.0	0.6567	0.0122	350.7	0.1016
A wet	1506.6	0.1185	8.53	2714.5	0.5650	0.0148	358.1	0.0953
B dry	926.4	0.1044	9.85	1462.1	0.4047	0.0136	94.3	0.0904
B wet	590.2	0.1163	8.82	1228.0	0.3864	0.0125	60.4	0.0862
C dry	1106.5	0.1290	8.22	1583.9	0.4798	0.0160	96.2	0.0889
C wet	896.9	0.0987	10.18	1425.4	0.3344	0.0525	68.0	0.0569

* *Wet E_R values are not used in the analysis. The reference parameters are those of the dry specimens.*
** *Using $S_i = S_{1000}$ in Equation 14*

It is important to note the difference between the viscoelastic properties used in calculating σ_{ve} and the DPSE in Equations 6.8 and 6.9, and those to estimate R in Equation 5. In calculating the DPSE, the viscoelastic properties and E_R are associated with the undamaged state, which is the dry state. Therefore, the values of E_1 and m in Equation 6.8, the value of S_i in Equation 6.9, and the value of E_R used to compute the pseudo strain, correspond to the dry state. However, based on the derivation of Schapery and Lytton et al., the values of E_1 and n in Equation 6.5 correspond to the material surrounding the crack, either dry or moisture conditioned (Schapery [1981]) and Lytton et al. [1993]).

The value of r for the three replicates of each type of asphalt mixture was calculated using Equation 6.3. In addition, the parameter R was computed using Equation 6.5. Table 6.5 presents the average of both results at $N = 1000$ load cycles along with their coefficients of variation. These results show that the variation in the results is reduced when using the crack growth parameter, R, normalized with respect to the tensile strength value

that exhibited the highest variability among the measured material properties. It is interesting to note that the coefficient of variation was higher under wet conditions for Mixtures B and C, which were more moisture susceptible as compared to Mixture A.

Table 6.5. Average Crack Growth Parameters and Coefficients of Variation.

	Crack Growth Parameter, *r*		Normalized Crack Growth Parameter, *R*	
Mixture	**Average**	**Coefficient of Variation (%)**	**Average**	**Coefficient of Variation (%)**
A dry	3.25	19.8	0.54	16.3
A wet	3.57	10.1	0.60	2.8
B dry	9.93	25.5	0.53	25.2
B wet	19.21	40.8	0.64	23.8
C dry	12.59	35.3	0.59	9.3
C wet	32.40	66.6	0.96	43.3

The values of R for the asphalt mixtures and the asphalt mastics were plotted against the number of load cycles as shown in Figures 6.3 and 6.4, respectively. According to Figure 6.3, Mixture A is the least moisture susceptible, and Mixture C is the most susceptible to moisture damage. Observing Figure 6.4, it is also apparent that the asphalt mastic fraction of Mixture C is the most susceptible to moisture damage. The asphalt mastic of Mixture B failed earlier than the asphalt mastic of Mixture A. The failure point for the asphalt mastic of Mixture B, around 4000 load cycles, corresponded to the number of load cycles at which the asphalt mastic of Mixture C started to exhibit a rapid increase in the wet to dry ratio.

To assess the effect of the adhesive bond energy between the asphalt and the aggregate in dry and wet conditions, the dry to wet ratio, $\Delta G_f^{dry} / \Delta G_f^{wet}$, previously presented in Table 6.3 was compared to the wet to dry ratio of the normalized crack growth index for the asphalt mixtures, R^{wet} / R^{dry}, obtained using Equation 6.5 at $N = 1000$. The relationship between these two parameters is presented in Figure 6.5. The mixture with the highest $\Delta G_f^{dry} / \Delta G_f^{wet}$ ratio and a ratio of R^{wet} / R^{dry} closer to 1 is expected to be more resistant to moisture damage (Bhasin et al. [2006]). Mixture C had the lowest $\Delta G_f^{dry} / \Delta G_f^{wet}$ value and the ratio of R^{wet} / R^{dry} at $N = 1000$ was equal to 1.64, the highest

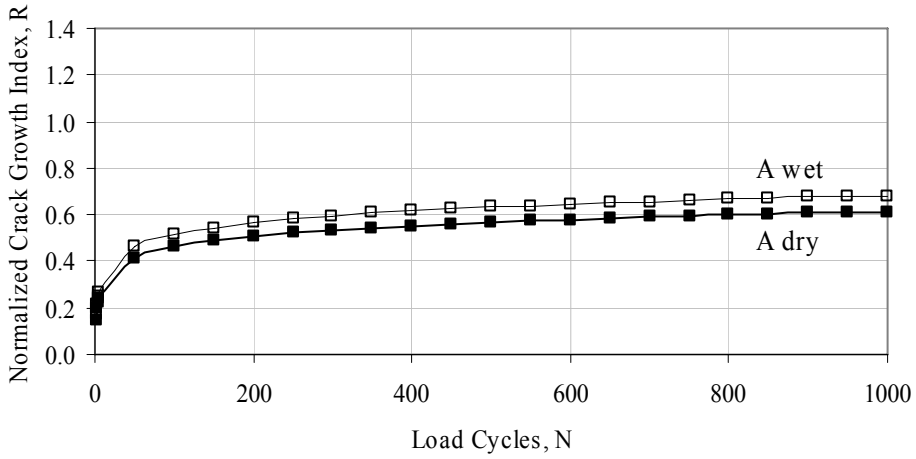

(a)

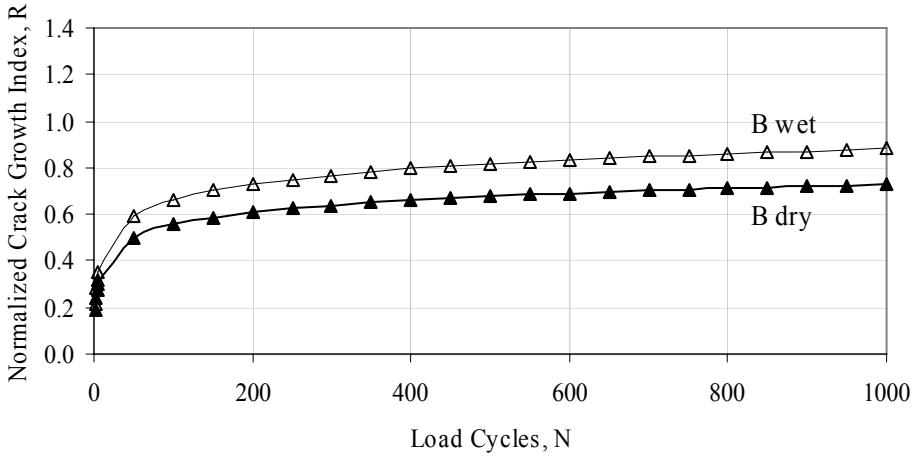

(b)

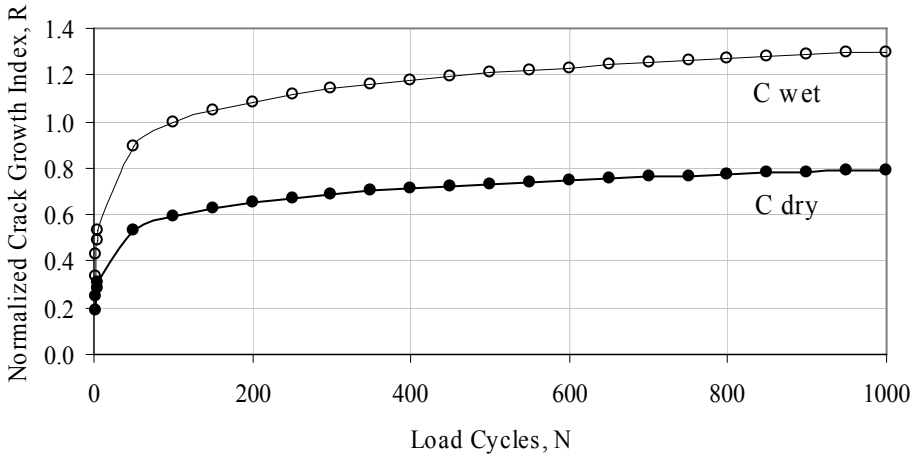

(c)

Figure 6.3. Normalized Crack Growth Parameter for Each Mixture Type. (a) Mixture A, (b) Mixture B, and (c) Mixture C.

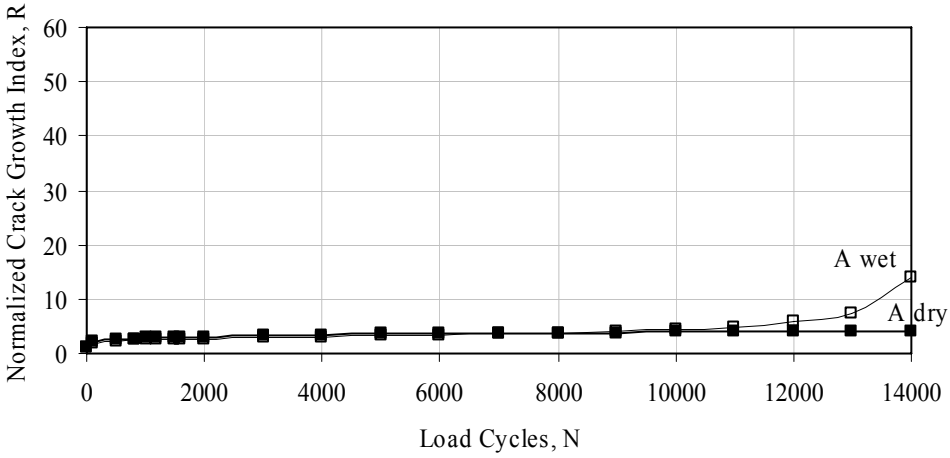

(a)

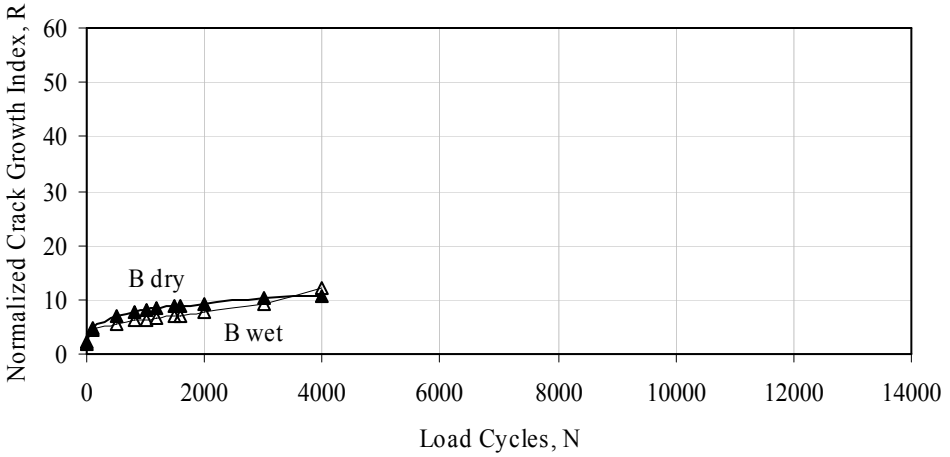

(b)

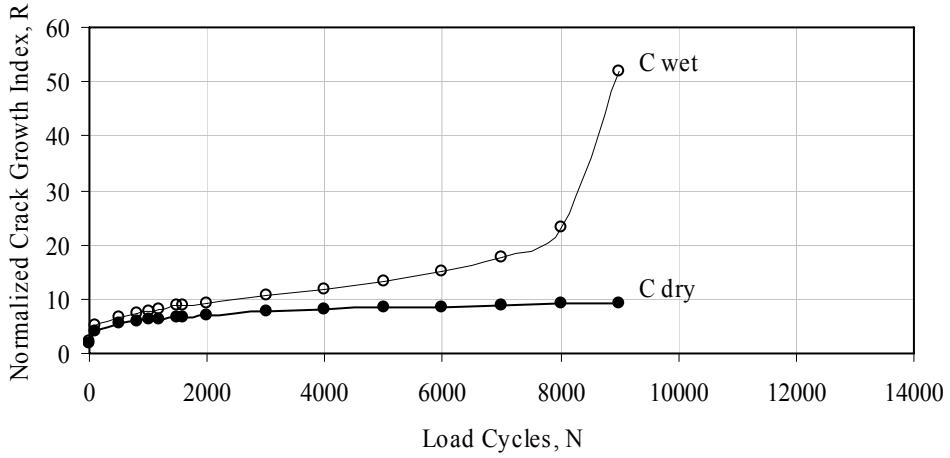

(c)

Figure 6.4. Normalized Crack Growth Parameter for the Asphalt Mastic Fraction of Each Mixture Type. (a) Mixture A, (b) Mixture B, and (c) Mixture C.

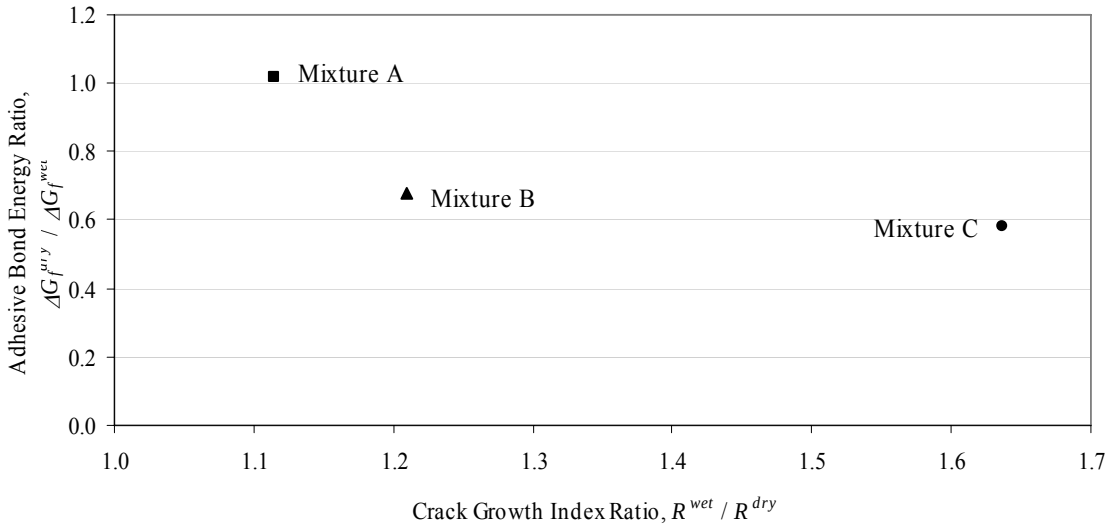

Figure 6.5. Adhesive Bond Energy Ratio versus the Asphalt Mixture Crack Growth Index Ratio.

among the three mixtures. This observation confirms that Mixture C is the most susceptible to moisture damage. On the other hand, Mixture A had the highest $\Delta G_f^{dry} / \Delta G_f^{wet}$ value and the lowest R^{wet} / R^{dry} value at N =1000 of 1.11. Therefore, mixture *A* is considered the least prone to moisture damage among the mixtures analyzed.

SUMMARY

Several qualitative and quantitative methods have been developed in the past for the evaluation of moisture damage. Qualitative methods are based on a subjective visual assessment of damage, while the majority of the quantitative methods rely on measuring the change of a single test parameter (indirect tensile strength, dynamic modulus, etc.) due to moisture conditioning. These approaches do not account for the interactions between the fundamental chemical and mechanical properties of the mix constituents that influence the resistance to moisture damage. Consequently, these methods offer only a limited understanding of the factors influencing moisture damage.

To overcome these shortcomings, a crack growth model based on Paris' law for viscoelastic materials was developed to assess the moisture susceptibility of asphalt mixtures and asphalt mastics. The advantages of this method are that its derivation is based on principles of fracture mechanics and that it accounts for several fundamental chemical and mechanical material properties. This method analyzed the resistance of asphalt mixtures and their asphalt mastic fraction to moisture damage. For the asphalt mixtures, the normalized crack growth index, *R*, and the wet to dry ratio of this index, R^{wet}/R^{dry}, agreed with the reported field performance. The parameters for estimating *R* for the asphalt mixtures were obtained from the analysis of mechanical tests (relaxation and uniaxial dynamic tension) and measurement of the adhesive bond energy between the asphalt binder and the aggregate. For the asphalt mastic fraction, the DMA was used to test the specimens and obtain the model parameters. The data analysis showed similar results to that for the asphalt mixtures in terms of good differentiation between the wet and dry behavior and a ranking of the mixtures according to the reported field performance. The authors highly recommend the use of the crack growth index presented in this project to assess moisture susceptibility of additional asphalt mixtures and asphalt mastics with known field performance.

CHAPTER 7
RESEARCH SUMMARY

BACKGROUND

Moisture damage in asphalt mixtures can occur within the asphalt mastic (cohesive fracture) or at the aggregate-mastic interface (adhesive fracture or failure). Whether or not a cohesive or adhesive failure occurs depends on the physio-chemical nature and the relative thickness of the mastic. The majority of previous studies on this subject focused on the development of tests and empirical parameters that quantify moisture sensitivity of whole asphalt mixtures. The main objective of this project was to develop a framework for the evaluation of moisture damage by carefully considering fundamental material properties and mechanisms that influence durability of the adhesive interface between aggregate and asphalt and the cohesive strength and durability of the mastic. The project was divided into two phases to achieve this objective.

The first phase of the study focused on the validation of the surface energy measurements and the DMA through the evaluation of moisture susceptibility of materials and mixtures with known field performance. The second phase of the project evaluated the surface energy and moisture susceptibility of wide combinations of aggregates and asphalts. The following are the main tasks conducted in this project:

- Develop test protocols to determine surface energy of binders and aggregates.
- Catalog surface energy properties of commonly used asphalt binders and aggregates in Texas.
- Evaluate the impact of liquid anti-strips, modifications made by the manufacturers of asphalt binders, and aging on the surface energy of asphalt binder and its consequence on mixture performance.
- Evaluate the impact of pH of the water on its surface free energy and, consequently, on mixture resistance to moisture damage.
- Develop a test protocol to conduct dynamic mechanical analysis of the fine aggregate matrix (mixture of asphalt binder and fine aggregates).

- Develop a framework with a tentative protocol to evaluate moisture sensitivity of asphalt mixtures based on surface energy measurements and dynamic mechanical analysis of the fine aggregate matrix.
- Provide specifications for the equipment that can be used for measuring the surface energy of asphalt binder and aggregates.

Following is a summary from the various tasks accomplished in this report.

SURFACE ENERGY OF BINDERS AND AGGREGATES

The WP device and the USD were used to measure the surface energy components of asphalt binders and aggregates, respectively. The detailed test protocols for these test methods were developed in a parallel study under the National Cooperative Highway Research Program. These test protocols in Association of American State and Transportation Officials (AASHTO) format are attached in Appendices D and E of this report.

The surface energy components of several different aggregates as well as unmodified and modified asphalt binders were determined and cataloged using these test procedures. Typical range of values for the surface energy components, work of cohesion and adhesion, and energy parameters with different aggregates were determined and reported to serve as a guideline for future measurements. The use of energy parameters computed using the surface energy components of asphalt binders and aggregates as a screening tool by which to select optimum combinations of asphalt binders and aggregates was demonstrated.

INFLUENCE OF MODIFICATIONS MADE TO ASPHALT BINDERS ON ITS SURFACE ENERGY

Addition of Liquid Anti-Strip

Addition of liquid anti-strip agents typically reduced the non-polar component of the surface free energy and, consequently, the work of cohesion of the asphalt binders. This addition can indirectly improve the fracture resistance by promoting better adhesion between the fines and the binder during the mixing and compaction process. Use of liquid

anti-strip agents either improved or did not significantly change the moisture resistance of asphalt binders with the selected aggregates. The liquid anti-strip agents from the two different sources demonstrated different levels of changes in the moisture resistance when used with the same combination of asphalt binder and aggregate. These conclusions were based on the energy parameter computed from surface energy components of the binder and aggregate.

Binder Aging

Aging can have different impacts on different asphalt binders depending on the initial chemistry of the asphalt binder. Furthermore, differences in kinetics of different compounds formed during oxidative aging also influence the chemistry and, consequently, the surface free energy components and performance of different asphalt binders after short-and long-term aging.

In most cases, long-term aging reduced the work of cohesion indicating lower fracture resistance of the aged binder. In the case of one unmodified binder and one modified binder, the work of cohesion increased after long-term aging. After long-term aging, asphalt binders from one source demonstrated a decrease in the moisture sensitivity, while asphalt binders from the other source demonstrated an increase or no change with the moisture sensitivity with the two aggregates used in this project. The difference in the behavior of the two asphalt binders is attributed to the influence of aging on the magnitudes of the polar functional groups.

Manufacturer Modifications

Modifications made to a base asphalt binder by the manufacturer to produce a higher PG grade typically increased the work of cohesion indicating better fracture resistance of the modified binders. These modifications did not change the moisture sensitivity of the asphalt binder–aggregate combinations significantly except when TRS was used as a modifier. In this case, the acid component of the asphalt binder increased, providing a potential improvement in the adhesive bond strength with most types of aggregates. For one of the asphalt binders, addition of SBS also showed improved moisture resistance after aging.

INFLUENCE OF pH OF WATER ON ITS SURFACE ENERGY

No significant changes in the total surface free energy or the acid and base components of surface free energy were observed with respect to the reference distilled water. Within the range of pH that was achieved by exposing distilled water to aggregates in this project, there is no significant correlation between the change in surface free energy components and the pH of the water.

DYNAMIC MECHANICAL ANALYSIS OF FINE AGGREGATE MATRIX

Dynamic mechanical analysis was conducted on the fine aggregate matrix (FAM) portion of different asphalt mixtures. The FAM is the portion of the asphalt mixture that is comprised of fine aggregates and the asphalt binders. The durability of the FAM is essential for the optimal performance of the asphalt mixture as a whole. The method to prepare and test DMA samples is provided in TxDOT Report 0-4524-02. Appendices B and C of this report include the methods for the design of FAM for DMA testing.

FRAMEWORK TO EVALUATE MOISTURE SENSITIVITY OF ASPHALT MIXTURES

The researchers developed a system of three steps to evaluate the influence of fundamental material properties, mixture modification, and mixture design on moisture susceptibility. In the first step, an energy-based parameter termed the energy ratio (ER) is calculated using the surface energy measurements and is used as a screening tool to select binders and aggregates that have good resistance to moisture damage. In the second step, the dynamic mechanical analysis of FAM specimens consisting of asphalt binder and fine portion of aggregates is used to evaluate moisture susceptibility. In the third step, researchers evaluated the moisture susceptibility of the full mixture.

The testing in steps 2 and 3 yields a crack growth index that is a function of fundamental material properties. The DMA testing is useful to evaluate moisture susceptibility of the materials without being influenced by mixture design and internal structure distribution. The evaluation of the full mixture is necessary, however, in order to verify that the mixture design and internal structure distribution are optimized to improve the resistance to moisture damage.

Figure 7.1 illustrates the framework with the logical progression of steps that need to be followed in order to design a mixture with desired resistance to moisture damage. Table 7.1 provides a preliminary recommendation for the values of the parameters that may be used for the decision steps illustrated in Figure 7.1. The values in Table 7.1 are preliminary and need to be refined by populating it with data based on several more real mixtures.

The framework and tentative protocols developed in this project can be used to select materials and design mixture that have a good resistance to moisture damage. In contrast to traditional methods that rely solely on testing of whole mixtures, this framework is based on a bottom up approach to quantify moisture sensitivity of asphalt mixtures. In other words, in this framework, materials are screened first, followed by tests on fine aggregate matrix and whole mixtures. As such, the results of this project will contribute to the reduction of asphalt pavement failures due to moisture damage. This will translate to longer pavement life and less maintenance and construction cost. Also, by identifying those combinations of asphalts and aggregates that bond well together, it will expand the range of options of alternative sources of aggregates and asphalt binders that will provide acceptable performance on any given project.

Table 7.1. Preliminary Recommendation of Values to be Used with Decision Tree Shown in Figure 7.1.

	Resistance to Moisture Damage			
Parameter	**Good**	**Fair**	**Poor**	**Notes**
Step 1: Energy Ratio*	≥ 0.8	≥ 0.8 < 0.5	≤ 0.5	The energy ratio is calculated from the binder cohesive energy, wet adhesive bond energy, and dry adhesive bond energy.
Step 2: Ratio of Crack Growth Index at 10,000 Cycles (DMA Testing of Asphalt and Fine Portion of the Mixture)	≤ 1.5	> 1.5 ≤ 2.0	> 2.0 Or Failure Under Wet Condition	The ratio is calculated as crack growth index under wet conditions to crack growth index under dry conditions.
Step 3: Ratio of Crack Growth Index at 1000 Cycles (Dynamic Testing of Full Mixture	≤ 1.2	> 1.2 ≤ 1.5	> 1.5 Or Failure Under Wet Condition	The ratio is calculated as crack growth index under wet conditions to crack growth index under dry conditions.

* Additional consideration must be made for aggregates with very low specific surface area.

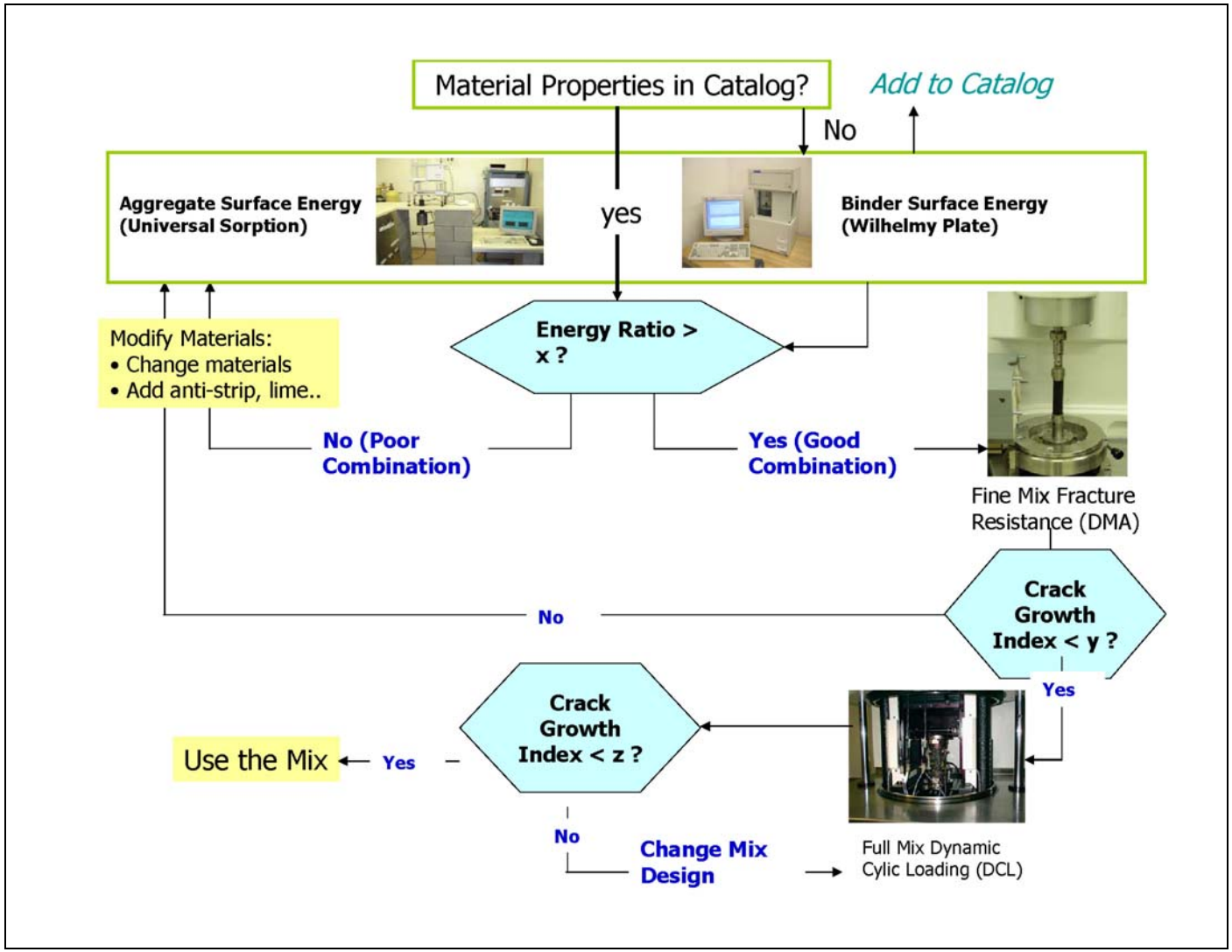

Figure 7.1. Framework to Select Mixtures Resistant to Moisture Damage.

REFERENCES

Adamson, A.W., and A.P. Gast. (1997). Physical Chemistry of Surfaces, John Wiley & Sons, Inc., New York.

Arambula, E., E. Masad, and A.E. Martin. (In Press). The Influence of Air Void Distribution on the Moisture Susceptibility of Asphalt Mixes. *Journal of Materials in Civil Engineering*.

The Asphalt Institute. (1995). *Performance Graded Asphalt Binder, Specification and Testing*. Superpave Series No. 1, SP-1. The Asphalt Institute, Lexington, Kentucky.

Bhasin, A., E. Masad, D. Little, and R.L. Lytton. (2006). Limits on Adhesive Bond Energy for Improved Resistance of Hot Mix Asphalt to Moisture Damage. *Transportation Research Record 1970*, Transportation Research Board, National Research Council, Washington, D.C. pp 3-13.

Birgisson, B., R. Roque, and G.C. Page. (2003). Evaluation of Water Damage Using Hot Mix Asphalt Fracture Mechanics. *Journal of the Association of Asphalt Paving Technologists*, Vol. 72, pp. 424-462.

Cheng, D.X., D.N. Little, R.L. Lytton, and J.C. Holste. (2002) "Surface Energy Measurement of Asphalt and its Application to Predicting Fatigue and Healing in Asphalt Mixture," *Transportation Research Record 1810*, Transportation Research Board, National Research Council, Washington, D.C. pp 44-53.

Cheng, D. (2002). *Surface Free Energy of Asphalt-Aggregate System and Performance Analysis of Asphalt Concrete.* Ph.D. Thesis, Texas A&M University, College Station, Texas.

Emery, J., and H. Seddik. (1997). *Moisture Damage of Asphalt Pavements and Anti-stripping Additives: Causes, Identification, Testing, and Mitigation*. Transportation Association of Canada, Ottawa, Canada.

Griffith, A.A. (1921). The Phenomenon of Rupture and Flow in Solids. *Philosophical Transactions of the Royal Society of London*, Vol. A221, pp.163-198.

Hefer, A.W., A. Bhasin, and D.N. Little. (2006). Bitumen Surface Energy Characterization Using a Contact Angle Approach. *Journal of Materials in Civil Engineering (ASCE)*, 18(6), pp. 759-767.

Hefer, A.W. (2004). *Adhesion in Bitumen-Aggregate Systems and Quantification of the Effects of Water on the Adhesive Bond*. Ph.D. Dissertation, Texas A&M University, College Station, Texas.

Hughes, R.I., Lamb, D.R. and Pordes, O. (1960). "Adhesion in Bitumen Macadam," Journal of Applied Chemistry, Vol. 10, pp 433-443.

Kiggundu, B.M., and F.L. Roberts. (1988). "The Success/Failure of Methods Used to Predict Stripping Potential in the Performance of Bituminous Pavement Mixtures," Submitted to Transportation Research Board, Washington D.C.

Kim, Y.R., D.N. Little, and R.L. Lytton. (2004). Effect of Moisture Damage on Material Properties and Fatigue Resistance of Asphalt Mixtures. In *Proceedings 83rd Annual Transportation Research Board Meeting.* CD-ROM. Transportation Research Board of the National Academies, Washington, D.C.

Kim, Y.R., and D.N. Little. (2003). "Development of Specification-Type Tests to Assess Damage and Healing Properties of Bitumens and Mastics," Federal Highway Administration FHWA/473630, Texas Transportation Institute, Texas A&M University, College Station, Texas.

Kringos, N., and A. Scarpas. (2005). Raveling of Asphaltic Mixes Due to Water Damage: Computational Identification of Controlling Parameters. In *Proceedings 84th Annual Transportation Research Board Meeting*. CD-ROM. Transportation Research Board of the National Academies, Washington, D.C.

Little, D.N., and A. Bhasin. (2006). *Using Surface Energy Measurements to Select Materials for Asphalt Pavement.* Texas Transportation Institute, Draft final report under Project 9-37 submitted to National Cooperative Highway Research Program, Washington, D.C.

Lucic, S., V. Kovacevic, and D. Hace. (1998). Mechanical Properties of Adhesive Thin Films. *International Journal of Adhesion and Adhesives*, Vol. 18, pp. 115-123.

Lytton, R.L., E. Masad, C. Zollinger, R. Bulut, and D. Little. (2005). *Measurements of Surface Energy and Its Relationship to Moisture Damage*, TxDOT Report Number 0-4524-2, Texas Transportation Institute, Texas A&M University, College Station, Texas.

Lytton, R.L., J. Uzan, E.G. Fernando, R. Roque, D. Hiltmen, and S. Stoffels. (1993). Development and Validation of Performance Prediction Models and Specifications for Asphalt Binders and Paving Mixtures. SHRP Report No. A-357, Strategic Highway Research Program, National Research Council, Washington, D.C.

Lu, X., and U. Isacsson. (2000). Artifical Aging of Polymer Modified Bitumens. *Journal of Applied Polymer Science*, Vol. 76, pp.1811-1824.

Masad, E., V. Castelo Branco, D.N. Little, and R. Lytton. (2006). An Improved Method for the Dynamic Mechanical Analysis of Fatigue Failure of Sand Asphalt Mixtures. Federal Highway Administration, Texas Transportation Institute, Texas A&M University, FHWA/473630.

Masad, E., C. Zollinger, R. Bulut, D.N. Little, and R.L. Lytton. (2006). Characterization of HMA Moisture Damage Using Surface Energy and Fracture Properties. *Proceedings Association of Asphalt Paving Technologists,* Vol. 75, pp 713-748.

Masad, E., A. Castelblanco, and B. Birgisson. (2006). Moisture Damage as a Function of Air Void Size Distribution, Pore Pressure, and Bond Energy. *Journal of Testing and Evaluation*, Vol. 34, No. 1, pp 15-23.

Masad, E., V.Castelo Branco, and D.N. Little. (2006). *Fatigue Damage: Analysis of Mastic Fatigue Damage Using Stress Controlled and Strain Controlled Test.* Final Report No. 473630, Texas Transportation Institute in cooperation with Federal Highway Administration and Western Research Institute.

McGennis, R.B., T.W. Kennedy, and R.B. Machemehl. (1984). *Antistripping and Moisture Damage in Asphalt Mixtures*. Publication 253-1. Center for Transportation Research, Austin, Texas.

Medani, T.O., M. Huurman, and A.A.A. Molenaar. (2004). On the Computation of Master Curves for Bituminous Mixes. In *Proceedings Third EuroBitumen Congress*, Vienna, Austria.

Miller, J.S., and W.Y. Bellinger. (2003). *Distress Identification Manual for the Long-Term Pavement Performance Program*. Publication FHWA-RD-03-031. FHWA, Office of Infrastructure Research and Development, McLean, Virginia.

Ohio Department of Transportation (ODOT). (2005). *2005 Construction and Material Specification*. Columbus, Ohio.

Schapery, R.A. (1984). "Correspondence Principles and a Generalized J Integral for Large Deformation and Fracture Analysis of Viscoelastic Media," *International Journal of Fracture*, Vol. 25, pp. 195-223.

Schapery, R.A. (1981). Nonlinear Fracture Analysis of Viscoelastic Composite Materials Based on a Generalized J Integral Theory. In *Proceedings Japan-U.S. Conference on Composite Materials*, Tokyo, Japan.

Scott, J.A.N. (1982). "Adhesion and Disbonding Mechanisms of Asphalt Used in Highway Construction and Maintenance," *Proceedings*, Association of Asphalt Paving Technologist, Vol. 47, pp 19-24.

Si, Z. (2001). *Characterization of Microdamage and Healing of Asphalt Concrete Mixtures*. Ph.D. Dissertation, Texas A&M University, College Station, Texas.

Solaimanian, M., J. Harvey, M. Tahmoressi, and V. Tandon. (2003). Test Methods to Predict Moisture Sensitivity of Hot Mix Asphalt Pavements. In *Proceedings National Seminar on Moisture Sensitivity of Asphalt Pavements*, San Diego, California.

Taylor, M.A., and N.P. Khosla. (1983). Stripping of Asphalt Pavements: State of the Art," Transportation Research Record 911, pp. 150-158.

Terrel, R.L., and S. Al-Swalilmi. (1994). "Water Sensitivity of Asphalt-Aggregate Mixes: Test Selection," SHRP Report No. A-403 Strategic Highway Research Program, National Research Council, Washington, D.C.

Texas Department of Transportation (TxDOT). (2004). *Standard Specifications for Construction and Maintenance of Highways, Streets, and Bridges*. Austin, Texas.

van Oss, C.J. (1994). *Interfacial Forces in Aqueous Media.* Marcel Dekker Inc., New York.

Vassiliev, N.Y., R.R. Davison, and C.J. Glover. (2001). Development of Stirred Airflow Test Procedure for Short-Term Aging of Asphaltic Materials. *Transportation Research Record 1810*, Transportation Research Board, National Research Council, Washington, D.C. pp. 25-32.

Walubita, L., A.E. Epps, S.H. Jung, C.J. Glover, G. Cleveland, and R.L. Lytton. (2005). Two Approaches to Predict Fatigue Life of Hot Mix Asphalt Concrete Mixtures. Presented at *84th Annual Meeting of the Transportation Research Board,* Washington, D.C.

Wasiuddin, N.M., C.M. Fogle, M.M. Zaman, and E.A. O'Rear. (2006). Effect of Anti-Strip Additives on Surface Free Energy Characteristics of Asphalt Binders for Moisture-Induced Damage Potential, *Journal of Testing and Evaluation*, ASTM, Vol. 35, No. 1, pp 1-9.

Western Research Institute. (2006). *Fundamental Properties of Asphalts and Modified Asphalts*, *Vol. I, Interpretive Report,* Draft final report submitted to FHWA.

Wolf, P.R., and C.D. Ghilani. (2002). *Elementary Surveying: An Introduction to Geomatics.* Addison-Wesley Prentice Hall, Upper Saddle River, New Jersey.

Yoon, H.J., and R.R. Tarrer. (1989) "Effect of Aggregate Properties on Stripping," *Transportation Research Record 1171,* Transportation Research Board, National Research Council, Washington, D.C. pp. 37-43.

Zollinger, C.J. (2005). Application of Surface Energy Measurements to Evaluate Moisture Susceptibility of Asphalt and Aggregates. M.S. Thesis, Texas A&M University, College Station, Texas.

APPENDIX A
CURRENT SAND ASPHALT MIXTURE DESIGN METHOD

The following protocol describes the sand asphalt mix design method used in this report to fabricate sand asphalt mix samples. This methodology was originally proposed by Kim et al. and later improved by Zollinger Kim et al. [2003]) and Zollinger [2005]). The main steps involved in the design process of DMA mixtures are described below.

STEP

1. Obtain the following information about the full HMA mixture:

    a. aggregate gradation,
    b. specific gravity of each filler (passing sieve No. 200) used in the mix,
    c. percentage of binder by weight of the mixture, and
    d. maximum specific gravity of the mixture.

2. Determine the percentage of each aggregate that passes sieve No. 16 (1.18 mm).
3. Calculate the aggregate batch weight of material passing sieve No. 16 through material retained on sieve No. 200. This is the batch weight used to prepare the sand asphalt mixture sample in the Superpave gyratory compactor. Equation A.1 can be used to estimate the aggregate batch weight:

$$Aggregate\ batch\ weight\ (g) = \pi \times r^2 \times h \times G_{mm}(1 - Vv\%) \quad \text{(A.1)}$$

    where r is the sample radius (typically 6 in), h is the sample height (typically 3 in), G_{mm} is the maximum specific gravity of the full mixture, and Vv percent is desired percent air voids in the sand asphalt mixture (recommended value is 11 percent).
4. Use the proportions of aggregates passing sieve No. 16 (1.18 mm) through material retained on sieve No. 200 from the full HMA gradation to calculate the mass of each size fraction of the aggregate required in the sand asphalt mixture.
5. Calculate the amount of binder required for the sand asphalt mixture using Equation A.2:

$$Binder\ (g) = Aggregate\ Batch\ Size \times A/FA \quad \text{(A.2)}$$

where *A/FA* is the ratio of the asphalt binder plus filler to fine aggregate (passing sieve No. 16 and retained on sieve No. 200) by mass used in the sand asphalt mixture batch. According to Kim et al. (2003), researchers recommend using an A/FA ratio of 8 percent.

6. Obtain the mass of each filler used in the DMA mixture using Equation A.3:

$$Filler(g) = \%Filler \times F/A \times binder\ weight \times filler\ specific\ gravity \quad \text{(A.3)}$$

where *F/A* is the ratio of all fillers to asphalt by volume, and *percent Filler* is the percentage of the filler for which calculations are being conducted with respect to all fillers. According to Kim et al. (2003), the recommended filler to binder (*F/A*) ratio is 10 percent.

EXAMPLE: SAND ASPHALT MIX DESIGN METHOD

Step 1:

The asphalt mixture selected for this example is the full HMA Mixture No. 7. Tables A.1 and A.2 present aggregate gradation and composition for the full HMA mixture. The asphalt binder used in this example was rated as a PG 64-22 and is manufactured by Tri-State Asphalt out of Rayland, Ohio. 5.4 percent asphalt binder by weight of aggregate was added to the mixture. DMA samples were prepared using aggregate passing sieve No. 16 (1.18 mm). Only aggregates that have more than 50 percent passing sieve No. 16 are used for preparing DMA specimens. Aggregate gradations that have less than 50 percent passing sieve No. 16 do not contribute enough material to be of consequence and are, therefore, not included. For this case, only limestone sand and natural sand were used for DMA sample fabrication; see bolded portion of Table A.1. Rap was not in the DMA mixture design for this example. The overall specific gravity for the fillers was 2.3, and the maximum specific gravity (G_{mm}) for this mix was 2.302.

Table A.1. Aggregates Gradations for Full HMA Mixture (Mixture No. 7).

Sieve (mm)	% Passing				
	#8 Limestone	#8 Gravel	Limestone Sand	Natural Sand	Rap (Project 159-86 & 209 98)
2" (50.80)	100.0	100.0	100.0	100.0	100.0
1 1/2" (37.50)	100.0	100.0	100.0	100.0	100.0
1" (25.40)	100.0	100.0	100.0	100.0	100.0
3/4" (19.05)	100.0	100.0	100.0	100.0	100.0
1/2" (12.70)	100.0	100.0	100.0	100.0	98.0
3/8" (9.50)	88.0	95.0	100.0	100.0	83.0
#4 (4.75)	18.0	20.0	100.0	100.0	55.0
#8 (2.36)	2.0	2.0	90.0	92.0	34.0
#16 (1.18)	2.0	2.0	**63.0**	**67.0**	25.0
#30 (0.6)	2.0	2.0	**40.0**	**44.0**	16.0
#50 (0.3)	2.0	2.0	**20.0**	**18.0**	12.0
#100 (0.15)	2.0	2.0	**9.0**	**5.0**	10.0
#200 (0.075)	2.0	2.0	**6.40**	**4.30**	7.6

Table A.2. Aggregate Composition for Full HMA Mixture (Mixture No. 7).

Aggregate	#8 Limestone	#8 Gravel	Limestone Sand	Natural Sand	Rap (Project 159-86 & 209 98)
% in the Mix	22	22	10	26	20

Step 2:

To ensure the DMA sample is accurate, based on the full HMA mixture, the aggregate proportions from the full mixture are used for the DMA sample. The limestone sand and natural sand comprise the entire DMA sample, so the new proportions used for limestone sand and natural sand are 28 and 72 percent, respectively.

Step 3:

The estimation of the DMA mixture batch weight is done using Equation A.1. The mixture in this example had an estimated batch weight of approximately 3346 g. The dimensions of an ideal specimen are used—a 15.2 cm diameter and a height of 9 cm—along with an air void content of 11 percent.

Step 4:

Table A.3 displays the weight of each size fraction of the aggregate required in the DMA sample. These values were calculated using the aggregate batch weight found in Step 3 and the aggregate proportions determined during Steps 1 and 2.

Table A.3. Aggregates Weight for DMA Mixture (Mix #7).

Sieve (mm)	Weight (g)	
	Limestone Sand	Natural Sand
#30 (0.6)	377.69	886.46
#50 (0.3)	328.43	1002.08
#100 (0.15)	180.63	501.04
#200 (0.075)	42.70	26.98

Steps 5 and 6:

The mass of asphalt determined in this example was 267.68 g, or 8 percent of the mass of the batch size calculated in Step 3. The mass of each filler, material passing sieve # 200 (0.075 mm), was found using Equation A.2. They were calculated to be 17.10 g for limestone sand and 44.46 g for natural sand.

Figure A.1 presents full HMA and DMA mixtures gradation curves.

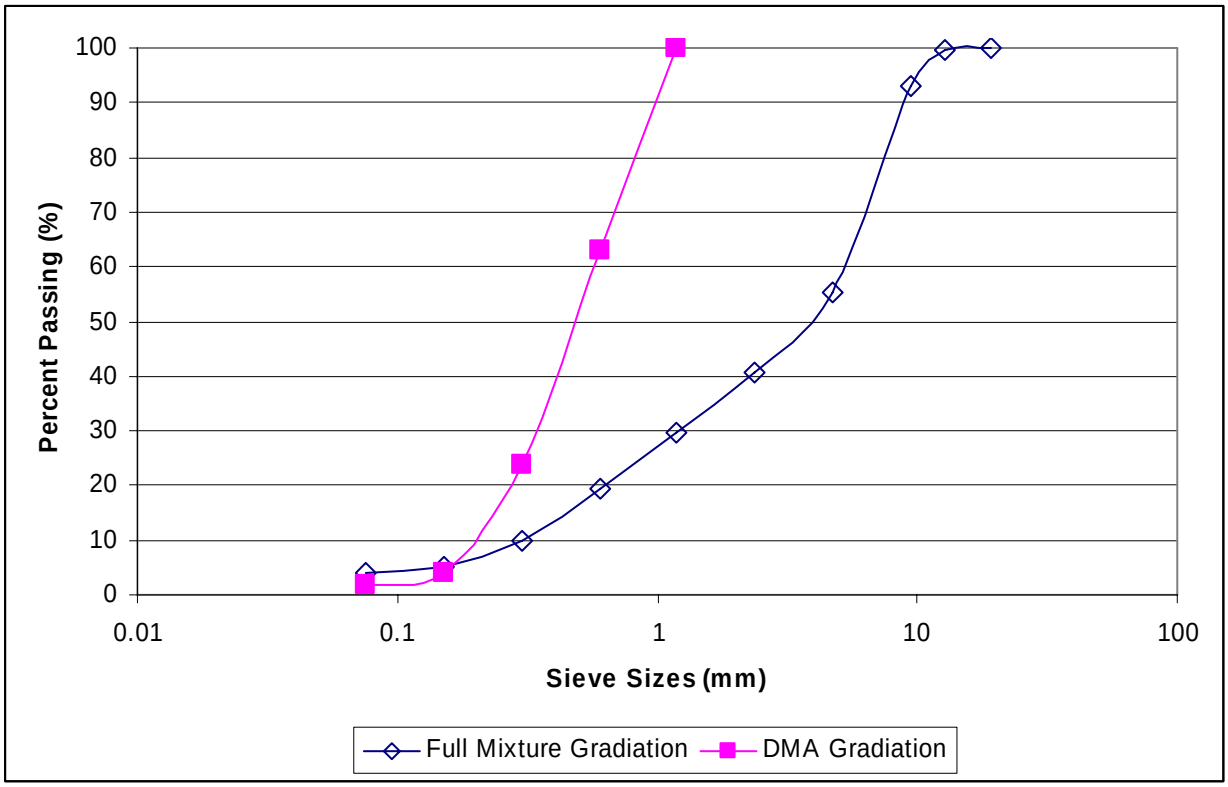

Figure A.1. Full HMA and DMA Mixtures Gradation Curves.

APPENDIX B
IMPROVED DESIGN METHOD FOR SAND ASPHALT MIXTURES

The following protocol describes a new method for the design of sand asphalt mixtures for DMA testing. The main feature of this method is the development of a more quantitative method for the calculation of the *A/FA* ratio.

STEP

1. Obtain the following information about the full HMA mixture:
    a. aggregate gradation,
    b. specific gravity of each filler (passing sieve No. 200) used in the mix,
    c. percent of binder by weight of the mixture, and
    d. Maximum specific gravity of the mixture.
2. Determine the percentage of each aggregate that passes sieve No. 16 (1.18 mm).
3. Calculate the aggregate batch weight of material passing sieve No. 16 and retained on sieve No. 200. This is the batch weight used to prepare the sand asphalt mixture sample in the Superpave gyratory compactor. Equation B.1 can be used to estimate the aggregate batch weight:

$$Aggregate\ batch\ weight\ (g) = \pi \times r^2 \times h \times G_{mm}(1 - Vv\%) \qquad \text{(B.1)}$$

    where r is the sample radius (typically 6 in), h is the sample height (typically 3 in), G_{mm} is the maximum specific gravity of the full mixture, and $Vv\%$ is desired percent air voids in the sand asphalt mixture (recommended value is 11 percent).
4. Calculate the mass of aggregate retained on each sieve using the aggregate batch size (Step 3) and the percent of material retained on each sieve.
5. Obtain the aggregate bulk specific gravity.
6. Calculate the volume of aggregates retained on each sieve using the mass of aggregate retained on each sieve (Step 4) and the aggregate bulk specific gravity (Step 5).
7. Assuming a spherical shape for particles, calculate the number of aggregates retained on each sieve by dividing the volume of the total material retained on each sieve (Step 6) by the volume of one sphere. The volume of a spherical particle is calculated using the average particle size on the sieve.

8. Estimate binder film thickness according to the percent of binder used in the full HMA mixture. Binder film thickness, T_F, can be estimated using Equation B.2.

$$T_F = \frac{V_{asp}}{SA \times W}(1{,}000) \tag{B.2}$$

where V_{asp} is the effective volume of asphalt binder, the volume of absorbed binder is subtracted from the volume of binder, SA is the surface area of all the combined aggregates in the full HMA mixture, and W is the weight of the aggregates. Common values for binder film thickness are between 4 and 10 μm.

9. Calculate the volume of aggregate (retained in each sieve) plus binder using Equation B.3:

$$v = \frac{4}{3}\pi R^3 \tag{B.3}$$

where R is the radius of aggregate (assuming that aggregate particles are spheres with diameter equal the average diameter of the sieve) plus the binder film thickness (Step 8).

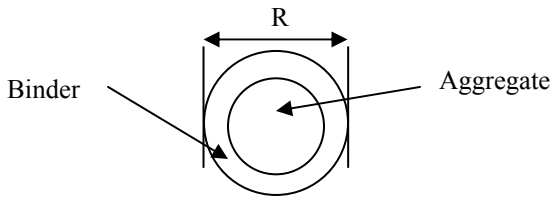

10. Calculate the volume of binder covering the aggregates retained in each sieve in the full HMA mixture by subtracting the volume of aggregate (Step 6) from volume of aggregate plus binder (Step 9).
11. Calculate the total volume of binder in the sand asphalt mixture by summing the volumes obtained in Step 10 for aggregates passing sieve No. 16 through aggregates retained on sieve No. 200.

12. Calculate the percent asphalt binder in the sand asphalt mixture.
13. Obtain the weight of each filler by using Equation B.4:

$$Filler(g)=\%Filler\times F/A\times binder\ weight\times filler\ specific\ gravity \quad \text{(B.4)}$$

where *F/A* is ratio of all fillers to asphalt by volume, and *%Filler* is the percentage of the filler for which calculations are being conducted with respect to all fillers. According to Kim et al. (2003), the recommended filler to binder ratio (*F/A*) is 10 percent.

14. Calculate the ratio of binder plus filler to fine aggregates in mass (*A/FA*) using the amount of binder found in Step 12.
15. Based on experience, researchers found that the calculated asphalt content (Step 12) was too high due to the assumption of a spherical particle shape. The calculated percent binder should be reduced based on particle shape. However, it is recommended to start by initially reducing the asphalt content of the DMA mixture by 30 percent.

EXAMPLE: IMPROVED SAND ASPHALT MIX DESIGN METHOD

Step 1:

The asphalt mixture selected for this example is the full HMA Mixture No. 7. Aggregate gradation and composition for the full HMA mixture are presented in Tables B.1 and B.2. The asphalt binder used in this example was rated as a PG 64-22 and is manufactured by Tri-State Asphalt out of Rayland, Ohio. 5.4 percent asphalt binder by weight of aggregate was added to the mixture. DMA samples were prepared using aggregate passing sieve No. 16 (1.18 mm). Only aggregates that have more than 50 percent passing sieve No. 16 are used for preparing DMA specimens. Aggregate gradations that have less than 50 percent passing sieve No. 16 do not contribute enough material to be of consequence and are, therefore, not included. For this case, only limestone sand and natural sand were used for DMA sample fabrication; see bolded portion of Table B.1. Rap was not in the DMA mixture design for this example. The overall specific gravity for the fillers was 2.3, and the maximum specific gravity (G_{mm}) for this mix was 2.302.

Table B.1. Aggregates Gradations for Full HMA Mixture (Mixture No. 7).

Sieve (mm)	% Passing				
	#8 Limestone	#8 Gravel	Limestone Sand	Natural Sand	Rap (Project 159-86 & 209 98)
2" (50.80)	100.0	100.0	100.0	100.0	100.0
1 1/2" (37.50)	100.0	100.0	100.0	100.0	100.0
1" (25.40)	100.0	100.0	100.0	100.0	100.0
3/4" (19.05)	100.0	100.0	100.0	100.0	100.0
1/2" (12.70)	100.0	100.0	100.0	100.0	98.0
3/8" (9.50)	88.0	95.0	100.0	100.0	83.0
#4 (4.75)	18.0	20.0	100.0	100.0	55.0
#8 (2.36)	2.0	2.0	90.0	92.0	34.0
#16 (1.18)	2.0	2.0	**63.0**	**67.0**	25.0
#30 (0.6)	2.0	2.0	**40.0**	**44.0**	16.0
#50 (0.3)	2.0	2.0	**20.0**	**18.0**	12.0
#100 (0.15)	2.0	2.0	**9.0**	**5.0**	10.0
#200 (0.075)	2.0	2.0	**6.40**	**4.30**	7.6

Table B.2. Aggregate Composition for Full HMA Mixture (Mixture No. 7).

Aggregate	#8 Limestone	#8 Gravel	Limestone Sand	Natural Sand	Rap (Project 159-86 & 209 98)
% in the mix	22	22	10	26	20

Step 2:

To ensure the DMA sample is accurate, based on the full HMA mixture, the aggregate proportions from the full mixture are used for the DMA sample. The limestone sand and natural sand comprise the entire DMA sample, so the new proportions used for limestone sand and natural sand are 28 and 72 percent, respectively.

Step 3:

The estimation of the DMA mixture batch weight is done using Equation B.1. The mixture in this example had an estimated batch weight of approximately 3346 g. The dimensions of an ideal specimen are used—a 15.2 cm diameter and a height of 9 cm—along with an air void content of 11 percent.

Step 4:

Table B.3 displays the weight of each size fraction of the aggregate required in the DMA sample. These values were calculated using the aggregate batch weight found in Step 3 and the aggregate proportions determined during Steps 1 and 2.

Table B.3. Aggregates Weight for DMA Mixture (Mixture No. 7).

Sieve (mm)	Weight (g)	
	Limestone Sand	Natural Sand
#30 (0.6)	377.69	886.46
#50 (0.3)	328.43	1002.08
#100 (0.15)	180.63	501.04
#200 (0.075)	42.70	26.98

Step 5:

To simplify the example, the bulk specific gravity of the mixture (G_{mb}) was used instead of the bulk specific gravity of each aggregate size fraction. It is recommended to use the bulk specific gravity of each aggregate size fraction in the calculations if the information is available.

Step 6:

Table B.4 displays the volume of aggregates retained on each sieve for the full HMA mixture. For this example, a batch weight of 4500 g was used. The diameters of the sieves were taken as an average of two consecutives sieves.

Steps 7 through 11:

In this design method, aggregates are considered to have a spherical shape. The number of spheres retained in each sieve was obtained by dividing the volume of aggregate retained on each sieve (Table B.4) by a sphere representing the volume of the aggregate particle (Equation B.3). The volume of aggregates plus binder was calculated assuming a binder film thickness equal to 8 μm. The volume of binder was calculated by subtracting the volume of aggregate (Table B.4) from the volume of aggregate plus binder (Table B.5). In Table B.5, researchers noted that 90.16 percent of the asphalt binder goes to the fine portion (below sieve No. 16) of the full HMA mixture. This large amount of binder can be justified by the high surface area per mass of the fine aggregates.

Table B.4. Volume of Aggregates Retained on Each Sieve for the Full HMA Mixture (Mix No. 7).

Sieve	Sieve Size (mm)	Sieve Size (cm)	Diameter (cm)	% Retained	Mass (g)	Volume of Aggregates (cm^3)
2"	50.80	5.08	4.415	0.00	0.00	0.00
1 1/2"	37.50	3.75	3.145	0.00	0.00	0.00
1"	25.40	2.54	2.2225	0.00	0.00	0.00
3/4"	19.05	1.905	1.5875	0.00	0.00	0.00
1/2"	12.70	1.27	1.11	0.40	17.03	7.39
3/8"	9.50	0.95	0.7125	6.74	286.92	124.59
#4	4.75	0.475	0.3555	37.50	1596.38	693.17
#8	2.36	0.236	0.177	14.76	628.33	272.83
#16	1.18	0.118	0.089	11.00	468.27	203.33
#30	0.60	0.06	0.045	10.08	429.11	186.32
#50	0.30	0.03	0.0225	9.56	406.97	176.71
#100	0.15	0.015	0.01125	4.88	207.74	90.20
#200	0.075	0.0075	0.0075	0.92	39.25	17.04
<#200	0.075	0.0075	0.00375	4.16	177.01	76.86

Table B.5. Volume and Mass of Binder Retained in Each Sieve for Full HMA Mixture (Mixture No. 7).

Sieve	Spheres nº	Volume Aggregate + Binder	Volume Binder (cm^3)	% Volume Binder	% Accumulated	% Accumulated	Mass Binder (g)	% Mass Binder
2"	0.00E+00	0.00E+00	0.000	0.00%	0.00%		0.00	0.00%
1 1/2"	0.00E+00	0.00E+00	0.000	0.00%	0.00%		0.00	0.00%
1"	0.00E+00	0.00E+00	0.000	0.00%	0.00%		0.00	0.00%
3/4"	0.00E+00	0.00E+00	0.000	0.00%	0.00%		0.00	0.00%
1/2"	1.03E+01	7.43E+00	0.032	0.01%	0.01%	9.84%	0.03	0.01%
3/8"	6.58E+02	1.25E+02	0.841	0.29%	0.30%		0.87	0.29%
#4	2.95E+04	7.03E+02	9.401	3.20%	3.50%		9.68	3.20%
#8	9.40E+04	2.80E+02	7.466	2.54%	6.04%		7.69	2.54%
#16	5.51E+05	2.14E+02	11.164	3.80%	9.84%		11.50	3.80%
#30	3.91E+06	2.07E+02	20.590	7.01%	16.84%		21.21	7.01%
#50	2.96E+07	2.17E+02	40.443	13.76%	30.60%		41.66	13.76%
#100	1.21E+08	1.34E+02	44.221	15.05%	45.65%		45.55	15.05%
#200	7.72E+07	3.04E+01	13.400	4.56%	50.21%	90.16%	13.80	4.56%
<#200	2.78E+09	2.23E+02	146.324	49.79%	100.00%		150.71	49.79%

Step 12:

The mass of asphalt binder needed for the DMA mixture can be calculated once the amount of fine aggregate retained on each sieve, the aggregate batch weight, and the mass of asphalt binder for the full HMA mixture are known. For this example, the percentage of asphalt binder by weight for the DMA mixture was found to be 14.52 percent.

Step 13:

The amount of filler for each aggregate type to be used in the DMA mixture was calculated using Equation B.4.

Step 14:

The ratio of asphalt binder plus filler to fine aggregates by mass (A/FA) was found to be 18 percent. This was accomplished by using the mass of asphalt binder found in Step 12.

APPENDIX C

FRACTURE ANALYSIS AND MOISTURE SUSCEPTIBILITY OF ASPHALT MIXTURES

SECTION 1

Overview

Use this test method to analyze the fracture potential of compacted hot mix asphalt concrete (HMAC) mixtures. The fundamental material properties required are the tensile strength, the elastic relaxation modulus, the stress relaxation rate, and the rate of accumulation of fracture damage.

Use the following to obtain the parameters necessary to compute the crack growth index, denoted by *r*:

- Part I–Tensile strength test to obtain the maximum tensile strength under direct tensile loading,
- Part II–Relaxation modulus test to obtain the elastic relaxation modulus and the stress relaxation rate under static direct loading, and
- Part III–Repeated direct tension test to determine the rate of accumulation of fracture damage under repeated direct tensile loading

Units of Measurements

The values given in parentheses (if provided) are not standard and may not be exact mathematical conversions. Use each system of units separately. Combining values from the two systems may result in nonconformance with the standards.

SECTION 2

Apparatus

Use the following apparatus:

- Loading Mechanism (see Figure C.1 for the loading configuration)
  - Capable of applying a continuous direct axial tensile load at a constant elongation (deformation) rate of 0.01 inches/min (0.25 mm/min) for a specified period (see Part I for the tensile strength test description),

- Capable of applying a tensile and compressive load to maintain a constant axial strain (deformation or displacement) in tension or compression mode for a specified loading period (see Part II for the relaxation modulus test description),
- Capable of applying a uniaxial repeated direct tensile load at a given strain level for a specified number of load cycles (see Part III for the RDT test description).
- A load cell capable of measuring the axial load to an accuracy of ±2 percent of the applied axial load.
- A load cell calibrated and/or checked prior to initiation of any program of testing, rechecked monthly thereafter, and recalibrated semiannually.

- Temperature Control System
  - The system is capable of controlling temperature within a range of 50 to 86°F (10 to 30°C).
  - The system includes a temperature-controlled cabinet or chamber large enough to hold at least three specimens.
  - The temperature should be monitored and recorded via a thermocouple probe inserted inside a HMAC specimen, also placed in the temperature chamber.
  - The temperature must be held to within ±2°F (±1°C) of the specified test temperature.
  - The specimens should be pre-conditioned to the test temperatures (in the temperature chamber) for a minimum period of 2 hrs prior to testing.
  - CO_2 can be used to maintain temperature inside the test chamber.
- Loading Platens
  - Two loading platens must be used for the upper and lower ends of the specimen.
  - Both loading platens must be of the same diameter as the specimen being tested to provide for positive centering of the specimen under load.
  - The upper loading platen provides attachment to the load cell, and the lower loading platen is used to fix the sample to the base plate of the loading frame (Figure C.1).
  - The loading platens must be thoroughly cleaned, wiped with acetone, and dried prior to use. The side of the loading platens attaching to the specimen should be rough to provide an effective connection to the specimen.
  - LVDT Attachments

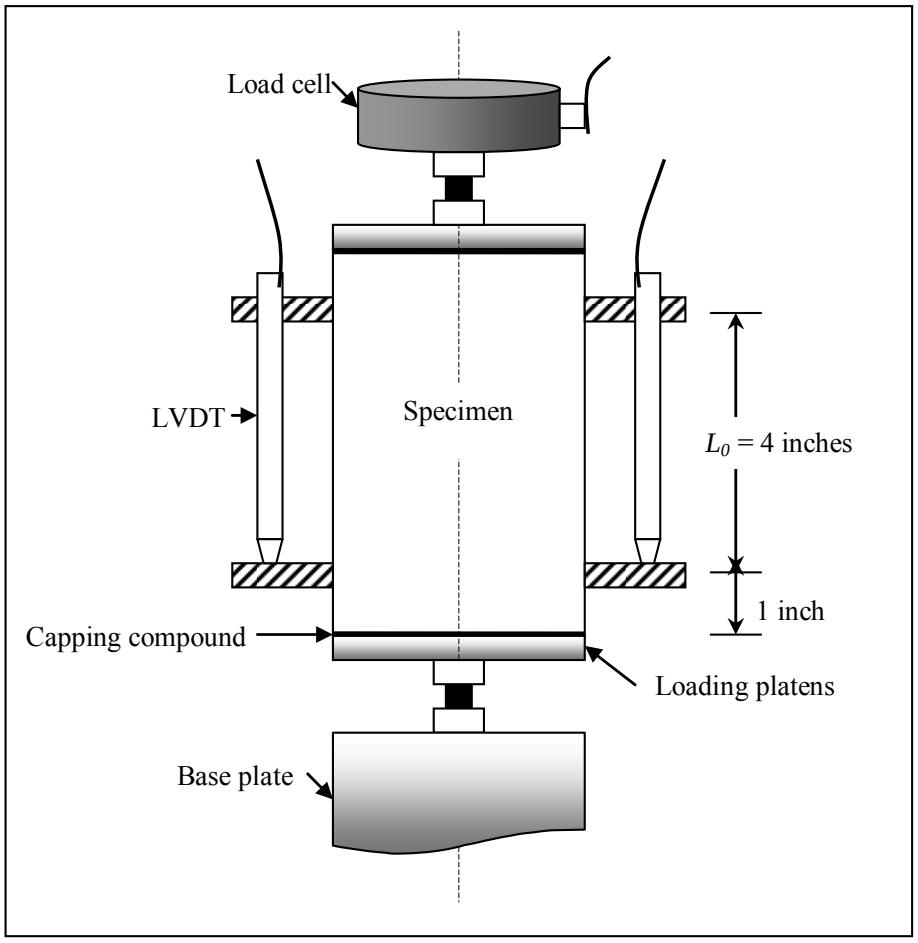

Figure C.1. Specimen Setup and LVDT Configuration.

- Use three LVDTs for deformation measurements.
- Attach the LVDTs at three radial equidistances around the specimen. For 6 in (150 mm) height specimens, the vertical distance between the LVDT holders should be 4 in (100 mm) center to center and 1 in (25 mm) from the specimen end as shown in Figure C.1.
    - Measurement and Recording System
    - Measure the vertical deformation with the LVDTs; the resolution of each LVDT must be at least of 0.0001 in (0.0025 mm).
    - Measure load with an electronic load cell capable of measuring vertical loads of up to 5000 lb (22 241 N) with an accuracy of ±2 percent of the load level being applied.

- Continuously monitor and record the load and axial deformations during the test at the specified frequency, according to the type of test being performed. Temperature should also be continuously monitored and recorded at least every 5 s.

SECTION 3

Materials and Test Specimens

- Capping compound (such as 2 ton Epoxy) that is able to withstand at least 1000 lb (5000 N) load without cracking for attaching the loading platens to the specimen.
- Gluing compound (such as Pro CA Cyanoacrylate and an accelerator) that is used for attaching the LVDT fixtures to the specimen.
- Laboratory Molded Specimen
- Prepared according to test methods "Laboratory Method of Mixing Bituminous Mixtures," and or "Tex-241-F, Superpave Gyratory Compacting of Test Specimens of Bituminous Mixtures."
- The recommended size for the cylindrical specimen is 4 in (100 mm) diameter and 6 in (150 mm) height to a tolerance of ± 0.1 in (± 2.5 mm).
- Specimens may initially be molded to 6 in (150 mm) diameter by 7 in (175 mm) height and then saw and cored to a final dimension of 4 in (100 mm) diameter by 6 in (150 mm) height.
- Specimen end surfaces must be sawn smooth and parallel.
- Density of test specimens must be 93 ± 1 percent (i.e., 7±1 air voids).

- Field Cored Specimen
  - Cylindrical specimen of diameter of 4 in (100 mm) and height of 6 in (150 mm) with ± 0.1 in (± 2 mm) tolerance.
  - End surfaces must be smooth and parallel.

SECTION 4

Part I–Tensile Strength Test

Use this test method to characterize the maximum tensile strength of compacted HMAC mixtures. The measured fundamental material properties from this test are the tensile strength and the tensile failure strain at break under direct-tensile loading. For additional information on this test procedure, please refer to the TxDOT technical report 0-4468-3: "*Application of Calibrated Mechanistic Fatigue Analysis with Aging Effects*" by L.F. Walubita, A. Epps Martin, S. Jung, C.J. Glover, and E. Park.

The loading mechanism should apply a continuous axial tensile load at a constant elongation (deformation) rate of 0.01 in/min (0.25 mm/min) until the specimen breaks or the peak load drops by 25 percent, whichever occurs first. See Figure C.2 for the loading configuration.

The recommended test temperature is 68°F (20°C) or the reference temperature used to construct the relaxation master curve (see Section 5). The load and axial deformation during the test should be recorded at every 0.1 s and the temperature monitored at least every 5 s.

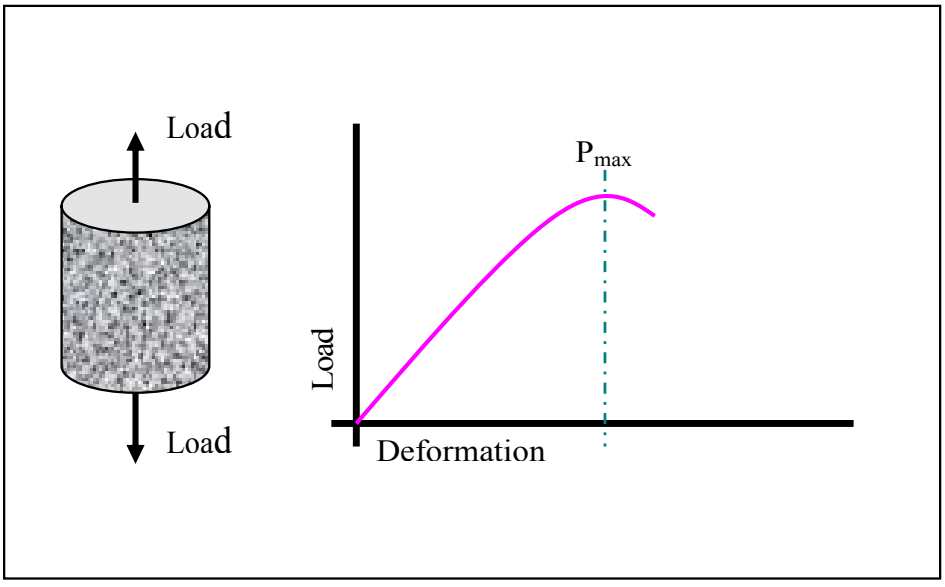

Figure C.2. Tensile Strength Test Loading Configuration.

Procedure

Follow the next procedure to perform the tensile strength test:

TENSILE STRENGTH TEST

Step	Action
1.	Fabricate at least three specimens as described in Section 3.
2.	Measure and record for each specimen: • Dimensions (diameter and height) • Relative density and air voids according to test methods "Tex-207-F, Determining Density of Compacted Bituminous Mixtures" and "Tex-227-F, Theoretical Maximum Specific Gravity of Bituminous Mixtures."
3.	Attach loading platens and LVDT fixtures: • Mix the capping compound specified in Section 3, apply it to the loading platens using a spatula, and attach them to the end surfaces of the specimen. Two loading platens are required for each specimen. • Apply some pressure (such as extra weights) to the loading platens while allowing the capping compound to dry for about 24 hours. • Use the gluing compound specified in Section 3 to attach the LVDT fixtures to the specimen as described in Section 2.
4.	Precondition the specimen to the test temperature for a minimum of 2 hours prior to testing.
5.	Attach the specimen to the loading mechanism and load cell as shown in Figure C.1. Make sure to align the specimen along the central axis of loading to minimize the possibility of erroneous or misleading results.
6.	Fix the LVDTs in the LVDT fixtures and zero their readings prior to testing.
7.	In load-controlled mode, apply a continuously increasing tensile load at a deformation rate 0.01 inches/min (0.25 mm/min) until the specimen breaks or the peak load drops by 25 percent, whichever occurs first.

8.a. During Step 7, record every 0.1 s:

- Time (t [s]),
- Load (P [lbs or kips])
- Deformation (ΔL[in or mm])

8.b. Monitor every 5 s:

- Temperature (T [°F or °C])

9. When testing is done, detach the LVDTs from the fixtures and remove the specimen from the machine setup

Calculations

- Calculate the maximum tensile strength and failure strain as follows:

  Maximum tensile strength

$$\sigma_{t\max} = \frac{P_{\max}}{\pi r^2} \tag{C.1}$$

  Failure tensile strain

$$\varepsilon_f = 10^6 \frac{\Delta L_{\max}}{L_0} \tag{C.2}$$

  where:

  σ_{tmax} = Maximum tensile strength, psi (or MPa),

  P_{max} = Peak tensile load, lbs (or kN),

  r = Radius of the cylindrical HMAC specimen, inches (or mm),

  ε_f = Failure tensile strain at P_{max} in microns, in/in (or mm/mm),

  ΔL_{max} = Deformation at P_{max}, inches (or mm),

  L_0 = Initial distance between the LVDT holders (see Figure C.1), inches (or mm).

- For each specimen, ε_f should be calculated as the average of the three LVDTs.
- Figure C.3 is a typical plot of tensile stress versus strain, where:

  Tensile Stress

$$\sigma_t = \frac{P}{\pi r^2} \tag{C.3}$$

Tensile microstrain

$$\varepsilon = 10^6 \frac{\Delta L}{L_0} \quad \text{(C.4)}$$

- From this plot, obtain:
  - The maximum tensile strength, σ_t (psi) as the peak tensile stress, e.g., 93.5 psi in Figure C.3.
  - The corresponding failure tensile strain, ε_f, e.g., 3,908.0 με in Figure C.3.
- A minimum of three replicate specimens are recommended for the test.

- If the computed coefficient of variation (COV) for the σ_t of the three specimens differs by more than 15 percent, researchers recommend testing additional specimens. Note that 15 percent is a typically acceptable COV for HMAC mixtures/specimens due to HMAC heterogeneity and test variability.

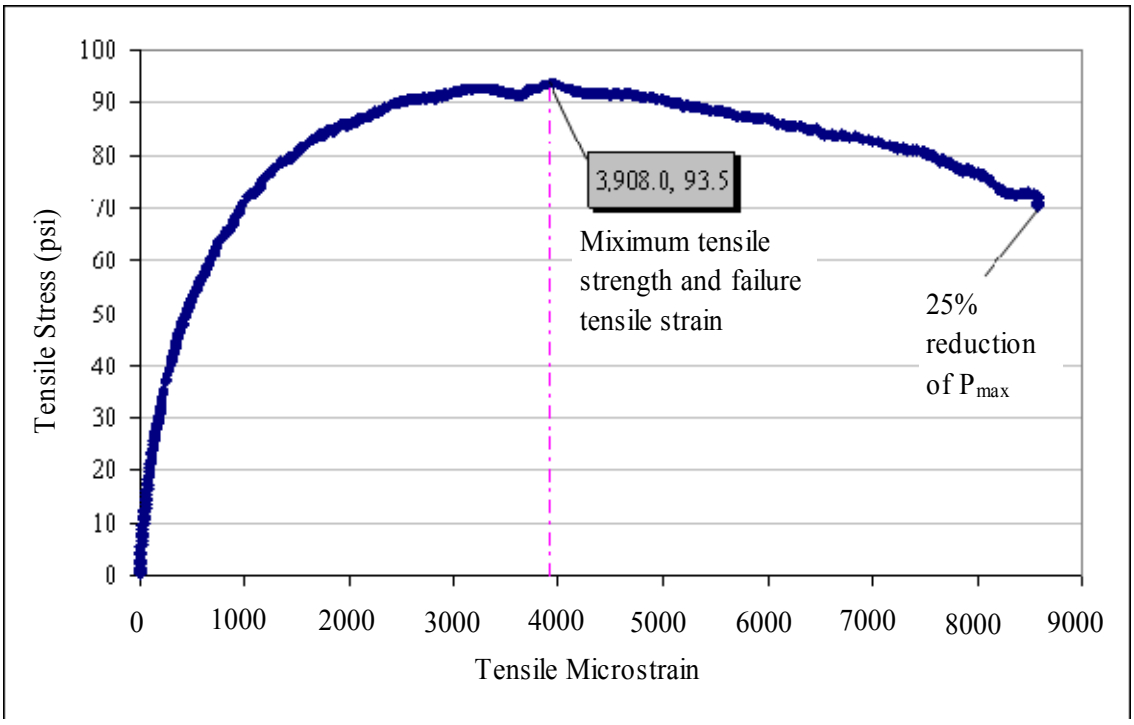

Figure C.3. Typical Plot of Tensile Stress versus Strain Performed at a Temperature of 68°F (20°C).

Report

The results and data to be reported for subsequent analyses include:

- the air void content (and density),
- the binder content,
- the peak tensile load (P_{max}),
- the average maximum tensile strength (σ_t),
- the average failure tensile strain (ε_f) in microns,
- the loading rate,
- the test temperature, and
- the COV of σt and εf.

SECTION 5

Part II–Relaxation Modulus Test

Use this test method to characterize the elastic relaxation modulus and stress relaxation rate of HMAC mixtures. The test involves applying a constant axial strain (or displacement) to a cylindrical HMAC specimen in tension for 60 s, releasing the strain for 600 s to allow the specimen to relax (elastic recovery), and finally applying a constant axial strain in compression for another 60 s.

The test should be run in strain-controlled (displacement or LVDT mode), and one of the three LVDTs (preferably the one designated as LVDT 1) should be used as the control. The loading mechanism should apply a tensile and compressive load to maintain a constant axial strain (deformation or displacement) equivalent to 20 percent of the failure tensile strain (i.e., $0.2\varepsilon_f$) obtained from the tensile strength test performed at a test temperature of 68°F (20°C). If a higher temperature is used to perform the tensile strength test, the percent of the failure tensile strain should be reduced. Likewise, if a lower temperature is used during the tensile strength test, the percentage of the failure tensile strain should be increased. Ten percent of the tensile strain (i.e., $0.1\varepsilon_f$) is recommended for a tensile strength test performed at 86°F (30°C). The input strain waveform is trapezoidal-shaped as shown in Figure C.4. The time required to achieve the target strain level from 0 to $+0.2\varepsilon_f$ (tension) or from 0 to $-0.2\varepsilon_f$ (compression) should not exceed 6 s.

The test must at least be performed at three temperatures to facilitate generation of a master-curve. The three recommended test temperatures are 50, 68, and 86°F (10, 20, and 30°C). However, other preferred temperatures may be used. The test should start with the lowest temperature, and once the tensile and compressive loading sequence is done, the next highest temperature should be set and the specimens preconditioned to perform the test again.
The load and axial deformations should be recorded during the test at least every 0.5 s, and the temperature should be monitored at least every 5 s. The measurable fundamental material properties from this test are the elastic relaxation modulus and the stress relaxation rate denoted by the parameter *m*. For additional information on this test procedure, please refer to the TxDOT technical report 0-4468-3: "*Application of Calibrated Mechanistic Fatigue Analysis with Aging Effects*" by L.F. Walubita, A. Epps Martin, S. Jung, C.J. Glover, and E. Park.

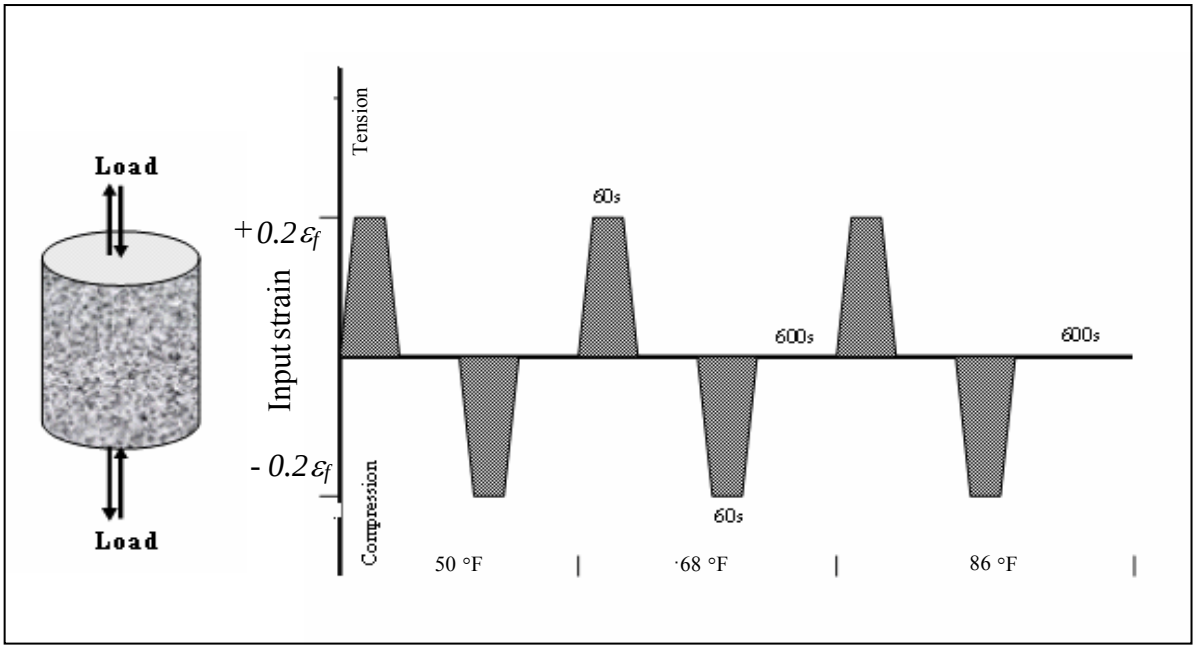

Figure C.4. Relaxation Modulus Test Loading Configuration.

Procedure

Follow the next procedure to perform the tensile strength test:

TENSILE STRENGTH TEST

Step	Action
1.	Fabricate at least three specimens as described in Section 3.
2.	Measure and record for each specimen: • Dimensions (diameter and height) • Relative density and air voids according to test methods "Tex-207-F, Determining Density of Compacted Bituminous Mixtures" and "Tex-227-F, Theoretical Maximum Specific Gravity of Bituminous Mixtures."
3.	Attach loading platens and LVDT fixtures: • Mix the capping compound specified in Section 3, apply it to the loading platens using a spatula, and attach them to the end surfaces of the specimen. Two loading platens are required for each specimen. • Apply some pressure (such as extra weights) to the loading platens while allowing the capping compound to dry for about 24 hours. • Use the gluing compound specified in Section 3 to attach the LVDT fixtures to the specimen as described in Section 2.
4.	Precondition the specimen to a given test temperature for a minimum of 2 hours prior to testing. *Note: The test should start with the lowest temperature and once the tensile and compressive loading sequence is done, the next highest temperature should be set and the specimens preconditioned to perform the loading sequence again.*
5.	Attach the specimen to the loading mechanism and load cell as shown in Figure C.1. Make sure to align the specimen along the central axis of loading to minimize the possibility of erroneous or misleading results.
6.	Fix the LVDTs in the LVDT fixtures and zero their readings prior to testing.
7.	For a given test temperature: • In displacement-controlled (strain-controlled) mode, apply a load to induce the selected target tensile strain (e.g., $+0.2\varepsilon_f$) for a period of 60 s.

- Release the load and allow the specimen to relax for 600 s.
- In displacement-controlled (strain-controlled) mode, apply a compressive load to achieve the selected target tensile strain (e.g., -0.2ε_f) for a period of 60 s.
- Release the load and allow the specimen to relax for 600 s

8. During Step 7, record every 0.5 s:
   - Load (P [lbs or kips])
   - Deformation (ΔL[in or mm])
   - Time (t [s])

Note that it is not necessary to capture data during the last rest period since it is not used in the calculations.

   - Monitor every 5s:
   - Temperature (T [°F or °C])

9. Repeat Steps 4 to 8 for the rest of the specified test temperatures.
   Note: The same specimen can be used for all test temperatures.
10. When the testing sequence has been performed at all the different temperatures, detach the LVDTs from the fixtures and remove the specimen from the machine setup.

Calculations

- Calculate the time-dependent elastic relaxation modulus as follows:

$$E(t) = \frac{P(t)}{\pi r^2 \varepsilon} \tag{C.5}$$

where:

E(t) = Time-dependent elastic relaxation modulus, psi (or MPa),
P(t) = Load, lb (or kN),
R = Radius of the cylindrical HMAC specimen, in (or mm),
ε = Applied target tensile strain (e.g., +0.2ε_f).

- Using the time-temperature superposition principle, generate a master-curve of *E(t)* versus reduced time ξ (s) in the form of simple power function illustrated below:

$$E(t) = E_1 \xi^{-m} \tag{C.6}$$

where:

$E(t)$ = Time-dependent elastic relaxation modulus, psi (or MPa),

E_1 = Elastic relaxation modulus at a reduced loading time of 1 s, psi (or MPa),

ξ = Reduced loading time, s,

m = Stress relaxation rate ($0 \leq m < 1$).

- Reduced time is determined as a function of the actual loading time (t) and temperature correction factors (a_T):

$$\xi = \frac{t}{a_T} \tag{C.7}$$

- The temperature correction factors can be obtained using the Arrhenius equation:

$$\log a_T = \log e \frac{\Delta H}{R}\left(\frac{1}{T} - \frac{1}{T_{ref}}\right) \tag{C.8}$$

where:

T = actual temperature, K,

T_{ref} = reference temperature, K,

ΔH = activation energy, J/mol,

R = gas constant [8.314 J/(mol K)].

Alternatively to Equation C.8, the Williams-Landel-Ferry (WLF) equation can also be used to estimate the temperature correction factors:

$$\log a_T = \frac{-C_1(T - T_{ref})}{C_2 + T - T_{ref}} \tag{C.9}$$

where:

T	=	actual temperature, °C,
T_{ref}	=	reference temperature, °C,
C_1 and C_2	=	regression constants.

The values of E_1, m, and ΔH (Arrhenius equation) and C_1 and C_2 (WLF equation) are obtained using the *solver* tool in Excel, by minimizing the sum of squared errors between the measured and the predicted modulus values using Equation C.6.

- The recommended reference temperature for the master curve is 68°F (20°C), but a higher or lower temperature can also be used and should be consistent with the temperature of the tensile strength test.
- Figure C.5 presents a typical plot of the relaxation modulus master curve for tension loading mode at a reference temperature of 68°F (20°C).

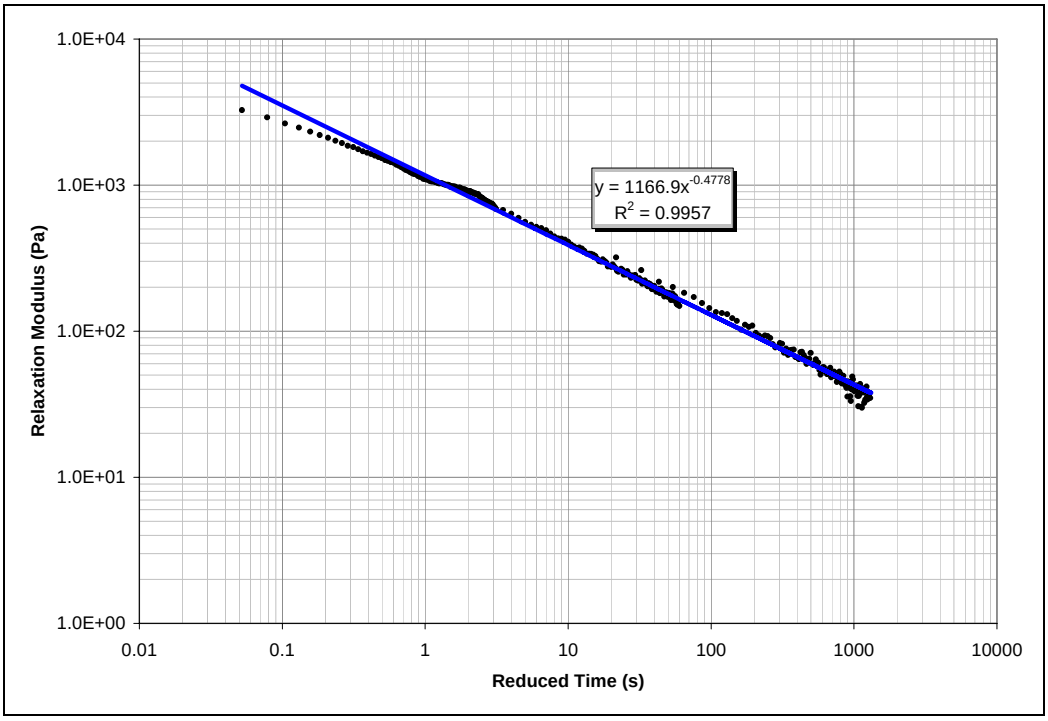

Figure C.5. Typical Plot of the Relaxation Modulus Master Curve (Tension, T_{ref} = 68°F).

- From the master curve constructed using the tension results, obtain:
    - the elastic relaxation modulus, E_1 (psi) as the $E(t)$ at a reduced loading time of 1 s, e.g., 1187.7 MPa in Figure C.5, and
    - the stress relaxation rate (m), which is the slope of the master curve, e.g., 0.4293 in Figure C.5.
- A minimum of two replicate specimens are recommended for this test.
- If the computed COV for the E_1 values of the two specimens differs by more than 15 percent, it is recommended to test additional specimens. Note that 15 percent is a typically acceptable COV for HMAC mixtures/specimens due to HMAC heterogeneity and test variability.

Report

The results and data to be reported for subsequent analyses include:

- the air void content (and density),
- the binder content,
- the (average) tensile elastic relaxation modulus (E_1),
- the (average) tensile stress relaxation rate (m),
- the reference temperature for the master-curve (T_{ref}),
- the temperature correction factors (a_T), and
- the COV of E_1 and m.

SECTION 6

Part III–Uniaxial Repeated Direct Tension Test

Use this test method to characterize the fracture damage potential of HMAC mixtures under repeated direct tensile loading. The measurable fundamental material property from this test is the rate of accumulation of fracture damage under repeated direct tensile loading, a parameter denoted as b, and the reference modulus, E_R.

The test should be run in strain-controlled (displacement or LVDT mode), and one of the three LVDTs (preferably the one designated as LVDT 1) should be used as the control. The input strain waveform is haversine-shaped as shown in Figure C.6. The loading frequency is 1 Hz.

Therefore, the complete load cycle is 1.0 s with a loading period of 0.1 s and a resting period of 0.9 s between load pulses. The total number of load repetition should be 1000. The test must be setup so that it ends automatically, after the number of load repetitions reaches 1000.

The loading mechanism should apply load equivalent to induce a deformation of 35 percent of the failure tensile strain from the tensile strength test (i.e., 0.35 ε_f) performed at a test temperature of 68°F (20°C). If a higher temperature is used to perform the tensile strength test, the percent of the failure tensile strain should be reduced. Likewise, if a lower temperature is used during the tensile strength test, the percentage of the failure tensile strain should be increased. About 18 percent of the tensile strain (i.e., 0.18 ε_f) is recommended for tensile strength tests performed at 86°F (30°C).

The recommended temperature for this test is 68°F (20°C) or the temperature used to perform the tensile strength test and to construct the relaxation master curve (see Sections 4 and 5).

For additional information on this test procedure, please refer to the TxDOT technical report 0-4468-3: "*Application of Calibrated Mechanistic Fatigue Analysis with Aging Effects*" by L.F. Walubita, A. Epps Martin, S. Jung, C.J. Glover, and E. Park.

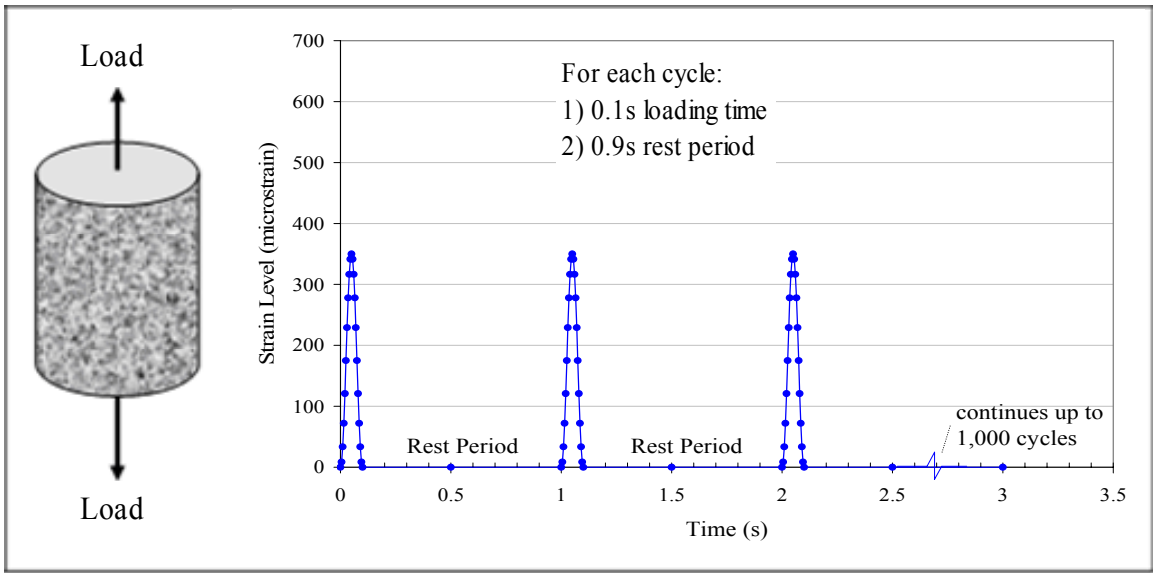

Figure C.6. Repeated Direct Tension Loading Configuration.

UNIAXIAL REPEATED DIRECT TENSION TEST

Step	Action
1.	Fabricate at least three specimens as described in Section 3.
2.	Measure and record for each specimen: • Dimensions (diameter and height) • Relative density and air voids according to test methods "Tex-207-F, Determining Density of Compacted Bituminous Mixtures" and "Tex-227-F, Theoretical Maximum Specific Gravity of Bituminous Mixtures."
3.	Attach loading platens and LVDT fixtures: a. Mix the capping compound specified in Section 3, apply it to the loading platens using a spatula, and attach them to the end surfaces of the specimen. Two loading platens are required for each specimen. b. Apply some pressure (such as extra weights) to the loading platens while allowing the capping compound to dry for about 24 hours. • Use the gluing compound specified in Section 3 to attach the LVDT fixtures to the specimen as described in Section 2.
4.	Precondition the specimen to a given test temperature for a minimum of 2 hours prior to testing.
5.	Attach the specimen to the loading mechanism and load cell as shown in Figure C.1. Make sure to align the specimen along the central axis of loading to minimize the possibility of erroneous or misleading results.
6.	Fix the LVDTs in the LVDT fixtures and zero their readings prior to testing.
7.	In displacement-controlled (strain-controlled) mode, repeatedly apply a tensile load equivalent to the selected target tensile strain from the tensile test (e.g., 0.35 ε_f) up to a specified number of load cycles.
8.a.	During Step 7, record every 0.005 s: • Load (P [lb or kips]) • Deformation (ΔL[inch or mm]) • Time (t [s])
8.b.	Monitor every 5 s: • Temperature (T[°F or °C])

9. When testing is done, detach the LVDTs from the fixtures and remove the specimen from the machine setup.

Calculations

- Calculate the measured stress as follows:

$$\sigma_m(t) = \frac{P(t)}{\pi r^2} \quad \text{(C.10)}$$

where:

$\sigma_m(t$ = Measured time-dependent tensile stress, psi (or MPa),

$P(t)$ = Load, lb (or kN),

= Radius of the cylindrical HMAC specimen, in (or mm).

- Calculate the viscoelastic stress as follows:

$$\sigma_{VE}(t) = \Sigma_{i=1}^{n} E_1(\tau - t_i)^{-m}\left(\frac{d\varepsilon}{dt}\right)_i dt \quad \text{(C.11)}$$

where:

$\sigma_{VE}(t)$ = Calculated time-dependent viscoelastic tensile stress, psi (or MPa),

E_1 = Elastic relaxation modulus at a reduced loading time of 1 s, psi (or MPa),

τ = Last value of time in the load cycle, s,

T = *ith* value of time in the load cycle, s,

M = Stress relaxation rate ($0 \leq m < 1$),

$(d\varepsilon/dt)_I$ = *C*hange in strain for every *ith* time increment *dt*,

dt = Time increment,

n = Number of data points recorded during each load cycle.

- Calculate the reference modulus as follows:

$$E_R = \frac{\sigma_m(t)_{\max}}{\varepsilon_{\max}} \quad \text{(C.12)}$$

where:

E_R = Reference modulus, psi (or MPa),

$\sigma_m(t)_{max}$ = Maximum measured time-dependent tensile stress, psi (or MPa), usually corresponds to the first load cycle,

ε_{max} = Applied target tensile strain (for example, $+0.35\varepsilon_f$).

- Calculate the pseudo strain as follows:

$$\varepsilon_R(t) = \frac{\sigma_{VE}(t)}{E_R} \quad \text{(C.13)}$$

where $\varepsilon_R(t)$ is the pseudo strain, psi/psi (or MPa/MPa).

- Calculate the dissipated pseudostrain energy (DPSE).
  - When the values of $\sigma_m(t)$ are plotted against $\varepsilon_R(t)$, they form an oval-shaped loop, as shown in Figure C.7. The area inside the loop, which represents the DPSE in each load cycle, is computed using the area by coordinates method.
  - Normalize the DPSE to account for the reduction in material that is capable of dissipating energy:

$$W_R = \frac{DPSE}{\left(\frac{S_i}{S_1}\right)} \quad \text{(C.14)}$$

where:

S_i = Pseudostiffness, computed for load cycle i as the ratio of $\sigma_m(t)_{max}$ and $\varepsilon_R(t)$,

S_1 = Maximum pseudostiffness, usually corresponds to the first load cycle.

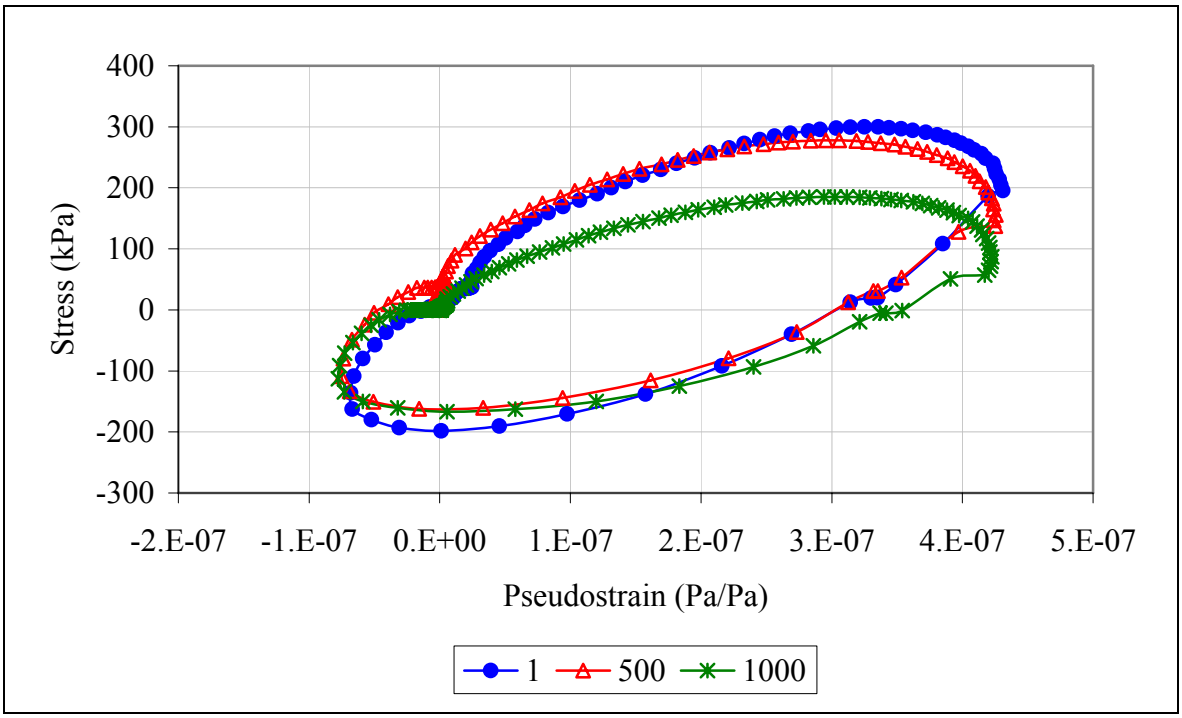

Figure C.7. Typical Stress versus Pseudostrain Plot Showing the DPSE for Load Cycle N = 1 and N = 1000 for a Test Performed at a Temperature of 86°F (30°C).

- Determine the rate of fracture damage accumulation (parameter *b*).
- As shown in Figures C.8 and C.9, when WR is plotted against the number of load cycles in a semi-log scale, the relationship yields a linear expression of the following form:

$$W_R = a + bLog(N) \tag{C.15}$$

where:

W_R = Normalized DPSE (J/m^3),

A = Intercept, represents the energy associated with the initial damage and the material nonlinearity,

B = Slope, represents the rate of fracture damage accumulation with respect to load cycles,

N = Load cycle.

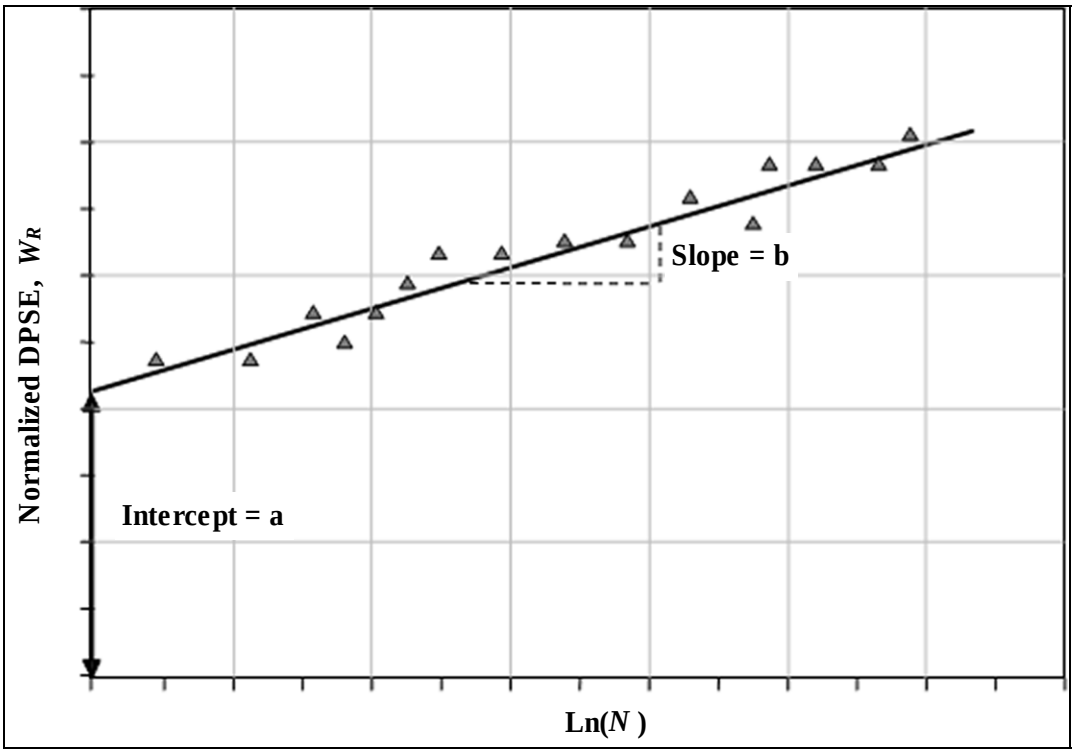

Figure C.8. Schematic Plot of W_R versus *Ln(N)*.

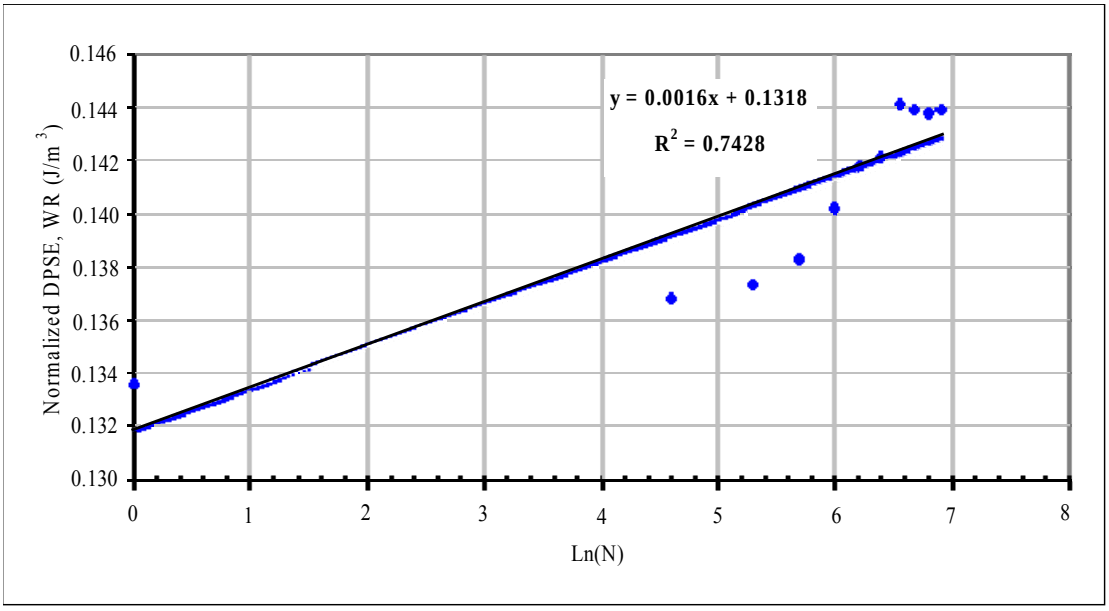

Figure C.9. Typical Plot of W_R versus *Ln(N)* for a Test Performed at a Temperature of 86°F (30°C).

- From the W_R versus *ln(N)* plot, obtain the rate of fracture damage accumulation, *b*, as the slope of the plot of DPSE versus Log N, e.g., 0.0016 in Figure C.9.
- A minimum of three replicate specimens are recommended for this test.
- If the computed COV for the *b* values of the two specimens differs by more than 15 percent, it is recommended to test additional specimens. Note that 15 percent is a typically acceptable COV for HMAC mixtures/specimens due to HMAC heterogeneity and test variability.

Report

The results and data to be reported for subsequent analyses include:

- the air void content (and density),
- the binder content,
- the applied number of load cycles,
- the loading frequency (Hz),
- the (average) *b* value,
- the test temperature, and
- the COV of *b*.

APPENDIX D

PROPOSED TEST METHOD TO USE A WILHELMY PLATE DEVICE TO DETERMINE SURFACE ENERGY COMPONENTS OF ASPHALT BINDERS

Disclaimer

"The proposed test methods are recommendations of the National Cooperative Highway Research Program (NCHRP) Project 9-37 staff at Texas Transportation Institute. These methods have not been approved by NCHRP or by any AASHTO Committee or formally accepted for the AASHTO specifications."

1. Scope

1.1 This test method covers the procedures for preparing samples and measuring contact angles using the Wilhelmy Plate device to determine the three surface energy components of asphalt binders.

1.2 This standard is applicable to asphalt binders that do not contain particulate additives such as crumb rubber.

1.3 This method must be used in conjunction with the manual for mathematical analysis to determine surface energy components from contact angle measurements or the computerized spreadsheets that were developed to carry out this analysis.

1.4 *This standard may involve hazardous material, operations, and equipment. This standard is not intended to address all safety problems associated with its use. It is the responsibility of the user of this procedure to establish appropriate safety and health practices and to determine the applicability of regulatory limitations prior to its use.*

2. Referenced Documents

2.1 AASHTO Standards

T40 Sampling of Bituminous Materials

3. Definitions

3.1 *Surface Energy*, γ, or surface free energy of a material is the amount of work required to create unit area of the material in vacuum. The total surface energy of a material is divided into three components, namely the Lifshitz-van der Waals component, the acid component, and the base component.

3.2 *Contact Angle,* θ, refers to the equilibrium contact angle of a liquid on a solid surface measured at the point of contact of the liquid-vapor interface with the solid.

3.3 *Advancing Contact Angle*, within the context of this test, refers to the contact angle of a liquid with the solid surface as the solid surface is being immersed into the liquid.

3.4 *Receding Contact Angle*, within the context of this test, refers to the contact angle of a liquid with the solid surface as the solid surface is being withdrawn from the liquid.

3.5 *Probe Liquid*, within the context of this test, refers to any of the pure, homogeneous liquids that do not react chemically or dissolve with asphalt binders and are used to measure the contact angles with the binder. The three surface energy components of the probe liquid must be known at the test temperature from the literature.

3.6 *Mixing Temperature*, within the context of this test, refers to the temperature at which the viscosity of the asphalt binder is approximately 0.170 Pa's, or any other temperature that is prescribed or determined by the user for use as the mixing temperature with aggregates to prepare hot mix asphalt.

4. Summary of Method

4.1 A glass slide coated with the asphalt binder and suspended from a microbalance is immersed in a probe liquid. From simple force equilibrium conditions, the contact angle of the probe liquid with the surface of the asphalt binder can be determined. The analysis to obtain the contact angle is carried out using software accompanying the device.

4.2 Contact angles measured with different probe liquids are used with equations of work of adhesion to determine the three surface energy components of the asphalt binder.

4.3 Figure D.1 presents a schematic of the Wilhelmy Plate device.

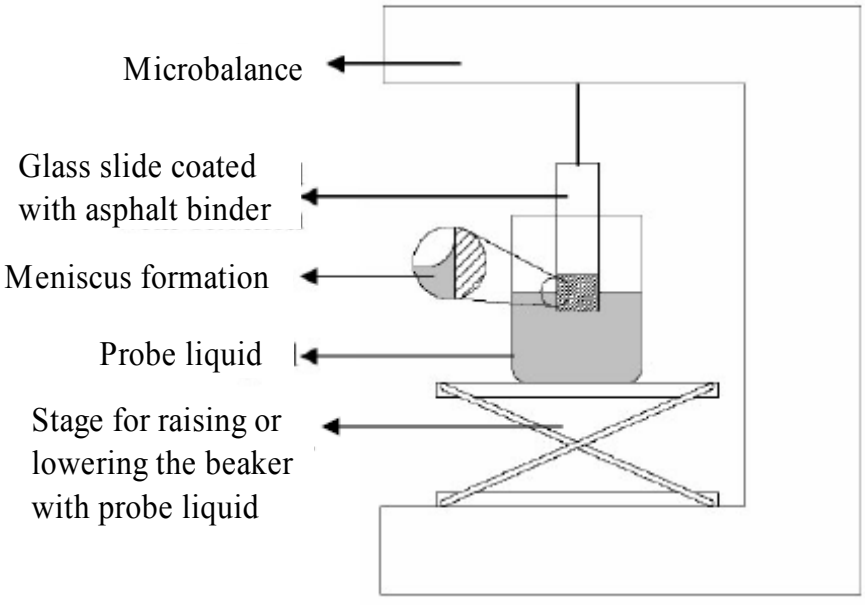

Figure D.1. Schematic of the Wilhelmy Plate Device.

5. Significance and Use

5.1 Surface energy components of asphalt binders are important material properties that are related to the performance of hot mix asphalt. Surface energy components of asphalt binders can be used to determine the total surface energy and cohesive bond strength of this material. The cohesive bond strength of asphalt binders is related to the work required for microcracks to propagate within the asphalt binder in an asphalt mix, which is related to the fatigue cracking characteristics of the mix.

5.2 Surface energy components of asphalt binders can also be combined with the surface energy components of aggregates to compute the work of adhesion between these two materials and the propensity for water to displace the asphalt binder from the asphalt binder-aggregate interface. These two quantities are related to the moisture sensitivity of the asphalt mix.

6. Apparatus

6.1 Microscope glass slides (24 mm x 60 mm No. 1.5) to serve as substrates for the asphalt binder.

6.2 An oven capable of heating up to 150°C to heat asphalt binders for sample preparation.

6.3 A vernier calipers with a least count of at least 0.01mm to measure the dimensions of the slide.

6.4 A heating plate with temperature control to maintain temperature of the asphalt binder during the sample preparation process.

6.5 A propane torch to heat and clean glass slides prior to sample preparation.

6.6 A slotted slide holder to hold the finished asphalt binder slides.

6.7 Wilhelmy Plate device—This device comprises a microbalance with a motor-controlled stage that can be raised or lowered at a desired speed to immerse a slide with asphalt binder in the probe liquid in advancing mode and to withdraw the slide from the probe liquid in receding mode. The tests are conducted at 25±1°C. If the room temperature is significantly different from the test temperature, then an appropriate environmental chamber may be required to house the apparatus.

6.8 The data acquisition and analysis software is used to collect the data and determine the contact angles.

6.9 Glass beaker to hold the probe liquid while the slide coated with asphalt binder is immersed in the liquid.

7. Sampling

7.1 Obtain a representative sample of the asphalt binder according to procedure T40. Approximately 50 g of asphalt binder stored in a small metallic container is required for this test.

8. Preparation of Test Samples

8.1 Heat the container with asphalt binder in an oven to the mixing temperature for about 1 hour, and transfer the container to the heating plate.

8.2 Set the temperature of the heating plate so that the asphalt binder remains at the mixing temperature. Stir the liquid asphalt binder from time to time throughout the sample preparation process.

8.2 Pass the end of the glass slide intended for coating six times on each side through the blue flame of a propane torch to remove any moisture (Figure D.2). Dip the slide into the molten bitumen to a depth of approximately 15 mm (Figure D.3). Drain excess binder from the plate until a very thin (0.18 to 0.35 mm) and uniform layer at least 10 mm thick remains on the plate. A thin coating is required to reduce variability of the results. Turn the plate with the uncoated side downward (Figure D.4), and carefully place it in the slotted slide holder (Figure D.5).

8.3 If necessary, the heat-resistant slide holder with all the coated slides is placed in the oven after coating for 15 to 30 s to obtain the desired smoothness.

8.4 Place the binder-coated plates in a desiccator overnight.

Figure D.2. Glass Slide Dried before Immersion by Passing it over a Propane Flame.

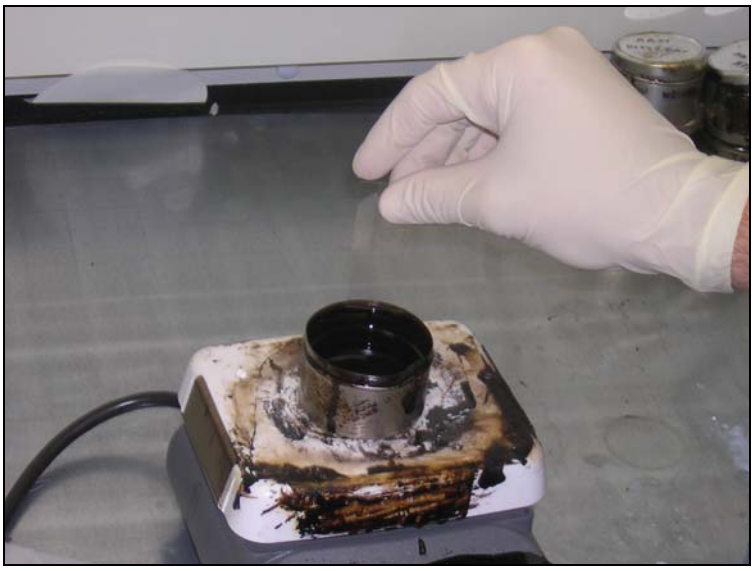

Figure D.3. Clean Glass Slide Dipped in Molten Asphalt Binder to Create Coating.

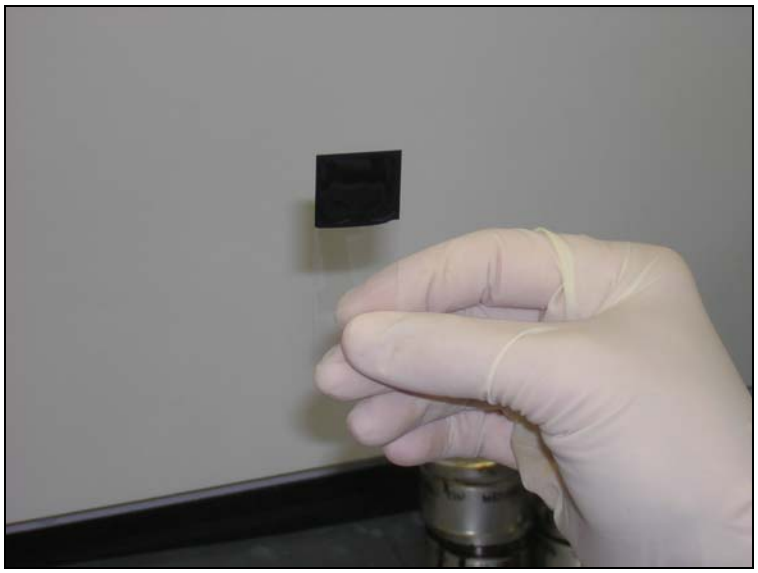

Figure D.4. Glass Slide Coated with Asphalt Binder for Testing with the Wilhelmy Plate Device.

Figure D.5. Finished Slides Stored on Slotted Holder in Desiccator Prior to Testing.

9. Procedure

9.1 User must ensure that the microbalance is calibrated in accordance with the manufacturer specifications prior to the start of the test.

9.2 One asphalt binder coated slide is removed from the desiccator at a time. Use the vernier calipers to measure the width and thickness of the asphalt binder slide to an

accuracy of 0.01 mm. The measurements must be made just beyond 8 mm from the edge of the slide to avoid contamination of the portion of coating that will be immersed in the probe liquid.

9.3 Suspend the glass slide coated with asphalt binder from the microbalance using a crocodile clip. Ensure that the slide is horizontal with respect to the base of the balance.

9.4 Fill a clean glass beaker with the probe liquid to a depth of at least 10 mm, and place it on the balance stage. Raise the stage manually to bring the top of the probe liquid in proximity to the bottom edge of the slide (Figure D.6).

Figure D.6. Asphalt Binder Sample Suspended from Microbalance for Immersion in Probe Liquid.

9.5 During the test, the stage is raised or lowered at the desired rate via a stepper motor controlled by the accompanying software. A rate of 40 microns per second is recommended to achieve the quasi-static equilibrium conditions for contact angle measurement. The depth to which the sample is immersed in the probe liquid is set to

8 mm. Larger depths up to 15 mm may be used if the thickness of asphalt coating on the slide is uniform. The weight of the slide measured by the microbalance is recorded continuously by the software accompanying the device during the advancing (stage is raised to dip the slide) and receding (stage is lowered to retract the slide from the liquid) process.

9.6 At least five probe liquids are recommended for use with this test. These are water, ethylene glycol, methylene iodide (diiodomethane), glycerol, and formamide. All reagents must be high-purity grade (>99 percent). Contact angles must be measured for at least three replicates with each probe liquid for each asphalt binder.

9.7 Since methylene iodide is a light-sensitive material, cover the beaker containing methylene iodide with black tape to reduce the effect of light.

9.8 Dispose of the probe liquid in the beaker after testing with three asphalt binder slides, and use a fresh sample of the probe liquid for each different type of binder. Store all probe liquids in air tight containers, and do not use after prolonged exposure to air in open-mouthed beakers.

9.9 Tests must be completed within 24 to 36 hours from the time of preparation of the slides.

10. Calculations

10.1 From simple force equilibrium considerations, the difference between weight of a plate measured in air and partially submerged in a probe liquid (ΔF) is expressed in terms of buoyancy of the liquid, liquid surface energy, contact angle, and geometry of the plate. The contact angle between the liquid and surface of the plate is calculated from this equilibrium as:

$$\cos\theta = \frac{\Delta F + V_{im}\left(\rho_L - \rho_{air} g\right)}{P_t \gamma_L^{Tot}} \qquad \text{(D.1)}$$

where P_t is the perimeter of the bitumen coated plate, γ_L^{Tot} is the total surface energy of the liquid, θ is the dynamic contact angle between the bitumen and the liquid, V_{im} is the volume immersed in the liquid, ρ_L is the density of the liquid, ρ_{air} is the air

density, and g is the local acceleration due to gravitation. The accompanying software requires the density of the liquid, total surface tension of the liquid, dimensions of the sample, and local acceleration due to gravity as inputs to compute the contact angle using the force measurements from the microbalance.

10.2 Buoyancy correction based on slide dimensions and liquid density can introduce unwanted variability into the resulting contact angles. To eliminate these effects, the accompanying software performs a regression analysis of the buoyancy line and extrapolates the force to zero depth. The user must select a representative area of the line for regression analysis (Figure D.7). The software reports the advancing and receding contact angles based on the area selected using the aforementioned equation.

10.3 If the force measurements are not smooth, i.e., if sawtooth-like force measurements are observed due to slip-stick behavior between the probe liquid and the asphalt binder, then report this along with the advancing and receding contact angles.

10.4 The typical standard deviation of the measured contact angle for each pair of liquid and asphalt binder based on measurements with three replicate slides is less than 2°.

10.5 The contact angle of each replicate and probe liquid is used with the surface energy analysis workbook that conducts the required analysis to determine the three surface energy components of the asphalt binder and the standard deviations of these components. This workbook also verifies the accuracy and consistency of the measured contact angles and integrates data from other test methods such as the surface energy components of aggregates to determine various parameters of interest that are related to the performance of asphalt mixes.

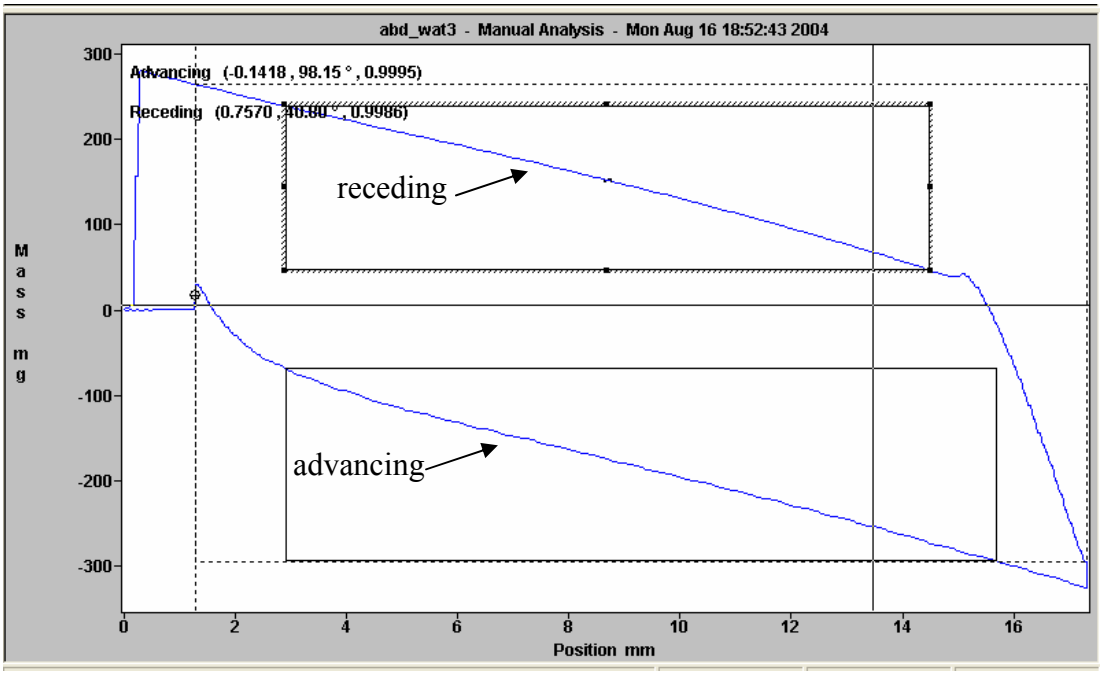

Figure D.7. Selection of Representative Area to Determine Advancing and Receding Contact Angles (screen image).

APPENDIX E
PROPOSED TEST METHOD TO USE A SORPTION DEVICE TO DETERMINE SURFACE ENERGY COMPONENTS OF AGGREGATES

Disclaimer

"The proposed test methods are recommendations of the NCHRP Project 9-37 staff at the Texas Transportation Institute. These methods have not been approved by NCHRP or by any AASHTO Committee or formally accepted for the AASHTO specifications."

1. Scope

1.1 This test method covers the procedures for preparing samples and measuring adsorption isotherms using a sorption device with an integrated Surface Energy Measurement System (SEMS) to determine the three surface energy components of asphalt binders.

1.2 This standard is applicable to aggregates that pass through a 4.75 mm sieve (No. 4) and are retained on a 2.36 mm sieve (No. 8).

1.3 This method must be used in conjunction with the manual for mathematical analysis to determine surface energy components from spreading pressures or the computerized spreadsheets that were developed to carry out this analysis.

1.4 *This standard may involve hazardous material, operations, and equipment. This standard is not intended to address all safety problems associated with its use. It is the responsibility of the user of this procedure to establish appropriate safety and health practices and to determine the applicability of regulatory limitations prior to its use.*

2. Referenced Documents

2.1 AASHTO Standards

T2 Practice for Sampling Aggregates

3. Definitions

3.1 *Surface Energy,* γ , or surface free energy of a material is the amount of work required to create a unit area of the material in a vacuum. The total surface energy of a material is divided into three components, namely the Lifshitz-van der Waals component, the acid component, and the base component.

3.2 *Equilibrium spreading pressure*, π_e , is the reduction in surface energy of the solid due to adsorption of vapors at its saturation vapor pressure on the surface of the solid.

3.5 *Probe Vapor*, within the context of this test, refers to vapors from any of the pure, homogeneous liquids that do not chemically react or dissolve with aggregates and are used to measure the spreading pressure with the aggregate.

The three surface energy components of the probe vapor must be known at the test temperature from the literature.

3.6 *Relative Vapor Pressure,* within the context of this test, refers to the ratio of the pressure of the vapor to its saturation vapor pressure and can vary from 0 (complete vacuum) to 1 (saturation vapor pressure).

3.7 *Adsorption Isotherm* of a vapor with an aggregate is the relationship between the equilibrium mass of vapor adsorbed per unit mass of the aggregate and the relative vapor pressure of the vapors at a constant temperature.

4. Summary of Method

4.1 Clean aggregate samples are degassed under high temperature and vacuum in an air-tight sorption cell. Vapors of probe liquids are introduced into the sorption cell in controlled and gradually incremental quantities to achieve different relative pressures. The equilibrium mass of the vapor adsorbed to the solid surface is recorded for each relative pressure to obtain the adsorption isotherm. The adsorption isotherm computes the equilibrium spreading pressure of the probe vapor with the aggregate.

4.2 Equilibrium spreading pressure with different probe vapors is used with equations of work of adhesion to determine the three surface energy components of the aggregate.

5. Significance and Use

5.1 Surface energy components of aggregates are important material properties that are related to the performance of hot mix asphalt. Surface energy components of aggregates can be combined with the surface energy components of asphalt binders to quantify the work of adhesion between these two materials and the propensity for water to displace the asphalt binder from the asphalt binder-aggregate interface. These two quantities are related to adhesive fracture properties and moisture sensitivity of the asphalt mix.

6. Apparatus

6.1 A sorption device integrated with the SEMS comprises an air-tight adsorption cell, a magnetic suspension balance that measures the mass of the sample in the sorption cell in noncontact mode, a manifold with vacuum pump, temperature control, probe liquid containers with appropriate valves and controls to regulate the flow of vapors into the sorption cell, and associated software for test control and analysis (Figure E.1). The microbalance must have a precision of 10 μg with a capacity to weight of at least 50 g.

6.2 Temperature of the sorption cell, piping that carries vapors, and a buffer tank is maintained using a water bath that is automatically controlled by the SEMS software.

6.3 An oven capable of heating up to 150°C is required to prepare aggregate samples before testing.

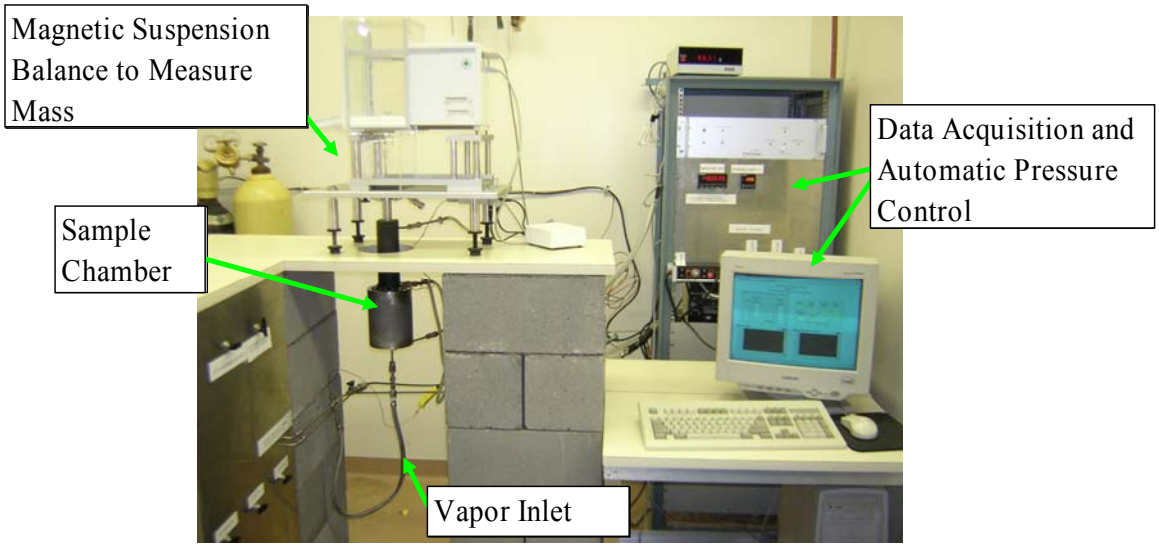

Figure E.1. Universal Sorption Device.

7. Sampling

7.1 Obtain a representative sample of the aggregate according to procedure T2. Sieve the sample to obtain about 100 g of aggregates passing a 4.75 mm sieve (No. 4) and retained on a 2.36 mm sieve (No. 8).

8. Preparation of Test Samples

8.1 Thoroughly wash about 25 g of the aggregate in a 2.36 mm sieve with deionized or distilled water. The quality of water used for the cleaning of the aggregates must be comparable to the quality of water used for gas chromatography. Place the clean aggregate sample in an oven at 150°C for 8 hours, and thereafter, transfer it to a desiccator at room temperature for at least 8 hours before testing.

9. Procedure

9.1 The samples are held in a wire mesh basket during the test. Rinse the basket with acetone and air dry. Transfer the aggregate sample to the basket (Figure E.2), and suspend the basket from the hook underneath the suspension balance (Figure E.3). Seal the sorption cell with the coupling with the suspension balance using a viton® O-ring (Figure E.4). A metal jacket connected to a water bath is used around the sorption cell to maintain temperature (Figure E.5).

Figure E.2. Basket with Aggregate Sample for Testing with the USD.

Figure E.3. Sample Basket Suspended from the Magnetic Suspension Balance.

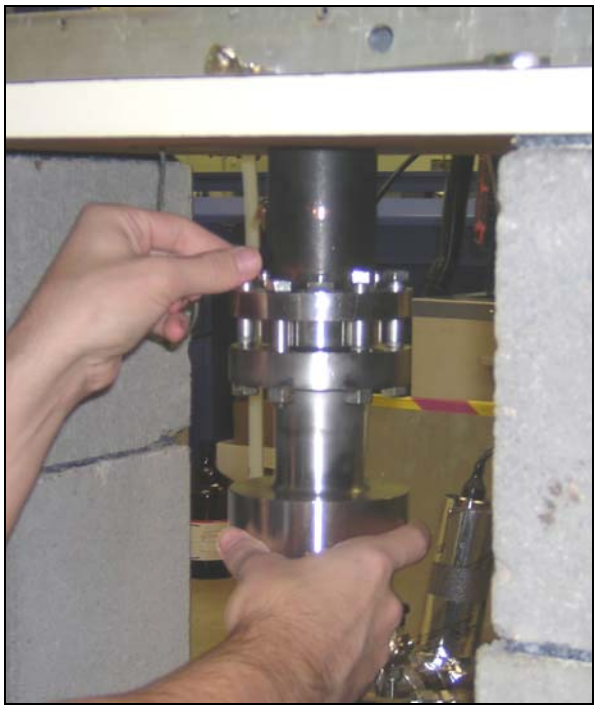

Figure E.4. Adsorption Cell Raised and Sealed with Sample Basket Inside.

Figure E.5. Temperature Jacket Raised to Cover Adsorption Cell.

9.2 In order to obtain stable and consistent readings with the magnetic suspension balance, it is necessary that the sample basket and magnetic suspension coupling are in vertical and horizontal alignment with each other. Activate and deactivate the magnetic suspension coupling repeatedly until stable and consistent readings are observed. This is an indication that the balance is aligned. This process, referred to as centering of balance, can also be automatically executed with the "Horizontal Centering" module of the SEMS software (Figure E.6).

9.3 Degas the sample and the test manifold by drawing vacuum from the system using a mechanical vacuum pump. After the first 2 hours of degassing at 70°C, reduce the temperature of the manifold to 25°C (test temperature), and continue degassing for another 4 hours. The pressure in the cell must be maintained below 20 millitorr during the last 4 hours of degassing. The temperature and degassing times can be controlled manually or automatically using the "Degassing" module of the SEMS software (Figure E.7). Monitor

the mass of the sample for the last 1 hour of the degassing time to ensure that it is stable. If the mass continues to decrease, it indicates that the sample is still losing physically adsorbed particles from its surface and more degassing time is required.

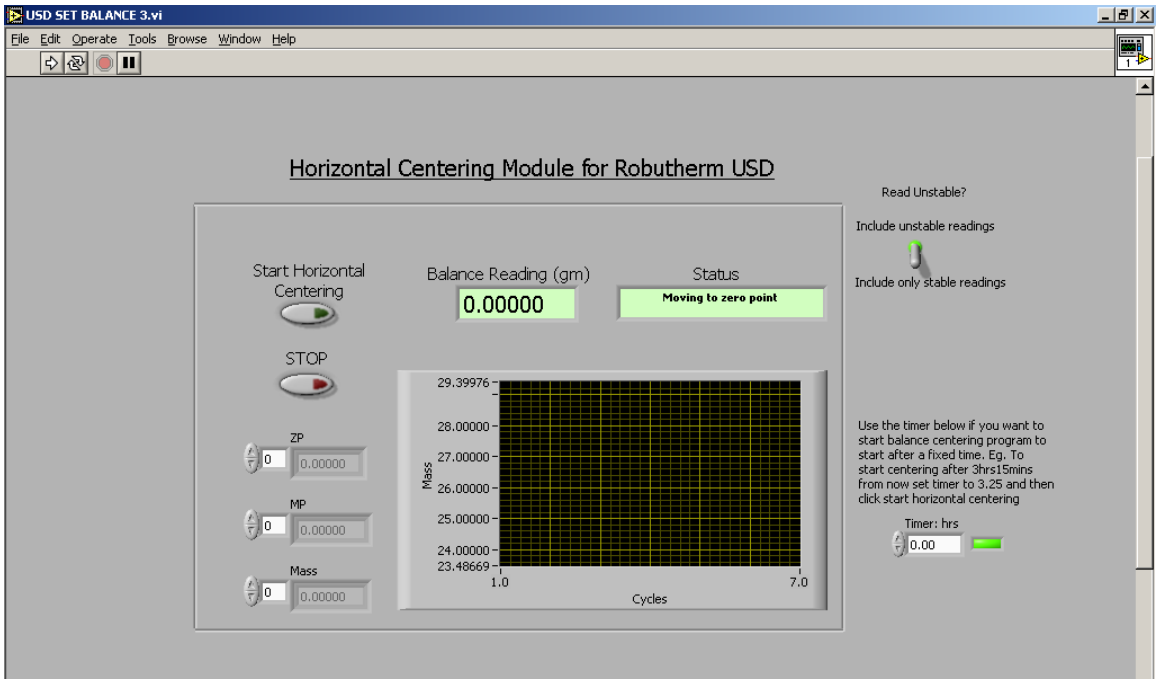

Figure E.6. Auto Centering Module in SEMS Software.

Figure E.7. Degassing Module in SEMS Software.

9.4 After completion of degassing, isolate the vacuum pump from the adsorption system. Monitor the pressure of the system for a few minutes to ensure that there is no significant leak. Typically, a leak that allows the system pressure to increase by more than 40 millitorr per hour is unacceptable. In such cases, retighten and replace the seal with the sorption cell, and repeat the degassing process.

9.5 Activate the "Adsorption Test" module of the SEMS software to control and execute the adsorption test (Figure E.8). Provide the necessary inputs to the software, such as volume of aggregate (computed by dividing the mass of the aggregate by its density) and probe vapor to execute the test. Other inputs such as name and description of the sample, name and location of the summary and raw data file for saving results, and minimum equilibrium time for each increment of relative pressure are also required. A minimum time of 15 minutes for equilibrium of each increment is recommended. Start the test from the SEMS software. A mechanical isolation valve is used between each of the probe liquid tanks and the system to prevent accidental exposure of the system to the probe vapors. Open the valve corresponding to the probe vapor for the

test. Close this valve after completion of the test and before changing or degassing samples.

9.6 The test is controlled, and data are acquired using the SEMS software. The software regulates valves to dose probe vapors into the system in 10 steps to achieve an increment of 0.1 in the relative pressure with each step. The mass of the sample is continuously acquired during this process by the SEMS software. The software computes the mass of vapor adsorbed in real time as the difference in the mass of sample at any time from the mass of the sample in vacuum after applying for corrections due to buoyancy. The software also corrects for any drift in the measurements due to the magnetic suspension coupling. Each increment of relative pressure is applied by the software after the mass of the sample comes into equilibrium due to adsorption of vapors from the previous increment, or after the minimum time for equilibrium is achieved, whichever is later. The test is complete after the saturation vapor pressure of the probe liquid is achieved in 10 increments and the equilibrium mass of vapor adsorbed is recorded for each increment.

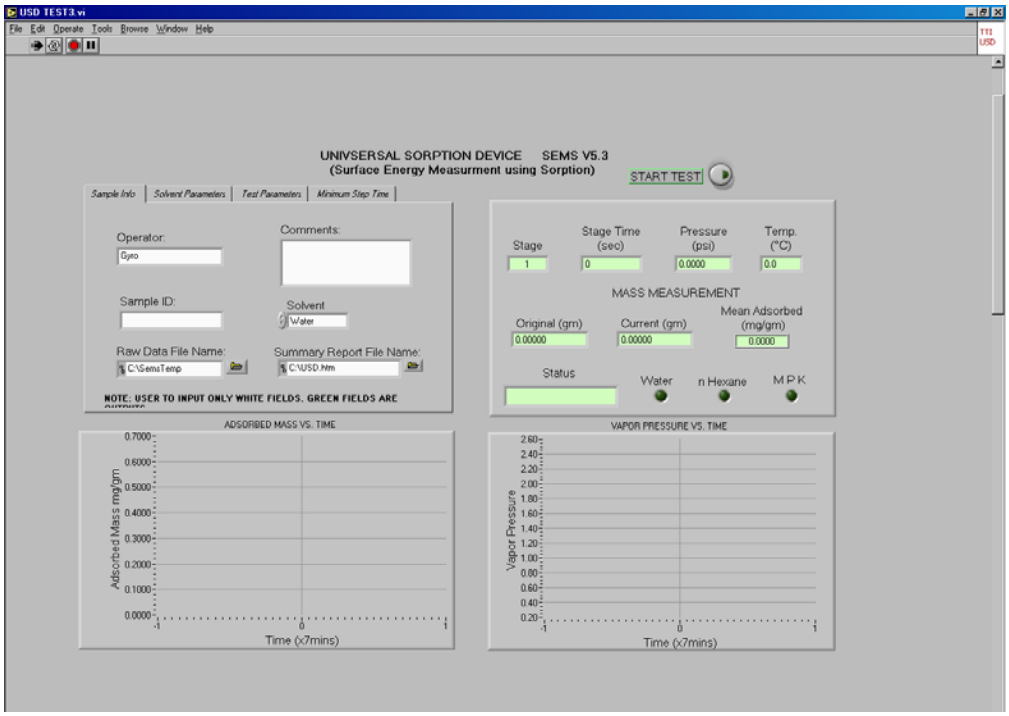

Figure E.8. Adsorption Test Module in SEMS Software.

9.7 Three probe vapors are recommended for this test. These are water, methyl propyl ketone (MPK), and hexane. All reagents must be high-purity grade (>99 percent). After filling the respective liquid tanks in the manifold for the first time, degas the tanks to remove any air trapped during the process of refilling. Typically, 100 ml of n-hexane lasts for approximately 15 tests, and 100 ml of MPK and water last for 60 tests.

10. Calculations

10.1 After completion of all 10 increments in vapor pressure, the software reports a summary of final results that includes the adsorption isotherm, specific surface of the aggregate with Brunauer-Emmett-Teller (BET) equations, and spreading pressure based on the specific surface area and the adsorption isotherm (Figure E.9).

10.2 The typical coefficient of variation (standard deviation/average) for the spreading pressure for each pair of probe vapor and aggregate based on three replicate measurements is about 15 percent.

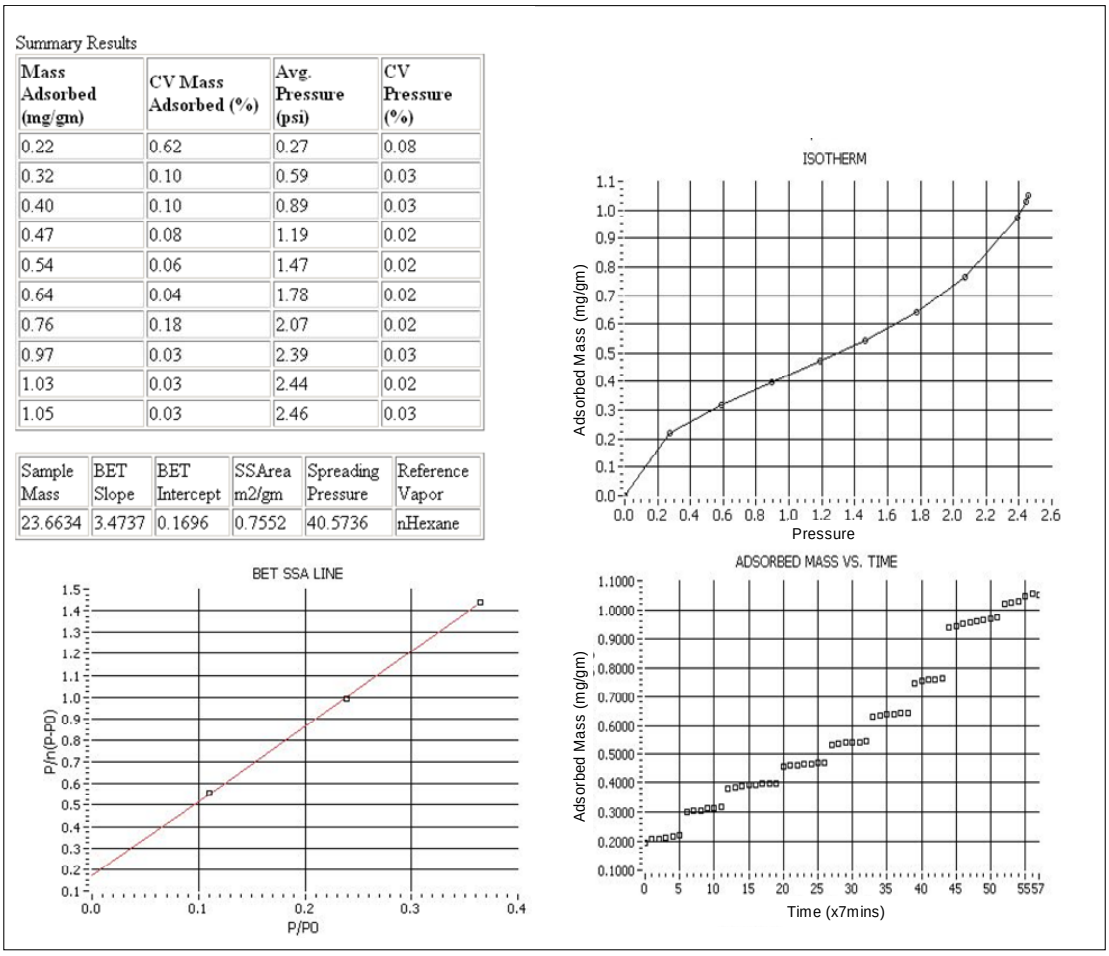

Figure E.9. Results Reported by SEMS Software.

10.3 Although the SEMS software reports specific surface areas and spreading pressures for each test, certain corrections must be applied in order to obtain the correct specific surface area and spreading pressures that can be combined to determine the three surface energy components. Therefore, the adsorption isotherms for each of the three probe vapors reported by SEMS are used with the surface energy analysis workbook that conducts the required analysis to determine the specific surface area and the three surface energy components of the aggregate and the standard deviations of these components. This user-friendly workbook also integrates data from other tests such as the surface energy components of asphalt binders to determine various parameters of interest that are related to the performance of asphalt mixes.

APPENDIX F
DESCRIPTION OF TEST EQUIPMENT

Specifications for the DMA

The following are the requirements for the DMA to be able to test a fine aggregate matrix sample.

No.	Description	Requirement
Test Device:		
1	Torque range	0.1 x10^{-6} to 200 x 10^{-3} Nm
2	Torque resolution	Minimum 10^{-9} Nm
3	Range for measurable speed	10^{-8} to 600 rad/s
4	Range for detectable speed	10^{-8} to 600 rad/s
5	Angular position resolution	Minimum 0.05 x 10^{-6} rad
6	Frequency range	10^{-6} to 150 Hz
7	Gap resolution	Minimum 1 micron
8	Range for sample height	1 to 50 mm
9	Normal force measurement range	0.1 to 2000 g
Accessories:		
10	Environmental chamber: Temperature range	-20°C to 150° C
11	Environmental chamber: Temperature control accuracy	±1° C
12	Attachments to the device to accommodate 12.5 mm diameter cylindrical samples	
13	Software: Must provide user with the following information based on the data acquired during the test	- maximum and minimum strain per cycle - maximum and minimum stress per cycle - phase angle - maximum and minimum torque per cycle - preferably a minimum of 50 data points per cycle for the torque, stress, and strain with respect to time

Specifications for the Wilhelmy Plate Device:

The Wilhelmy Plate device consists of two components:

1. A microbalance with a base can be lowered or raised using a stepper motor that allows controlled immersion and retraction of asphalt binder coated slides in beakers filled with probe liquids.
2. A software controls the immersion of the slide, acquires force data from the balance and computes the advancing and receding contact angles using the following physical and material properties: physical dimensions of the slide, total

surface tension of the probe liquid, density of the probe liquid, and local acceleration due to gravity.

No.	Description	Requirement
Test Device:		
1	Microbalance capacity	Minimum 10 gm
2	Microbalance resolution	Minimum 0.001 mg
3	Immersion speed range	2 to 250 microns/s
4	Immersion motor resolution	Minimum 0.1 micron
5	Overall contact angle resolution	Minimum 0.01°
Accessories:		
6	Software: Must provide user with the following information based on the data acquired during the test	- advancing contact angle - receding contact angle - regression fit parameters for buoyancy correction line

Specifications for the USD

The USD consists of two components:

1. A microbalance measures the mass of a sample in noncontact mode via a magnetic suspension coupling.
2. A computer controlled test manifold allows controlled exposure of the aggregate to various probe vapors by regulating pressure in the sorption cell.

No.	Description	Requirement
Test Device:		
1	Microbalance range	1-50 gm
2	Microbalance resolution	Minimum 0.01 mg
3	Pressure transducer range	0-1 atmosphere
4	Pressure transducer resolution	Minimum 5 millitorr
Accessories:		
5	Water bath circulator: Temperature range	20-80°C
6	Water bath circulator: Temperature control accuracy	±1°C
4	Software: Must provide user with the following information based on the data acquired during the test	Adsorption isotherm with equilibrium adsorbed mass corrected for buoyancy and fractional vapor pressures